THE UNIVERSITY OF QUEENSLAND

AUSTRALIA

Relativistic effects in atomic structure theory

Andoni Skoufris

Under the supervision of
Dr Benjamin Roberts

A thesis submitted to the University of Queensland in partial fulfilment of the degree of Bachelor of Advanced Science with Honours
School of Mathematics and Physics
June 2025

Typeset in LaTeX 2_ε.

The work presented in this Thesis is, to the best of my knowledge and belief original, except as acknowledged in the text, and has not been submitted either in whole or in part, for a degree at this or any other university.

Andoni Skoufris

Abstract

Despite the enormous success of theoretical atomic physics over the past 100 years, the majority of atomic physics calculations treat electron-electron interactions completely non-relativistically through the Coulomb interaction. Although this captures the leading order behaviour of the electron-electron interactions and is suitable for approximately non-relativistic systems, for heavy or highly-charged ions this can be an insufficient starting point. This can partly be remedied through the inclusion of relativistic corrections to the electron-electron interaction into these calculations. The Breit interaction represents the leading order relativistic correction to the Coulomb interaction, and captures the magnetic interactions, as well as retardation effects. While the Breit interaction can be included into high-precision atomic structure calculations, it can only currently be done to the second order of perturbation theory, where in heavy ions it is known to significantly modify energy corrections. In this thesis I will use the Feynman diagram method of perturbation theory in atomic physics to include the Breit interaction at the same time that certain many-body effects are summed to all orders of perturbation theory. By doing so, the Breit interaction can now be included into calculations that include important many-body corrections in a non-perturbative way. I will assess the impact of this on the accuracy of atomic structure calculations by comparing my calculations to experiment. I will also discuss an application of a generalisation of the Breit interaction to atomic physics calculations, and present results that indicate that its inclusion at the level of the zeroth order approximation to wave functions and energies may be important for an accurate understanding of highly relativistic atomic systems.

Acknowledgements

I would firstly like to thank my supervisor, Dr. Benjamin Roberts, for guiding me and the project for the past year, and for always being available to listen to and answer my endless questions.

I would also like to thank my friends and anyone else who ever took the time out of their day to listen to me ramble on about my thesis for 20 minutes or more. In particular, I'd like to pay special thanks to Narise Williams, Connor Tweedie, and my fellow Honours students: William McEniery, Harry Fung, Katelyn Smith, Rishi Goel, and Shannon Ray. It was an honour and a privilege to share my thoughts, and with some of you an office, for the past year.

Contents

List of Figures

List of Tables

Symbols and notation

Throughout this thesis the notation differs between the main body and the appendices. The following list of symbols should provide a relatively complete coverage of the symbols and conventions used in the main body of this thesis.

Dirac equation Throughout this thesis, the Dirac representation for the γ and Dirac matrices β and $\boldsymbol{\alpha} = (\alpha^1, \alpha^2, \alpha^3)$, will be used implicitly, particularly for the angular decomposition of the Breit interaction, in which,

$$\gamma^0 = \beta = \begin{pmatrix} I_{2\times 2} & 0 \\ 0 & -I_{2\times 2} \end{pmatrix} \quad \text{and} \quad \gamma^i = \gamma^0 \alpha^i = \begin{pmatrix} 0 & \sigma^i \\ -\sigma^i & 0 \end{pmatrix}, \tag{1}$$

where $\sigma^i = (\sigma^1, \sigma^2, \sigma^3)$ are the Pauli spin matrices and $I_{2\times 2}$ is the 2×2 identity matrix. The conventions for the Dirac spinors will be:

ψ, $\psi^\dagger$ ..... Quantum mechanical (spinor) wave function and its conjugate transpose

$\bar{\psi} = \psi^\dagger \gamma^0$ ... Dirac adjoint of the spinor ψ

Other notation Other notation and abbreviations used in this thesis are the following:

CHF ..... Coulomb-Hartree-Fock

BCHF ..... Breit-Coulomb-Hartree-Fock

ϕ, ε ..... Single-particle (spinor) solution to the CHF equation and its energy

$\bar{\phi}$, $\bar{\varepsilon}$ ..... Single-particle solution to the BCHF equation and its energy

t_{ijkl} $(\bar{t}_{ijkl})$ ... Matrix element of a two-particle operator with respect to CHF (BCHF) orbitals

t_{ij} $(\bar{t}_{ij})$ ..... Effective one-body matrix element of a two-particle operator with respect to CHF (BCHF) orbitals

$\Sigma^{(2)}$ ..... Second-order correlation correction

$\Sigma^{(\infty)}$ ..... All-orders correlation correction

Although overbarred spinors are used both to mean the Dirac adjoint and also BCHF orbitals, the distinction between the two should be clear from the context.

1 Introduction

The field of atomic physics has been enormously successful over the past 100 years, and the consequences of its predictions provide one of the most accurate low-energy tests of the Standard Model to date [1–3]. By combining experimental measurements of electromagnetically forbidden, parity-violating transitions in atoms with atomic structure calculations, one can provide a highly-precise and constraining bound on the possibility of new, as-yet undetected particles and fundamental forces. However, a common starting point for modelling atomic electrons and their interactions is through the non-relativistic Coulomb interaction. While this is known to work very well for a wide variety of atomic systems, in heavier and more highly-charged ions, relativistic effects become important and the Coulomb interaction is no longer sufficient to accurately model the electron-electron interactions. The most prominent example of this came in the late 1990's, when a high-precision measurement of the parity-nonconservation (PNC) amplitude in caesium [4], combined with high-accuracy atomic structure calculations [5, 6] predicted a deviation from the Standard Model for the value of the nuclear weak charge of 2.5 standard deviations. This tension was resolved in the early 2000's when the atomic structure calculations were reevaluated and it was found that contributions to the PNC amplitude due to relativistic corrections to the Coulomb interaction were underestimated [7, 8]. After including these corrections on the same footing as the Coulomb interaction, the conflict between between experiment and the Standard Model was reduced to just 1σ. For a heavy (and therefore relativistic) atomic system such as caesium, then, it is necessary that the electron-electron interactions are treated relativistically, with the magnetic interactions included on the same level as the completely non-relativistic Coulomb interaction.

The leading-order relativistic correction to the Coulomb interaction, known as the Breit interaction, emerges due to the exchange of a single transverse photon between two electrons in quantum electrodynamics. Physically, it accounts for the magnetic interactions between electrons that arise when the motion of electrons and their spin are taken into account to

lowest-order in inverse powers of the speed of light. It was by treating the Breit interaction on the same footing as the Coulomb interaction that the tension was resolved in the PNC amplitude in caesium. In more relativistic settings, the Breit interaction is known to lead to large corrections to calculated atomic properties of ions along the francium-isoelectronic sequence, for certain states making the agreement with experiment worse. This is of particular relevance now as there have recently been several high-precision measurements [9–11] of the excitation energy of a ^{229}Th nucleus, which has been proposed for the development of the world's first nuclear clock [12]. The nucleus of a thorium-229 atom is a particularly promising candidate for a nuclear clock due to its uniquely small nuclear excitation energy that is accessible to modern conventional lasers [13]. Such a clock would furnish the highest-accuracy probe to temporal changes in fundamental constants, as well as the strength of the strong interaction and quark masses [2]. These measurements pave the way for further investigation into the viability of the Th nucleus for the development of a nuclear clock, and one avenue through which this could be explored is in high-accuracy atomic studies of Th^{3+}. This ion lies along the francium-isoelectronic sequence and therefore undergoes large corrections due to the Breit interaction at only second order in perturbation theory. Because perturbation theory in atomic physics is known to not necessarily converge at low orders of perturbation theory [6, 14], we would therefore like to include the Breit interaction beyond just second order in perturbation theory.

With this motivation in mind, the aim of this thesis is to include the Breit interaction into high orders of perturbation theory using the Feynman method, in which corrections to energy levels are represented in terms of Feynman diagrams. The benefit of this approach, unlike other perturbative methods in atomic physics, is firstly its computational efficiency, and secondly that certain series of diagrams can be summed to all orders in perturbation theory [5]. This will allow us to determine whether the large corrections at second order for the ions along the francium-isoelectronic sequence are significantly modified upon including the higher order series of diagrams, and also whether this inclusion improves the accuracy of the atomic structure calculations with respect to experiment.

This thesis is structured as follows: In Chapter 2 I outline some of the main historical steps taken towards understanding relativistic interactions between charged particles, and how this led to the formulation of the Breit interaction. In this chapter I will also discuss the relevant theory of atomic physics and the different approaches that have been used in the past to include the Breit interaction into these calculations. In Chapter 3 I will perform a numerical study of the Breit interaction in caesium using the AMPSCI program [15], for the purpose of testing the numerical behaviour of the Breit interaction, as well as to reproduce the results of Derevianko [16]. Chapter 4 provides an overview of the Feynman method for perturbation theory, as well as the theory behind the all-orders correlation potential method and a broad outline of how I will be trying to include the Breit interaction into the Feynman method. In Chapter 5 I will discuss two methods I experimented with to include the Breit interaction into the Feynman method. I will show that the numerical structure of the Feynman diagrams in AMPSCI is insufficient for the inclusion of the Breit interaction and in the next chapter, Chapter 6, I will discuss the numerical details of the

Feynman method as it is currently implemented into AMPSCI, its shortcomings, and how I have corrected them. I demonstrate that after implementing these corrections, the Breit interaction can be included into the Feynman method, and agrees with the standard method of perturbation theory at second order validating my method of implementation. In Chapter 7, I will introduce a generalisation of the Breit interaction known as the frequency-dependent Breit interaction, that includes retardation effects to all orders in powers of the speed of light, and I will discuss how to numerically implement this into the Hartree-Fock approximation for electronic states. In Chapter 8, I will apply my implementation of the Breit interaction into the Feynman method to atomic structure calculations of energy levels and fine structure intervals in the all-orders Feynman method, and compare my results that include the Breit interaction to all-orders with calculations that before now could only be done to second order in perturbation theory.

2 Literature review

In this chapter I will provide an outline of the development of relativistic quantum mechanical equations of motion for interacting charged particles. I will first start by discussing the single-particle Dirac equation, and the difficulties associated with generalising it to two particles that describes their charge-charge interactions in an exact, Lorentz covariant way. I will then show that from second-order perturbation theory in quantum electrodynamics, one can derive the lowest-order description of such an interaction as the familiar instantaneous Coulomb interaction, plus a relativistic correction known as the Breit interaction. I will then outline some of the main theoretical methods that are used in modelling atomic structure, and the impact that including the Breit interaction makes to these calculations.

2.1 The Breit interaction

In relativistic quantum mechanics, the governing wave equation for a single spin-1/2 particle, such as an electron, in an external electromagnetic field is the minimal-coupled Dirac equation [17–20],

$$i\hbar\frac{\partial\psi}{\partial t} = \left[\beta mc^2 - c\boldsymbol{\alpha}\cdot\left(i\hbar\nabla - \frac{e}{c}\boldsymbol{A}\right) - eA_0\right]\psi. \tag{2.1}$$

Here, m and e are the electron mass and charge, $\hbar$ is the reduced Planck constant, c is the speed of light, $\beta = \gamma^0$ and $\boldsymbol{\alpha} = \gamma^0\boldsymbol{\gamma}$ are the Dirac matrices, and $A^\mu = (A_0, \boldsymbol{A})$ is the electromagnetic 4-potential [19, 20]. Neglecting radiative effects from quantum electrodynamics, this equation accurately predicts the properties of single electrons, such as the spin-own-orbit interaction, in a Lorentz covariant form [18, 20–22].

Given the success of the Dirac equation in describing the properties of a single electron in the presence of an electromagnetic field, there have been several attempts to write down an

analogous formula for two electrons, which should describe their magnetic interactions in a similarly Lorentz-covariant way. This problem is quantum-electrodynamical in nature, and no closed form expression for the fully relativistic equation is possible using a Hamiltonian formalism. This is because the Hamiltonian must be a local function of the coordinates and velocities of both particles, but since the speed of light is finite, the interaction felt by one electron will depend on the state of the other electron at earlier, or retarded, times [23–25]. Despite this, numerous expressions have been derived that take into account relativistic corrections to the free two-particle Dirac equation in which the electrons do not interact [18, 21].

As a lowest-order approximation to this equation, we can treat the kinematics of each particle fully relativistically by the free Dirac Hamiltonian of each particle, while the completely non-relativistic, static limit of the electron-electron interaction is the Coulomb interaction, e^2/r, where $r = |\boldsymbol{r}_1 - \boldsymbol{r}_2|$ is the distance between the two electrons. In this limit, the two-particle Dirac equation reads

$$i\hbar\frac{\partial\psi}{\partial t} = \left\{\sum_{j=1}^{2}\left[\beta_j mc^2 - c\boldsymbol{\alpha}_j\cdot\left(i\hbar\nabla_j - \frac{e}{c}\boldsymbol{A}(\boldsymbol{r}_j)\right) - eA_0(\boldsymbol{r}_j)\right] + \frac{e^2}{r}\right\}\psi \tag{2.2}$$

where the subscript index $j = 1, 2$ refers to the jth electron and $\psi = \psi(\boldsymbol{r}_1, \boldsymbol{r}_2, t)$ is now a 16-component spinor on which the Dirac matrices for the individual electrons operate [23, 26]. In 1929, Gaunt [27] and Eddington [28] modified the interaction energy from just the Coulomb interaction above according to the classical expression [26],

$$-\frac{e^2}{r}\left(1 - \frac{\boldsymbol{v}_1\cdot\boldsymbol{v}_2}{c^2}\right), \tag{2.3}$$

where the first (Coulomb) term accounts for the electrostatic interactions and the second term the magnetic interactions [26]. This can be promoted to a quantum mechanical operator by noting that in the first-quantised Hamiltonian, the right-hand side of Eq. (2.1), using $\boldsymbol{p} = -i\hbar\nabla$, and imposing the canonical commutation relation $[r_j, p_k] = i\hbar\delta_{jk}$, leads to the following Heisenberg equation of motion for $\boldsymbol{r}$ [24, 26, 29],

$$\frac{d\boldsymbol{r}}{dt} = \frac{i}{\hbar}[\boldsymbol{r}, H] = -c\,\boldsymbol{\alpha}. \tag{2.4}$$

This indicates that in the context of the Dirac equation, the Dirac matrices play the quantum mechanical role of the electron velocity, and so Eq. (2.3) can be included into the quantised Hamiltonian as

$$\frac{e^2}{r}\left(1 - \boldsymbol{\alpha}_1\cdot\boldsymbol{\alpha}_2\right), \tag{2.5}$$

which Gaunt applied in an analysis of helium [26, 27]. While this accounts for the magnetic effects to order $(v/c)^2$, Breit showed that there are other effects, namely retardation due to the propagation time of signals that travel at the speed of light, that are also present at this order. Including these additional terms, the complete expression is [19, 23, 26]

$$\frac{e^2}{r}\left\{1 - \frac{1}{2}\left[\boldsymbol{\alpha}_1\cdot\boldsymbol{\alpha}_2 + \frac{(\boldsymbol{\alpha}_1\cdot\boldsymbol{r})(\boldsymbol{\alpha}_2\cdot\boldsymbol{r})}{r^2}\right]\right\}, \tag{2.6}$$

where $\boldsymbol{r} = \boldsymbol{r}_1 - \boldsymbol{r}_2$. The term inside the square brackets is known as the Breit interaction,

$$H_{\mathrm{Br}} = -\frac{e^2}{2r}\left[\boldsymbol{\alpha}_1 \cdot \boldsymbol{\alpha}_2 + \frac{(\boldsymbol{\alpha}_1 \cdot \boldsymbol{r})(\boldsymbol{\alpha}_2 \cdot \boldsymbol{r})}{r^2}\right]. \tag{2.7}$$

It is often convenient to write the Breit interaction as a sum of the operator that Gaunt originally used, called the Gaunt interaction,

$$H_{\mathrm{G}} = -\frac{e^2}{r}\boldsymbol{\alpha}_1 \cdot \boldsymbol{\alpha}_2, \tag{2.8}$$

which accounts purely for the magnetic effects, plus the remaining terms,

$$H_{\mathrm{ret}} = \frac{e^2}{2r}\left[\boldsymbol{\alpha}_1 \cdot \boldsymbol{\alpha}_2 - \frac{(\boldsymbol{\alpha}_1 \cdot \boldsymbol{r})(\boldsymbol{\alpha}_2 \cdot \boldsymbol{r})}{r^2}\right], \tag{2.9}$$

called the retardation interaction, which accounts for the retardation effects [30, 31]. Including the Breit interaction into Eq. (2.2) at the same time as the Coulomb interaction gives an approximation to the relativistic two-particle Dirac equation that is correct up to terms of order $(v/c)^2$, known as the time-dependent Breit equation,

$$\begin{aligned} i\hbar\frac{\partial\psi}{\partial t} = \sum_{j=1}^{2}\left\{\beta_j mc^2 + c\boldsymbol{\alpha}_j \cdot \left[\boldsymbol{p}_j + \frac{e}{c}\boldsymbol{A}(\boldsymbol{r}_j)\right] - eA_0(\boldsymbol{r}_j)\right\}\psi \\ + \frac{e^2}{r}\left\{1 - \frac{1}{2}\left[\boldsymbol{\alpha}_1 \cdot \boldsymbol{\alpha}_2 + \frac{(\boldsymbol{\alpha}_1 \cdot \boldsymbol{r})(\boldsymbol{\alpha}_2 \cdot \boldsymbol{r})}{r^2}\right]\right\}\psi. \end{aligned} \tag{2.10}$$

The Breit interaction can be derived in a number of ways. In his original paper [26], Breit derived it from the classical Lagrangian for a system of interacting charged particles up to order $(v/c)^2$, known as the Darwin Lagrangian [32]. The interaction Lagrangian for a relativistic charged particle in an external electromagnetic field is [24, 25],

$$L_{\mathrm{int}} = -eA_0 + \frac{e}{c}\boldsymbol{v} \cdot \boldsymbol{A}. \tag{2.11}$$

In the rest frame of the first particle in the Coulomb gauge, $A_0 = e^2/r$ is simply the instantaneous Coulomb interaction to all orders in v/c, while the vector potential, to second order, is

$$\boldsymbol{A}(\boldsymbol{r}_1) = \frac{1}{c}\int \frac{\boldsymbol{J}_t(\boldsymbol{r}')}{|\boldsymbol{r}_1 - \boldsymbol{r}'|}\, d^3r', \tag{2.12}$$

where $\boldsymbol{J}_t$ is the transverse part of the current density generated by the second electron, satisfying $\nabla \cdot \boldsymbol{J}_t = 0$. The second electron generates a current $\boldsymbol{J} = e\boldsymbol{v}_2\delta^3(\boldsymbol{r} - \boldsymbol{r}_2)$ relative to the first, from which we can calculate $\boldsymbol{A}(\boldsymbol{r}_1)$. Eq. (2.11) then evaluates to [24, 32]

$$L_{\mathrm{int}} = -\frac{e^2}{r}\left\{1 - \frac{1}{2c^2}\left[\boldsymbol{v}_1 \cdot \boldsymbol{v}_2 + \frac{(\boldsymbol{v}_1 \cdot \boldsymbol{r})(\boldsymbol{v}_2 \cdot \boldsymbol{r})}{r^2}\right]\right\}. \tag{2.13}$$

FIGURE 2.1: Feynman diagrams contributing to $e^-e^- \to e^-e^-$ scattering at second order in quantum electrodynamics. Time runs from left to right, straight directed lines represent electrons, and wavy lines represent photons.

Breit derived the corresponding quantum mechanical interaction by making the replacements $\boldsymbol{v}_i \to -c\,\boldsymbol{\alpha}_i$, by generalising the result for a single particle, Eq. (2.4), yielding the Breit interaction. In the same paper Breit also derived this expression using an early version of quantum electrodynamics (QED) known as the Heisenberg-Pauli quantum theory of wave-fields [26, 33], but he later gave a more rigorous treatment using a more modern form of QED [34, 35]. In his paper, Breit demonstrates that his interaction appears due to the interaction of two electrons with a transverse photon [16, 23, 30, 36].

In order to see the origin of the Breit interaction, I will now present the outline of the derivation of the Breit interaction from a QED calculation in the Feynman gauge, as this gauge makes the origin of the retardation term explicit. In Section 7.1 I will present an alternative derivation in the *Coulomb* gauge, where the connection with transverse photons will be explicit. We consider the quantum-electrodynamical process of two electrons scattering via the exchange of a single photon, corresponding to the Feynman diagram on the left in Figure 2.1. The full amplitude for this process will involve a summation of higher order Feynman diagrams with more than one photon exchange, but those diagrams will contribute at higher orders than $(v/c)^2$, which is the order to which we are interested. We also will not need to calculate the contribution that comes from the second diagram shown in Figure 2.1, in which the two final electrons are swapped (describing the so-called exchange diagram), since from the first diagram we will derive the interaction operator that gives rise to this scattering process in the limit of a Schrödinger-type equation, and in this limit the exchange interaction can be included by appropriately anti-symmetrising the two-body wave function, i.e. by constructing it as a Slater determinant [37]. Using the Feynman rules for QED [38], the scattering matrix amplitude corresponding to this diagram is

$$S_{fi} = -ie^2 \int d^4x \int d^4y\, \bar{\psi}_f^{(1)}(x)\gamma_\mu \psi_i^{(1)}(x) D^F_{\mu\nu}(x-y) \bar{\psi}_f^{(2)}(y)\gamma_\nu \psi_i^{(2)}(y), \tag{2.14}$$

where $\bar{\psi} = \psi^\dagger \gamma^0$ is the Dirac adjoint of ψ, $\psi_i^{(k)}$ and $\psi_f^{(k)}$ are stationary eigenspinors,

$$H^{(k)}\psi_i^{(k)} = E_i^{(k)}\psi_i^{(k)} \quad \text{and} \quad H^{(k)}\psi_f^{(k)} = E_f^{(k)}\psi_f^{(k)}, \tag{2.15}$$

of a non-interacting, single-particle Dirac Hamiltonian with some stationary external potential,

$$H^{(k)} = -i\hbar c\,\boldsymbol{\alpha}_k \cdot \nabla_k + \beta_k mc^2 + V_{\text{ext}}^{(k)}, \tag{2.16}$$

and

$$D^F_{\mu\nu}(x-y) = -4\pi \int \frac{d^4k}{(2\pi)^4} \frac{e^{-ik\cdot(x-y)} g_{\mu\nu}}{k^2 + i\varepsilon} \tag{2.17}$$

is the photon propagator in the Feynman gauge. Separating out the time-dependence in the electron wave functions,

$$\bar{\psi}^{(k)}_f(x) = e^{iE^{(k)}_f t} \bar{\psi}^{(k)}_f(\boldsymbol{x}) \quad \text{and} \quad \psi^{(k)}_i(x) = e^{-iE^{(k)}_i t} \psi^{(k)}_i(\boldsymbol{x}), \tag{2.18}$$

allows us to define the transition currents,

$$j^{(k)\mu}_{fi}(x) = e\bar{\psi}^{(k)}_f(x)\gamma^\mu \psi^{(k)}_i(x) = e\bar{\psi}^{(k)}_f(\boldsymbol{x})\gamma^\mu \psi^{(k)}_i(\boldsymbol{x}) e^{i\left[E^{(k)}_f - E^{(k)}_i\right]t} = e^{i\omega^{(k)}_{fi} t} j^{(k)\mu}_{fi}(\boldsymbol{x}), \tag{2.19}$$

where $\omega^{(k)}_{fi} \equiv E^{(k)}_f - E^{(k)}_i$. If we consider a process where the energy of particle 1 is fully transferred to particle 2, $\omega^{(1)}_{fi} = -\omega^{(2)}_{fi}$ then the scattering amplitude can be written in the form [38]

$$S_{fi} = -i \int d^4x \, j^{(2)}_{fi}(x) \cdot A^{(1)}_{fi}(x), \tag{2.20}$$

where inside the integral we are taking a Minkowski scalar product, and

$$A^{(1)}_{fi}(x) = \int d^3y \, j^{(1)}_{fi}(\boldsymbol{y}) \frac{\exp\left[i\omega^{(1)}_{fi}(t - |\boldsymbol{y}-\boldsymbol{x}|/c)\right]}{|\boldsymbol{y}-\boldsymbol{x}|/c} \equiv \int d^3y \, \frac{j^{(1)}_{fi}(\boldsymbol{y}, t - |\boldsymbol{y}-\boldsymbol{x}|/c)}{|\boldsymbol{y}-\boldsymbol{x}|/c}. \tag{2.21}$$

Eqs. (2.20) and (2.21) therefore imply that the transition current of particle 2, $j^{(1)}_{fi}(\boldsymbol{x})$, interacts with the transition current of particle 1, $j^{(1)}_{fi}(\boldsymbol{y})$, not at the current time t but at an earlier time $t - |\boldsymbol{y}-\boldsymbol{x}|/c$, delayed exactly by how long light takes to travel from particle 1 to particle 2. Therefore, Eq. (2.21) is the *retarded potential* generated by the first particle relative to the second. The scattering amplitude can now be made to resemble a two-particle matrix element by integrating over the remaining time coordinate,

$$S_{fi} = -2\pi i\delta\left[\omega^{(1)}_{fi} + \omega^{(2)}_{fi}\right] e^2 \int d^3x \int d^3y \, \bar{\psi}^{(2)}_f(\boldsymbol{y})\gamma^\mu \psi^{(2)}_i(\boldsymbol{y}) \frac{e^{i|\omega_{fi}||\boldsymbol{y}-\boldsymbol{x}|/c}}{|\boldsymbol{y}-\boldsymbol{x}|/c} \bar{\psi}^{(1)}_f(\boldsymbol{x})\gamma_\mu \psi^{(1)}_i(\boldsymbol{x}). \tag{2.22}$$

This now has the form of a non-relativistic scattering matrix element, where the retarded interaction potential is sandwiched between initial and final states. For small particle velocities, we can Taylor expand the interaction term up to order $1/c^2$, leading to the amplitude (omitting the energy-conserving delta function)

$$\mathcal{A}_{fi} = e^2 \int d^3x \int d^3y \, \psi^{(2)\dagger}_f(\boldsymbol{y}) \psi^{(1)\dagger}_f(\boldsymbol{x}) \left[\frac{1}{r} - \frac{\boldsymbol{\alpha}_1 \cdot \boldsymbol{\alpha}_2}{2r} - \frac{(\boldsymbol{\alpha}_1 \cdot \boldsymbol{r})(\boldsymbol{\alpha}_2 \cdot \boldsymbol{r})}{2r^3}\right] \psi^{(2)}_i(\boldsymbol{y}) \psi^{(1)}_i(\boldsymbol{x}), \tag{2.23}$$

with $r = |\boldsymbol{x} - \boldsymbol{y}|$ and where we have used $\boldsymbol{\alpha} = \gamma^0\boldsymbol{\gamma}$. Up to this order, then, the effective interaction between the electrons is

$$U(\boldsymbol{x}-\boldsymbol{y}) = \frac{e^2}{r}\left\{1 - \frac{1}{2}\left[\boldsymbol{\alpha}_1\cdot\boldsymbol{\alpha}_2 + \frac{(\boldsymbol{\alpha}_1\cdot\boldsymbol{r})(\boldsymbol{\alpha}_2\cdot\boldsymbol{r})}{r^2}\right]\right\}, \tag{2.24}$$

which is just a sum of the Coulomb and Breit interactions [38]. Therefore, the Coulomb + Breit interaction is an approximation, correct up to order $1/c^2$, of the retarded magnetic interaction between two electrons due to the exchange of a single photon. Note also that because the first diagram in Figure 2.1 is the only Feynman diagram contributing to an $e^-e^- \to e^-e^-$ scattering process at second-order in QED (apart from the exchange diagram), if we had retained the full interaction potential, instead of Taylor-expanding it to terms of order $(v/c)^2$, then we would have derived the lowest-order correction to the Coulomb interaction in powers of the *coupling constant* e^2 that also captures retardation effects to all orders in v/c. In Chapter 7, we will see that in the Coulomb gauge this leads to a generalisation of the Breit interaction that depends on the energies of the interacting electrons known as the frequency-dependent Breit interaction.

What is important to note is that the Breit interaction arises from first-order perturbation theory in quantum electrodynamics. Because of this, it was originally believed that it should only be used to calculate the first-order energy shift from Coulomb wave functions satisfying Eq. (2.2), i.e.,

$$\Delta E = \langle\psi_1\psi_2|H_{\mathrm{Br}}|\psi_1\psi_2\rangle, \tag{2.25}$$

and that solving the Breit equation [Eq. (2.10)] exactly, using the Breit interaction in higher orders of perturbation theory, or using it to determine the self-consistent field in a procedure such as the Hartree-Fock method (see Section 2.2) is not physically meaningful [22, 23, 30, 39–41]. If we consider an interaction between an electron of positive energy and one of negative energy, then the frequency of the exchanged photon is of order $|\omega_{fi}| \sim 2mc^2$, and in that case we are not justified in Taylor expanding the retarded potential in Eq. (2.22) [22, 23, 39]. At second order in perturbation theory, where the energy shift for a given state would require a summation over intermediate negative energy states, the Breit interaction would therefore seem to give nonphysically large results [22, 23]. Despite this seemingly fundamental objection against including the Breit interaction as an additional term in the many-body Hamiltonian, this is now believed to be wrong and its inclusion generally improves the accuracy of calculations in comparison with experiment, and treating it on an equal footing with the Coulomb interaction greatly simplifies its inclusion into atomic structure calculations [16, 21, 42–47].

To gain some more physical insight into what the Breit interaction represents, one can take a non-relativistic limit known as the Pauli approximation. In this limit, the Breit interaction can be decomposed into a number of terms, representing spin-spin, spin(-other)-orbit, and velocity-velocity interactions between the two electrons, thereby capturing the magnetic interactions and retardation effects to second order in v/c [21, 23, 30, 37]. In this way,

including the Breit interaction into the many-body Dirac Hamiltonian means that the spin-own-orbit interaction of each electron is treated to all orders, while the spin-other-orbit and magnetic interactions between each pair of electrons are treated to only second order.

While the Breit equation takes into account magnetic effects to second order, it is not Lorentz invariant and does not include the effects of radiation emitted by the electrons (and hence, their self-energy), as radiation appears only at order $1/c^3$, and it is also not gauge-invariant [25, 34, 37, 48]. There are several other methods that permit us to go beyond second order in v/c. Some of these include the Tamm-Dancoff method [49, 50], a similar set of equations developed by Brown and Ravenhall [39], and the new Tamm-Dancoff method [51, 52], which each can be used to generate an infinite series of terms in powers of v/c [23]. Although the individual terms in these series are not Lorentz invariant, their complete sum is. Other perturbative expansion methods have been formulated in which each term in the perturbation series is individually Lorentz invariant. Schwinger [53, 54] formulated a method using Green's functions and Gell-Mann and Low [55] used a two-body Feynman kernel. In addition to these two examples, the most well-known method for covariantly treating the interaction between two charged particles is the Bethe-Salpeter equation [56], which involves an interaction operator $\bar{G}$ consisting of an infinite series of Lorentz invariant terms in powers of $e^2/\hbar c$ [57]. Although this equation is difficult to apply to highly relativistic systems, for non-relativistic systems $\bar{G}$ can be reduced to the instantaneous Coulomb operator plus small correction terms, which can be treated numerically [23]. This was first applied to the study of helium by Sucher [58] and then by Douglas and Kroll [59, 60]. Furthermore, one can show that in the limit where retardation effects are small, the Bethe-Salpeter equation reduces to the Breit equation [38].

2.2 The Hartree-Fock approximation

In order to understand how the Breit interaction is applied in understanding atomic structure, I will now briefly outline the starting point for many atomic theory calculations - the Hartree-Fock approximation. The non-relativistic limit of the many-body Dirac Hamiltonian for N electrons is [19, 21]

$$H(\boldsymbol{r}_1, \boldsymbol{r}_2, \ldots, \boldsymbol{r}_N) = \sum_{i=1}^{N} h_0(\boldsymbol{r}_i) + \sum_{i<j} \frac{1}{|\boldsymbol{r}_i - \boldsymbol{r}_j|} \tag{2.26}$$

with $h_0(\boldsymbol{r})$ the single-particle Dirac Hamiltonian in the presence of the nuclear potential

$$h_0(\boldsymbol{r}) = c\,\boldsymbol{\alpha} \cdot \boldsymbol{p} + \beta mc^2 - \frac{Z}{r}. \tag{2.27}$$

Trying to analytically, or even numerically, solve for the eigenstates of this equation is difficult. We can instead try to minimise the electron-electron interactions by rewriting the Hamiltonian as

$$H = \sum_{i=1}^{N} [h_0(\boldsymbol{r}_i) + U(\boldsymbol{r}_i)] + \sum_{i<j} \frac{1}{|\boldsymbol{r}_i - \boldsymbol{r}_j|} - \sum_{i=1}^{N} U(\boldsymbol{r}_i), \tag{2.28}$$

where $U(\boldsymbol{r})$ is a single-particle operator. The motivation behind writing the Hamiltonian in this way is that if $U(\boldsymbol{r})$ is a good approximation for the Coulomb potential, then the final two terms in the Hamiltonian, called the residual Coulomb interaction, should be small and can therefore be treated perturbatively. Since we want $U(\boldsymbol{r})$ to be a good approximation to the electron-electron interactions, but it is only a single-particle operator, we call U the mean-field potential. We can solve for each individual electron orbital by finding the eigenfunctions of the non-perturbative, single-particle part of the Hamiltonian,

$$[h_0(\boldsymbol{r}) + U(\boldsymbol{r})]\phi_i(\boldsymbol{r}) = \varepsilon_i \phi_i(\boldsymbol{r}), \tag{2.29}$$

and then the many-body wave function, in this mean field approximation, can be constructed as a Slater determinant of the single-particle solutions to Eq. (2.29), which ensures fermion anti-symmetry,

$$\Phi_{ab\ldots n}(\boldsymbol{r}_1, \boldsymbol{r}_2, \ldots, \boldsymbol{r}_N) = \frac{1}{\sqrt{N!}} \begin{vmatrix} \phi_a(\boldsymbol{r}_1) & \phi_b(\boldsymbol{r}_1) & \cdots & \phi_n(\boldsymbol{r}_1) \\ \phi_a(\boldsymbol{r}_2) & \phi_b(\boldsymbol{r}_2) & \cdots & \phi_n(\boldsymbol{r}_2) \\ \vdots & \vdots & \ddots & \vdots \\ \phi_a(\boldsymbol{r}_N) & \phi_b(\boldsymbol{r}_N) & \cdots & \phi_n(\boldsymbol{r}_N) \end{vmatrix}, \tag{2.30}$$

and which, it can be easily verified, is an eigenfunction of the single-particle Hamiltonian,

$$H_0 = \sum_{i=1}^{N} \left[h_0(\boldsymbol{r}_i) + U(\boldsymbol{r}_i) \right], \tag{2.31}$$

satisfying the eigenvalue equation [19]

$$H_0 \Phi_{ab\ldots n}(\boldsymbol{r}_1, \boldsymbol{r}_2, \ldots, \boldsymbol{r}_N) = (\varepsilon_a + \varepsilon_b + \cdots + \varepsilon_n)\Phi_{ab\ldots n}(\boldsymbol{r}_1, \boldsymbol{r}_2, \ldots, \boldsymbol{r}_N). \tag{2.32}$$

There are many choices for the mean field but a common choice in the literature is the so-called Hartree-Fock (HF) [or Coulomb-Hartree-Fock (CHF)] potential, which can be derived, for example, by minimising the expectation value of the full many-body Hamiltonian assuming a Slater determinant wave function [21]. For systems with only a single valence electron, it is typical to work in the V^{N-1} approximation, where each electron moves in the mean potential generated by only the $N-1$ core electrons. The action of the HF potential in this approximation on a single-particle orbital is given by

$$U^{\mathrm{CHF}}\phi_a(\boldsymbol{r}) \equiv \sum_{i \neq a}^{N_c} \left[\int \frac{\phi_i^\dagger(\boldsymbol{r'})\phi_i(\boldsymbol{r'})}{|\boldsymbol{r} - \boldsymbol{r'}|}\, d^3\boldsymbol{r'}\, \phi_a(\boldsymbol{r}) - \int \frac{\phi_i^\dagger(\boldsymbol{r'})\phi_a(\boldsymbol{r'})}{|\boldsymbol{r} - \boldsymbol{r'}|}\, d^3\boldsymbol{r'}\, \phi_i(\boldsymbol{r}) \right]. \tag{2.33}$$

The sum here extends over the quantum numbers of all electrons in the core of the atom, i.e. the electrons in the filled shells. The first term is called the direct, or Hartree potential, while the second, non-local term is called the exchange potential, and appears due to fermionic anti-symmetry under exchange of quantum numbers [19, 21, 61]. If this is used as the mean field when solving for the single-particle wave functions, this leads to the Hartree-Fock (or Dirac-Fock) equation,

$$\left(h_0 + U^{\mathrm{CHF}}\right) \phi_a(\boldsymbol{r}) = \varepsilon_a \phi_a(\boldsymbol{r}). \tag{2.34}$$

A further convenient property of using the HF potential as the mean field is that first-order corrections in the residual Coulomb interaction exactly vanish [19]. Furthermore, Koopman's theorem tells us that the Hartree-Fock energy eigenvalue ε_a is equal to the negative of the work required to remove the electron from the system, which is equivalent to the negative of the binding energy [21, 62].

Note that solving the HF equation for the core orbitals requires constructing the HF potential, which depends on the core orbitals themselves, so the state of each electron in the core must be constructed self-consistently: we start with an initial guess for the potential, which gives us an approximate set of core wave functions, which can then be used to generate a more accurate potential, which can then be used to generate more accurate wave functions, and so on, until the desired level of convergence is reached [19].

2.3 Correlation corrections

The HF potential is exact to first order in the residual Coulomb interaction, but higher order corrections become important for high-accuracy calculations. Corrections beyond the single-particle picture can be calculated using many-body perturbation theory and the corresponding corrections are known as correlation corrections. These correspond physically to the interaction of the valence electrons with the core. For a single-valence system, the second-order correlation correction to the energy of a valence state is given by [19, 21],

$$\delta^{(2)}\varepsilon_v = \sum_{amn} \frac{g_{vamn}(g_{nmav} - g_{nmva})}{\varepsilon_v + \varepsilon_a - \varepsilon_m - \varepsilon_n} + \sum_{abn} \frac{g_{vnab}(g_{banv} - g_{bavn})}{\varepsilon_v + \varepsilon_n - \varepsilon_a - \varepsilon_b}, \tag{2.35}$$

where the sums over a and b run over all states in the core, and the sums over m and n run over all virtual states (states not in the core). For a given valence state, we can calculate this directly using a complete set of states, but it is instead more useful to define a non-local (energy-dependent) operator $\hat{\Sigma}^{(2)}(\varepsilon)$, whose diagonal matrix elements correspond to the second-order correlation correction,

$$\Sigma^{(2)}_{ij}(\varepsilon) = \sum_{amn} \frac{g_{iamn}(g_{nmaj} - g_{nmja})}{\varepsilon + \varepsilon_a - \varepsilon_m - \varepsilon_n} + \sum_{abn} \frac{g_{inab}(g_{banj} - g_{bajn})}{\varepsilon + \varepsilon_n - \varepsilon_a - \varepsilon_b}. \tag{2.36}$$

It is easy to see that $\Sigma^{(2)}_{vv}(\varepsilon_v)$ returns Eq. (2.35). The operator $\hat{\Sigma}(\varepsilon)$ is referred to as the correlation potential, or the self-energy operator, and $\hat{\Sigma}^{(2)}(\varepsilon)$ is its second-order approximation [63]. Therefore, instead of calculating energy corrections using Eq. (2.35), we can instead directly solve for the single-particle wave functions in the presence of the non-local correlation potential,

$$\left[h_0 + U^{\mathrm{HF}} + \Sigma^{(2)}\right] \phi_i^{\mathrm{BO}}(\boldsymbol{r}) = \varepsilon_i^{\mathrm{BO}} \phi_i^{\mathrm{BO}}(\boldsymbol{r}). \tag{2.37}$$

This is known as the correlation potential method [64] and its solutions are known as Brueckner orbitals. Such orbitals include second-order correlation effects, and can therefore be used to calculate matrix elements with correlation effects included.

2.4 Second quantisation

Another way of understanding the origin of the Hartree-Fock potential is by writing the Hamiltonian in Eq. (2.28) in second-quantised form in the CHF basis,

$$H = \sum_i \varepsilon_i \, a_i^\dagger a_i + \sum_{i,j} (-U)_{ij} \, a_i^\dagger a_j + \frac{1}{2} \sum_{ijkl} g_{ijkl} \, a_i^\dagger a_j^\dagger a_l a_k, \tag{2.38}$$

where the summations are over all orbitals, and where the creation (annihilation) operator, $a_i^\dagger$ (a_i) creates (removes) an orbital described by the set of quantum numbers $i = \{n_i, j_i, l_i, m_i\}$ from the Slater determinant wave function. For example, $a_a^\dagger |0\rangle$ corresponds to $|\phi_a\rangle$ while

$$a_a^\dagger a_b^\dagger |0\rangle = -a_b^\dagger a_a^\dagger |0\rangle \quad \longleftrightarrow \quad \frac{1}{\sqrt{2}} \left[\phi_a(\boldsymbol{r}_1)\phi_b(\boldsymbol{r}_2) - \phi_b(\boldsymbol{r}_1)\phi_a(\boldsymbol{r}_2)\right] \tag{2.39}$$

which is ensured through the anti-commutation relations [21]

$$\{a_i, a_j\} = \{a_i^\dagger, a_j^\dagger\} = 0 \quad \text{and} \quad \{a_i, a_j^\dagger\} = \delta_{ij}. \tag{2.40}$$

In atomic physics, we often work in the frozen HF core approximation, in which the core orbitals are solved self-consistently using the HF procedure, and then valence orbitals are treated in perturbation theory [16, 19, 21]. In this way, the HF core is denoted as

$$|0_c\rangle = \prod_a^{\text{core}} a_a^\dagger |0\rangle, \tag{2.41}$$

which is then killed by any application of $a_{\text{core}}^\dagger$ or a_{virtual} (a virtual orbital being one that is unoccupied) due to the Pauli exclusion principle. It is therefore advantageous to normally order the Hamiltonian relative to the core by moving $a_{\text{core}}^\dagger$ and a_{virt} to the right of a_{core} and $a_{\text{virt}}^\dagger$ [21]. This yields a normal-ordered Hamiltonian

$$H_C = \sum_i \varepsilon_i \, :a_i^\dagger a_i: + \sum_{ij} (g_{ij} - U_{ij}) \, :a_i^\dagger a_j: + \frac{1}{2} \sum_{ijkl} g_{ijkl} \, :a_i^\dagger a_j^\dagger a_l a_k:, \tag{2.42}$$

where

$$g_{ijkl} \equiv \langle ij|\frac{1}{r}|kl\rangle = \int \frac{\phi_i^\dagger(\boldsymbol{r})\phi_j^\dagger(\boldsymbol{r}')\phi_k(\boldsymbol{r})\phi_l(\boldsymbol{r}')}{|\boldsymbol{r} - \boldsymbol{r}'|} \, d^3\boldsymbol{r} \, d^3\boldsymbol{r}', \tag{2.43}$$

and

$$g_{ij} = \sum_{a=1}^{N_c} \left(g_{iaja} - g_{iaaj}\right). \tag{2.44}$$

Note that the effective one-body matrix elements g_{ij} are exactly the matrix elements of the (Coulomb-)Hartree-Fock potential [cf. Eq. (2.33)]. Therefore, by normally ordering the Hamiltonian, it is clear that choosing the mean potential matrix elements to be those of the

CHF potential, $U_{ij} = g_{ij} \equiv U_{ij}^{\mathrm{CHF}}$, the second term in the Hamiltonian vanishes, so the CHF potential is exact to first order in many-body perturbation theory [16, 19, 21].

In the above equations, the Coulomb operator could be deconstructed into a sum of effective zero-, one-, and two-body contributions (with respect to a particular basis), respectively [16, 21],

$$g^{(0)} = \frac{1}{2}\sum_a g_{aa},\ g^{(1)} = \sum_{ij} g_{ij}\, :a_i^\dagger a_j:, \quad \text{and} \quad g^{(2)} = \frac{1}{2}\sum_{ijkl} g_{ijkl}\, :a_i^\dagger a_j^\dagger a_l a_k:. \tag{2.45}$$

In general, any two-particle operator, such as the Breit interaction, can be written in an analogous form.

2.5 Inclusion of the Breit interaction into the Hartree-Fock method

In the literature, the Breit interaction is included into atomic physics calculations typically in one of two ways. The first way is by using only the Coulomb interaction to generate the Hartree-Fock potential, forming the CHF potential, and treating the Breit interaction as a perturbative correction to the Hamiltonian. This is what was considered correct in the literature [23, 30] when it was believed that the Breit interaction should be used only to calculate the first-order energy shift via $\delta\varepsilon_v = b_{vv}$, where b_{ij} is the one-body part of the Breit interaction [cf. Eq. (2.44)]. In this same formalism, although it was believed to be incorrect to do so, any higher order term in the pertubation expansion could be calculated if desired [16, 23, 30]. Mathematically, the Hamiltonian in this first formalism is the sum of the conventional Coulomb Hamiltonian and the Breit interaction

$$H' = H_C + H_{\mathrm{Br}} = \sum_i \varepsilon_i\, :a_i^\dagger a_i: + \frac{1}{2}\sum_{ijkl} g_{ijkl}\, :a_i^\dagger a_j^\dagger a_l a_k: + \sum_{ij} b_{ij}\, :a_i^\dagger a_j^\dagger: + \frac{1}{2}\sum_{ijkl} b_{ijkl}\, :a_i^\dagger a_j^\dagger a_l a_k:, \tag{2.46}$$

which is not exact to first order in the Breit + Coulomb residual interaction, with corrections due to the Breit interaction being nonzero at this order. The second way is to treat the Coulomb and Breit interactions on an equal footing in the Hamiltonian and solving for the electron orbitals self-consistently in the Breit + Coulomb-HF (BCHF) potential,

$$\left(h_0 + U^{\mathrm{BCHF}}\right)\bar{\phi}_i(\boldsymbol{r}) = \bar{\varepsilon}_i\bar{\phi}_i(\boldsymbol{r}), \tag{2.47}$$

where $(U^{\mathrm{BCHF}})_{ij} = \bar{g}_{ij} + \bar{b}_{ij}$. Here, we adopt the convention of [16] in which overbarred quantities refer to those calculated in the BCHF potential, e.g. $\bar{g}_{ijkl} = \langle\bar{\phi}_i\bar{\phi}_j|\frac{1}{r}|\bar{\phi}_k\bar{\phi}_l\rangle$. This second method has the advantage that the Coulomb and Breit interactions are treated to the same order in the HF potential, and therefore the normal-ordered Hamiltonian takes on the much simpler form,

$$H = \sum_i \bar{\varepsilon}_i\, :\bar{a}_i^\dagger \bar{a}_i: + \frac{1}{2}\sum_{ijkl}(\bar{g}_{ijkl} + \bar{b}_{ijkl})\, :\bar{a}_i^\dagger \bar{a}_j^\dagger \bar{a}_l \bar{a}_k:, \tag{2.48}$$

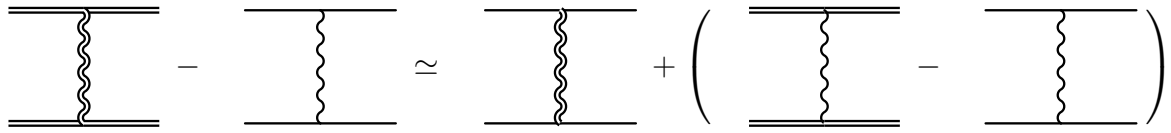

FIGURE 2.2: Diagrammatical representation of a generic contribution to a physical quantity from the inclusion of the Breit interaction. The left-hand side represents the full Breit correction, with single and double horizontal lines representing CHF and BCHF basis states, respectively, and single and double wiggly lines representing the Coulomb and the Breit + Coulomb two-body interactions, respectively. The first term on the right-hand side is the contribution from including Breit into the electron-electron interaction term in the full many-body Hamiltonian but not including it into the HF potential, while the term in parentheses is the correction that arises purely from the CHF to BCHF basis shift. Figure adapted from [16].

so in this formalism the one-body part of the Breit operator is absorbed into the BCHF orbitals, and the BCHF potential is therefore exact to first order in the residual Breit + Coulomb interaction.

These formalisms can help us classify the two types of contributions due to the inclusion of the Breit interaction. Shifts in energy eigenvalues, perturbative energy corrections, matrix elements, etc. that arise from using BCHF orbitals rather than CHF orbitals are called one-body Breit corrections, since the one-body part of the Breit operator modifies the HF potential used to generate the individual orbitals. On the other hand, contributions due to including the two-body part of the Breit interaction in the Hamiltonian are known as two-body contributions. This is because including the two-body part of the Breit interaction is equivalent to changing the two-body interaction from just the Coulomb interaction to the Coulomb + Breit interaction. We can separate the full Breit correction to a physical quantity into a one-body part – due to an orbital basis shift – and a two-body part – from including Breit into the two-particle electron-electron interaction [16, 44]. This is represented diagrammatically in Figure 2.2.

2.6 Numerical studies of the Breit interaction

2.6.1 Scaling behaviour

Because the Breit interaction is a first-order relativistic correction to the electron-electron interaction, it might be expected that the Breit interaction would be most significant in heavy atoms, where the electrons are more tightly bound to the atomic core. Indeed, while the Breit interaction is a relatively small perturbation for light atoms and ions, it becomes the dominant contribution to the ground state energy correction for closed-shell (He-like) atoms with high Z, where Z is the atomic charge of the nucleus [19]. Furthermore, in the case of lithium-like ions, one can show that the Breit interaction is expected to scale as Z^3 [23] and a numerical study of the Breit interaction by Johnson, Blundell and Sapirstein [40] for ions along the lithium isoelectronic sequence, from $Z = 3$ to $Z = 92$, found that, while the first-order Breit correction to the energy of the valence orbitals does not scale exactly as Z^3,

it does increase with Z, and approaches the expected cubic scaling for $Z \gtrsim 50$. Furthermore, in a study performed by Ishikawa and Koc [44], similar results were found for the noble gases up to radon, the group-IIB ions, and the ions of the neon isoelectronic sequence. In the neon isoelectronic sequence the difference in the second order energy correction with Breit included in the HF potential as well as in the residual electron-electron interactions, compared to the second order correction without Breit, increased greatly with increasing Z [65], whereas for the noble gases the difference remained relatively constant. This indicates that for heavy ions, the inclusion of the Breit interaction results in a significant modification of many-body effects at the second order of perturbation theory [44, 66–68]. A similar result was found for ions along the lithium isoelectronic sequence [40], as well as for ions along the beryllium isoelectronic sequence [69]. In particular, it was found that the contribution of the Breit interaction on the energy eigenvalues was enhanced for states closer to the nucleus, where the electrons are more tightly bound to the atom and therefore moving faster.

2.6.2 Gaunt and retardation contributions

Another important note is that, while the full Breit interaction is the complete first order correction to the Coulomb interaction, for heavy atoms the Gaunt interaction is seen to dominate compared to the retardation interaction, Eq. (2.9) [30, 31, 70]. This means that the Breit interaction can, to a good approximation, be approximated by only the Gaunt term if numerical simplicity is desired, especially since the retardation term is much harder to calculate than the Gaunt term [71]. For example, in Gaunt's original paper, he was successfully able to describe the fine structure of helium using only his interaction in place of the full Breit operator. This is because a decomposition of the Gaunt interaction in the non-relativistic Pauli approximation gives the same spin interaction terms as the full Breit interaction, but different velocity-velocity and Darwin terms [30], where the Darwin term accounts for the fact that, relativistically, particles cannot be localised to any accuracy greater than their Compton wavelength $\hbar/mc$, and so the potential that each electron sees is effectively smeared [72]. Therefore, for a light atom such as helium, a very accurate description of the fine structure can be made without the retardation interaction. Of course, because the matrix elements of the retardation term are generally nonzero, for high accuracy calculations both both the Gaunt and retardation terms should be used [16]. In more relativistic atoms, the retardation contribution becomes more important, although is generally an order of magnitude smaller than the Gaunt term [45]. Lastly, it is important to note that the Gaunt and retardation terms typically result in corrections that are opposite in sign to each other [30].

2.6.3 One- and two-body Breit contributions

It is also useful to examine separately the contribution that the one- and two-body parts of the Breit interaction make to energies, matrix elements etc. in atomic systems. The most prominent studies to do this were performed by Derevianko [16] and Kozlov et al. [31] (although they only used the Gaunt interaction in place of the full Breit operator) on the atomic properties of caesium. In these papers, the authors calculate the separate

contributions from the effective one- and two-body parts of the Breit interaction to energy levels up to second order in MBPT and to matrix elements at second order. Derevianko found that the contribution from the one-body part of the Breit interaction to the second-order energy correction of valence states was equally important as the correction at the level of the zeroth order, HF approximation, $\delta_{\mathrm{HF}}\varepsilon_v = \bar{\varepsilon}_v - \varepsilon_v$. Furthermore, for the s and p angular momentum orbitals this correction was opposite in sign to the HF level correction, and for the $7s_{1/2}$ state was exactly equal but opposite in sign. This means that at second order in perturbation theory, the one-body Breit correction is equally significant as at the Hartree-Fock level. In the cases where this cancellation occurs, the much less significant two-body Breit correction becomes important. In general, however, the two-body contribution is suppressed and can be neglected to a good approximation [31]. A similar trend was found in the Breit contribution to hyperfine structure constants, where the Breit contribution at second and third order was seen to be equally important as the contribution at the zeroth order, and in the case of the $6s$ and $7s$ states, the contributions at second and third order were two orders of magnitude larger than the respective contributions at the HF level. This systematic inclusion of the Breit interaction is in contrast to many prior calculations, e.g. [73], in which the Breit interaction was included into second order perturbative corrections, but not into the mean HF potential, thereby leading to large differences between the Breit corrections to hyperfine constants between the two studies.

2.6.4 Hyperfine structure and parity-nonconservation in caesium

One particular case where the Breit interaction has been shown to play an important role in reducing the deviation from experiment is in the calculation of hyperfine structure constants in caesium. Upon including the Breit interaction into atomic structure calculations the relative disagreement with experiment was decreased from -0.3% to -0.1% for the $6s_{1/2}$ and $7s_{1/2}$ orbitals; from 0.7% to 0.5% for the $6p_{1/2}$ orbital; and from 0.3% to 0.1% for the $7p_{1/2}$ orbital. These Breit corrections were added to calculations that only included Breit perturbatively [74], and which therefore missed out on comparably large corrections that come from including the Breit interaction into the HF procedure. It is therefore clear that the Breit interaction plays an important role in many-body corrections to hyperfine constants, and valence energy levels, often times being as significant as the lowest order corrections at the HF level. Since hyperfine structure constants sample the atomic wave functions close to the nucleus, this indicates that the Breit interaction is important in high-accuracy calculations of the properties of electrons close to the nucleus. For example, a 0.1% accuracy is required for testing parity non-conservation in atoms, a concept which has important implications for tests of the standard model of particle physics [1, 8, 16, 75–78].

In particular, the Breit interaction played a large role in the resolution of a large disagreement between the parity nonconservation (PNC) amplitude in caesium as predicted by the Standard Model, and the one measured experimentally. If the electrons in an atom interacted purely through the parity-conserving gravitational and electromagnetic forces, then the transition between the $6s$ and $7s$ states in caesium would be forbidden, due to being states of opposite parity. However, because electrons interact with the nucleus through the

parity-*violating* weak interaction, electrons in the $6s$ state can acquire an admixture of opposite parity states, and similarly for the $7s$ state [79]. Such an admixture causes the $6s$-$7s$ transition to become possible, with a small but experimentally measurable amplitude known as the PNC amplitude. The experimental amplitude can be related to a quantity known as the nuclear weak charge Q_W, which characterises the strength of the weak interactions between the nucleus and the atomic electrons, and whose value can be predicted purely theoretically using the Standard Model of Particle Physics [8, 63]. The experimentally measured amplitude can be used to determine the nuclear weak charge through atomic structure calculations, in which Q_W is treated as a parameter, and so a comparison of the theoretical PNC amplitude predicted through these atomic calculations and the experimental value allows the experimental value of the nuclear weak charge to be deduced. This provides one of the most accurate low-energy tests of the electroweak sector of the Standard Model, and in the late 1990s, the value of the nuclear weak charge predicted by the Standard Model and as measured experimentally [4, 80], and subsequently interpreted using high-precision atomic structure calculations, differed from each other by 2.5 standard deviations [78, 81]. This result prompted several proposals that explained this deviation in terms of new physics beyond the Standard Model [82, 83]. However, Derevianko [7] and then others [84] showed that this tension could be resolved down to just 1.2σ by including the Breit interaction into the atomic structure calculations. A later study [2, 47] showed that, in addition to other many-body corrections, inclusion of these Breit corrections into updated atomic structure calculations allowed the authors to reach perfect agreement with the Standard Model prediction, and thereby place constraints on several new physics models, such as the existence of a new Z boson, that have been predicted beyond the standard model [85–89].

It is therefore clear, given the numerical studies that have been performed involving the Breit interaction, that it is important to include into the Hartree-Fock potential, and also that its inclusion in the second order of perturbation theory leads to substantial modifications of these many-body corrections. In some cases, the contribution at second order in perturbation theory is as large or even larger than the correction at the HF (zeroth order) level, and improves the agreement between high-accuracy theoretical calculations and experimental values. It is thus important that the Breit interaction be included into high-accuracy MBPT calculations but, as yet, no one has done so beyond second order due to the complexity of the expressions that arise at higher orders. It would therefore be valuable to try and determine higher order corrections due to the Breit interaction.

2.7 Nuclear clock project

In addition to all the properties of the Breit interaction described above, the Breit interaction is known to lead to a very large modification of perturbative corrections in ions in the francium isoelectronic sequence, such as francium, singly-ionised radium, doubly-ionised actinium, etc. In particular, the f states of these ions have been shown to undergo very large Breit corrections at the second-order correlations level, with these being an order of magnitude larger even than the correction at zeroth order in perturbation theory [90]. This result is unexpected since the f states should be concentrated further away from the nucleus,

where relativistic effects such as the Breit interaction should be negligible. What's more, there is a large discrepancy between experiment and the highest accuracy theory calculations for these, as well as the d states, even after including Breit corrections into calculations. This means there is a large gap in the theoretical understanding of these ions, especially since the f states are the ground state in some Fr-like ions, so having close agreement between theory and experiment for these states is crucial in understanding the atomic properties of the ion [91].

This is significant as there are plans to develop the first nuclear clock using Th^{3+} [12, 92], which is part of the francium isoelectronic sequence, and which therefore also exhibits this sensitivity towards the Breit interaction. Nuclear clocks are desirable since they offer the possibility of a highly sensitive probe to the effects of temporal variation in the fundamental constants, including the fine structure constant α, strong interaction, quark mass [2], as well as detecting violations of Einstein's principle of equivalence, with a potential accuracy 1-2 orders of magnitude more precise than the current most-precise optical *atomic* clocks [93]. Furthermore, because the nucleus is shielded by electrons, it is expected that a nuclear clock would be much more stable than an atomic clock, and the fact that nuclear resonances can be determined highly precisely in solids means that nuclear clocks could potentially be formed from a much larger number of nuclei, thereby generating a much stronger signal than atomic clocks [94]. Nuclear clocks maintain time through the excitation energy of the nucleus of an atom, and although there are heavier nuclei with relatively narrow nuclear excitation energies, and in which the effects of changes in the fundamental constants over time would be enhanced to a similar degree as in ^{229}Th, such as a 76 eV transition energy in ^{235}U, such an excitation energy cannot be easily reached with usual lasers. A thorium-229 nucleus, on the other hand, has an excitation energy of only a few electron-volts, which *can* be reached by conventional lasers [95]. Although the proposal to use thorium nuclei for a nuclear clock was first made in 2003 [12], there remained a gap of 17 orders of magnitude between the uncertainty in the nuclear transition frequency and the natural linewidth of the transition [94]. This limited its viability for this application until 2024, when three separate research groups [9–11] each independently excited a ^{229}Th nucleus to achieve a nuclear transition, thereby greatly narrowing the uncertainty in the precise frequency required to do so.

In order to further investigate the long-term viability of using Th^{3+} as the basis for a nuclear clock, a better understanding of its nuclear structure is required. This can be done in a nuclear-theory independent way through improved high-precision atomic structure calculations [96]. For example, the nuclear magnetic-dipole and electric-quadrupole moments of an atom can be determined by comparing theoretically-calculated and experimentally-measured hyperfine structure constants (see, for example, [97]). Furthermore, the structure of the $^{229}Th^{3+}$ is well-suited for studies beyond just the magnetic-dipole and electric-quadrupole moments, as the angular momentum of the $5f_{5/2}$ ground state is large enough to couple to the nuclear octupole magnetic moment. Therefore, given that the Breit interaction seems to play such a large role in highly relativistic systems, such as the ions along the francium-isoelectronic sequence, and particularly strongly for the f states, it is advantageous to try to include Breit into the highest accuracy calculations possible.

3 The Breit interaction in caesium

In this chapter I will use the existing AMPSCI program [15] to study the atomic properties of caesium, firstly as a test that each part of the code is working, and second to gain some familiarity using the program to perform calculations. Although many papers in the literature include the Breit interaction into atomic structure calculations, few provide a systematic study of how it modifies many-body effects. One such paper that does do this is by Derevianko [16]; in it he calculates the contribution that the Breit interaction has on valence energies and matrix elements at the level of the Hartree-Fock approximation, and then also at second order in perturbation theory. In this chapter I will perform atomic structure calculations with the Breit interaction to try and reproduce the results in this paper, as well as to investigate the interplay between the Breit interaction and certain approximations made in the calculations of atomic properties. This can help to make it clear how important the Breit interaction actually is at different orders of perturbation theory, and therefore whether including the Breit interaction into higher orders of perturbation theory will be significant.

3.1 Breit corrections to valence energies

Derevianko's paper calculates the corrections to the energies of valence states due of caesium due to the inclusion of the Breit interaction. The correction at the level of the Hartree-Fock potential is just given by the difference between the BCHF and CHF single-particle eigenvalues,

$$\delta_{\mathrm{HF}} E_v = \bar{\varepsilon}_v - \varepsilon_v. \tag{3.1}$$

The contribution to the second order energy correction due to the one-body part of the Breit interaction was taken to be the difference between the second order energy correction to the HF valence energies when evaluated with the BCHF basis states and the HF valence

energies when evaluated with the CHF basis states. In both cases the two-body part of the Breit interaction was not added to the two-body Coulomb operator in the Hamiltonian, less the Hartree-Fock level correction. Finally, the contribution due to the two-body part of the Breit operator was taken to be the difference between the second order energy correction (calculated with the BCHF basis) with Breit included, and Breit not included into the two-body part of the Hamiltonian. Concretely, remember that the second-order correlation to the energy of a valence state v, excluding both the one- and two-body parts of Breit, is given by Eq. (2.35),

$$\delta^{(2)}\varepsilon_v = \sum_{amn} \frac{g_{vamn}(g_{nmav} - g_{nmva})}{\varepsilon_v + \varepsilon_a - \varepsilon_m - \varepsilon_n} + \sum_{abn} \frac{g_{vnab}(g_{banv} - g_{bavn})}{\varepsilon_v + \varepsilon_n - \varepsilon_a - \varepsilon_b}. \tag{3.2}$$

We can denote this expression symbolically as a function f of the matrix elements g_{ijkl} in the numerators and the single-particle CHF eigenvalues ε_i in the denominators,

$$\delta^{(2)}\varepsilon_v \equiv f(g, \varepsilon). \tag{3.3}$$

Then, the one-body Breit correction to the second-order correlation energy is defined as,

$$\delta^{(2)}\varepsilon_v,\ B^{(1)} = f(\bar{g}, \bar{\varepsilon}) - f(g, \varepsilon) - \delta_{\mathrm{HF}} E_v, \tag{3.4}$$

where recall that $\bar{g}_{ijkl} = \langle \bar{\phi}_i \bar{\phi}_j | \frac{1}{r} | \bar{\phi}_k \bar{\phi}_l \rangle$ and $\bar{\varepsilon}_i$ satisfies Eq. (2.47). What this quantity tells us is the difference between the correction that including the Breit interaction into has to the second-order energy and the difference that including the Breit interaction has to the Hartree-Fock energy. The two-body Breit contribution to the second-order energy correction is similarly defined as

$$\delta^{(2)}E_v,\ B^{(2)} \equiv f(\bar{g} + \bar{b}, \bar{\varepsilon}) - f(\bar{g}, \bar{\varepsilon}), \tag{3.5}$$

where $\bar{b}_{ijkl} = \langle \bar{\phi}_i \bar{\phi}_j | H_{\mathrm{Br}} | \bar{\phi}_k \bar{\phi}_l \rangle$ is the two-particle matrix element of the Breit interaction in the BCHF basis.

The calculated values of the three class of Breit corrections to the valence energies of caesium are shown in Table 3.1, as well as a comparison with Derevianko's results. As we can see from this table, the Coulomb-Hartree-Fock energies agree perfectly with the previous study, and the corrections due to the Breit interaction at the level of the HF approximation also agree exactly, excepting the correction for the $5d_{5/2}$ state, although this still matches very closely. We see in the third column that the one-body Breit correction to the second order perturbative correction to the valence energies are in relatively good agreement with Derevianko's result, but they do not agree exactly for all states. This is true also for the two-body corrections in the final column although these are generally so small that it just may be numerical noise that is appearing.

One potential reason for the disagreement between the values I have calculated and Derevianko's calculations is due to the methods used to obtain the BCHF orbitals. In AMPSCI, these orbitals are calculated by constructing the BCHF potential self-consistently

Table 3.1: Contributions from the Breit interaction to the energies of valence states of caesium in units of cm^{-1} compared to the calculations performed by Derevianko in Ref. [16]. The E_{CHF} column represents the Coulomb-Hartree-Fock energy eigenvalues, the $\delta_{\mathrm{HF}}E$ column represents the difference between the Hartree-Fock eigenvalues with Breit versus without Breit included into the HF potential. The final two columns represent the contributions to the second-order perturbative valence energy corrections from the one-body $[B^{(1)}]$ and two-body $[B^{(2)}]$ parts of the Breit interaction, respectively.

	E_{CHF}		$\delta_{\mathrm{HF}}E$		$\delta^{(2)}E$, $B^{(1)}$		$\delta^{(2)}E$, $B^{(2)}$	
State	This work	Derev.	This work	Derev.	This work	Derev.	This work	Derev.
$6s_{1/2}$	−27954.05	−27954	3.199	3.2	−6.097	−4.98	−0.298	−0.83
$7s_{1/2}$	−12112.221	−12112	1.078	1.1	−1.073	−1.1	−0.069	−0.28
$6p_{1/2}$	−18790.494	−18791	7.495	7.5	−0.177	−0.08	−0.376	−0.28
$7p_{1/2}$	−9222.621	−9223	2.685	2.7	−0.128	−0.1	−0.116	−0.1
$6p_{3/2}$	−18388.763	−18389	2.871	2.9	−2.303	−1.8	0.022	−0.25
$7p_{3/2}$	−9079.228	−9079	1.048	1	−0.651	−0.56	0.005	−0.09
$5d_{3/2}$	−14138.476	−14138	−10.152	−10.2	−15.792	−12	−1.174	−0.35
$5d_{5/2}$	−14162.647	−14163	−11.69	−11.8	−19.266	−14	0.348	−0.33

and then numerically solving the BCHF eigenvalue equation using a basis of B-splines. In his paper, Derevianko constructs the CHF orbitals self-consistently using a basis of B-splines, but then constructs the BCHF orbitals from the CHF orbitals via the unitary transformation,

$$\bar{\phi}_i = \sum_j d_{ij}\phi_j. \tag{3.6}$$

Substituting this into the single-particle BCHF eigenvalue equation,

$$\left(h_0 + U^{\mathrm{BCHF}}\right)\bar{\phi}_i = \left(h_0 + U^{\mathrm{CHF}} + \Delta U\right)\bar{\phi}_i = \bar{\varepsilon}_i\bar{\phi}_i, \tag{3.7}$$

where $\Delta U = U^{\mathrm{BCHF}} - U^{\mathrm{CHF}}$, results in the equation

$$\varepsilon_i d_{ij} + \sum_k (\Delta U)_{ik} d_{kj} = \bar{\varepsilon}_j d_{ij}, \tag{3.8}$$

where $(\Delta U)_{ij} = \langle\phi_i|\left(U^{\mathrm{BCHF}} - U^{\mathrm{CHF}}\right)|\phi_j\rangle$. This is the equation that Derevianko states he uses to find the BCHF orbitals. How to actually use this, however, is not made clear. The way that this can be done is by noting that fixing j to be a constant, e.g. $j = 1$, lets us write Eq. (3.8) as

$$\begin{pmatrix} (\Delta U)_{11} + \varepsilon_1 & (\Delta U)_{12} & (\Delta U)_{13} & \cdots \\ (\Delta U)_{21} & (\Delta U)_{22} + \varepsilon_2 & (\Delta U)_{23} & \cdots \\ (\Delta U)_{31} & (\Delta U)_{32} & (\Delta U)_{33} + \varepsilon_3 & \cdots \\ \vdots & \vdots & \vdots & \ddots \end{pmatrix} \begin{pmatrix} d_{11} \\ d_{21} \\ d_{31} \\ \vdots \end{pmatrix} = \bar{\varepsilon}_1 \begin{pmatrix} d_{11} \\ d_{21} \\ d_{31} \\ \vdots \end{pmatrix}, \tag{3.9}$$

which is an eigenvalue equation for eigenvalue $\bar{\varepsilon}_1$ and an eigenvector composed of the expansion coefficients for $\bar{\phi}_1$ in terms of the CHF orbitals, $\{d_{i1}\}$. A derivation of this equation

is presented in Appendix A. Since the $\{\varepsilon_i\}$ and $\{(\Delta U)_{ij}\}$ can be easily calculated from the CHF equation, we can calculate the expansion coefficients and the BCHF energies by solving the above eigenvalue equation. Note that because the matrix on the left-hand side is $N \times N$, where N is the basis size, this matrix will admit up to N eigenvalues and eigenvectors. So finding the eigenvalues and eigenvectors for this matrix will actually give us the energy and expansion coefficients for all N BCHF orbitals, not just for $j = 1$. This can be seen more clearly by noting that the matrix on the left-hand side of the above equation actually doesn't depend on j, and is therefore just a label for the solutions to the equation.

Since the CHF energies and HF level Breit corrections agree almost exactly between my own calculations and Derevianko's, it is obvious that the B-spline method that AMPSCI uses and the one that Derevianko employs result in the same BCHF eigenvalues. However, since the second order Breit corrections disagree, this may be a sign that the BCHF wave functions are different enough that it results in a meaningful discrepancy in the Breit corrections between the two methods.

3.1.1 Impact of basis size

In addition to reproducing the energies in Derevianko's paper, I also tested changing certain parameters in the calculations. The first parameter I tested was the size of the basis used to calculate perturbative corrections. In the second-order energy correlation correction to the energy of each valence state (for a single-valence system, with no Breit interaction present) is given by the summations in Eq. (2.35), so in order to calculate this for a valence state, we need to sum over the full set of complete single-particle states. In AMPSCI, these single-particle states are generated using a spline basis, the number of which can be controlled on execution of the code [61, 98]. In calculating the one- and two-body Breit corrections to the second-order correlation energy in caesium, I tested basis sizes of 30, 45, 60 and 80. This will help to determine how robust the parts of the code that include Breit into the calculations are, especially since the code for the two-body part of the Breit interaction hasn't been thoroughly tested yet.

TABLE 3.2: Comparison of the contributions to the second order energy correlation corrections of valence states in caesium due to the one-body $[B^{(1)}]$ and two-body $[B^{(2)}]$ parts of the Breit interaction for different number of basis states used, in units of cm^{-1}. The percentages in parentheses next to each number represent the percentage difference in that value from the corresponding value evaluated with the previous basis size.

	2nd order Breit correction							
	30 splines		45 splines		60 splines		80 splines	
State	$\delta^{(2)}E$, $B^{(1)}$	$\delta^{(2)}E$, $B^{(2)}$	$\delta^{(2)}E$, $B^{(1)}$	$\delta^{(2)}E$, $B^{(2)}$	$\delta^{(2)}E$, $B^{(1)}$	$\delta^{(2)}E$, $B^{(2)}$	$\delta^{(2)}E$, $B^{(1)}$	$\delta^{(2)}E$, $B^{(2)}$
$6s_{1/2}$	−5.966	−0.256	−6.087(2.02%)	−0.289(12.9%)	−6.095(0.13%)	−0.295(2.07%)	−6.097(0.03%)	−0.297(0.68%)
$7s_{1/2}$	−1.048	−0.059	−1.071(2.19%)	−0.067(13.6%)	−1.072(0.09%)	−0.068(1.49%)	−1.073(0.09%)	−0.068(0.0%)
$6p_{1/2}$	−0.171	−0.359	−0.177(3.51%)	−0.372(3.62%)	−0.177(0.0%)	−0.374(0.54%)	−0.177(0.0%)	−0.376(0.53%)
$7p_{1/2}$	−0.125	−0.111	−0.128(2.4%)	−0.115(3.6%)	−0.128(0.0%)	−0.116(0.87%)	−0.128(0.0%)	−0.116(0.0%)
$6p_{3/2}$	−2.282	0.032	−2.301(0.83%)	0.025(21.9%)	−2.302(0.04%)	0.023(8.0%)	−2.303(0.04%)	0.022(4.35%)
$7p_{3/2}$	−0.644	0.008	−0.651(1.07%)	0.006(25.0%)	−0.652(0.15%)	0.005(16.7%)	−0.651(0.15%)	0.004(20.0%)
$5d_{3/2}$	−15.493	−1.13	−15.758(1.71%)	−1.165(3.10%)	−15.786(0.18%)	−1.171(0.52%)	−15.792(0.04%)	-1.173(0.17%)
$5d_{5/2}$	−18.906	0.367	−19.225(1.69%)	0.354(3.54%)	−19.259(0.18%)	0.35(1.13%)	−19.266(0.04%)	0.349(0.29%)

As Table 3.2 shows, the effect of changing the basis size is relatively large in going from 30 splines to 45 splines, ranging from a modification of $0.83-3.51\%$ to the $B^{(1)}$ contribution and a widely varying $3.1-25\%$ modification in the $B^{(2)}$ corrections. However, as we go from a basis size of 45 to 60 we see that the $B^{(1)}$ and $B^{(2)}$ corrections undergo a much smaller change, and from 60 to 80 splines the change decreases again for most states. This trend is much more obvious in the $B^{(1)}$ corrections, which seem to be converging to a particular value as the basis size increases, but the $B^{(2)}$ corrections seem to be much more variable and the corrections to some states, such as $7p_{3/2}$, do not seem to be convergent with a basis size of 80. This is likely again due to the fact that the two-body Breit corrections are so small for these states that a small change in the parameters leads to a large modification in the resulting correction. Indeed, for the states with the larger $B^{(2)}$ corrections, such as $6s_{1/2}$, $7s_{1/2}$, $6p_{1/2}$ and $5d_{3/2}$, these do seem to be convergent. This therefore suggests that the code is numerically stable and, from the previous agreement we found with Derevianko's results, is producing accurate results. I will therefore be able to use these to test the validity of my code when I try including the Breit interaction into the Feynman method.

3.1.2 Non-linearity of the Breit interaction

Table 3.3: Comparison of the Breit corrections to valence energies at the HF level and the one- and two-body corrections at the second order in caesium in units of cm^{-1} at a scaling of $\lambda = 0.5$ and a scaling of $\lambda = 1$. Since we don't want non-linear terms in Breit to contribute to the corrections, each class of correction should be twice as large with $\lambda = 1$ as they are with $\lambda = 0.5$. The third column for each class of correction is the percentage error from a ratio of 2 between the two.

	$\delta_{\mathrm{HF}}E$			$\delta^{(2)}E$, $B^{(1)}$			$\delta^{(2)}E$, $B^{(2)}$		
State	$\lambda = 0.5$	$\lambda = 1$	$\Delta\lvert\frac{\lambda=1}{\lambda=0.5} - 2\rvert$	$\lambda = 0.5$	$\lambda = 1$	$\Delta\lvert\frac{\lambda=1}{\lambda=0.5} - 2\rvert$	$\lambda = 0.5$	$\lambda = 1$	$\Delta\lvert\frac{\lambda=1}{\lambda=0.5} - 2\rvert$
$6s_{1/2}$	1.601	3.199	−0.09%	−3.048	−6.095	−0.02%	−0.148	−0.295	−0.34%
$7s_{1/2}$	0.54	1.078	−0.19%	−0.537	−1.072	−0.19%	−0.034	−0.068	0.00%
$6p_{1/2}$	3.75	7.495	−0.07%	−0.088	−0.177	0.57%	−0.188	−0.374	−0.53%
$7p_{1/2}$	1.343	2.685	−0.04%	−0.064	−0.128	0.00%	−0.058	−0.116	0.00%
$6p_{3/2}$	1.436	2.871	−0.03%	−1.151	−2.302	0.00%	0.012	0.023	−4.17%
$7p_{3/2}$	0.524	1.048	0.00%	−0.326	−0.652	0.00%	0.003	0.005	−16.67%
$5d_{3/2}$	−5.071	−10.152	0.10%	−7.889	−15.786	0.05%	−0.584	−1.171	0.26%
$5d_{5/2}$	−5.837	−11.69	0.14%	−9.619	−19.259	0.11%	0.174	0.35	0.57%

An additional technical point about the Breit interaction I have investigated in my project is its non-linearity when used in atomic physics calculations. Because the Breit interaction is of order $1/c^2$, this means that any expressions that are quadratic in the Breit interaction are of order $1/c^4$, and these should not be physically meaningful. This is because terms of order $1/c^3$ and higher should, in principle, come from higher-order corrections to the Coulomb interaction beyond Breit. Therefore, when including Breit into energies, matrix elements, etc., which involve the product of matrix elements, we need to check if non-linear terms are contributing to the corrections. In order to do so, we should include Breit into the calculation as λBr, with λ being a scaling factor; if the non-linear terms are insignificant then we would expect that the correction from including Breit with $\lambda = 0.5$ should be half

as large as the correction with $\lambda = 1$, as this would indicate that only the linear terms are actually contributing [16, 31]. I have done this, again for the valence energies of caesium, for the HF level correction, as well as the $B^{(1)}$ and $B^{(2)}$ second order corrections. The results of this are shown in Table 3.3 and we can see from the third columns that each Breit correction scales linearly, as desired.

3.1.3 Impact of relativistic components

Finally, in testing the second-order valence energies, the last calculation that I have performed is in testing the contribution of the non-relativistic component of the correlation potential, Eq. (2.36), to the valence energies in caesium. In calculating the second-order energy correction to valence states, AMPSCI constructs the correlation potential using the spline-generated basis states and then the second-order energy correction is calculated by taking the expectation value $\Sigma^{(2)}_{vv}(\varepsilon_v)$. In spinor space, the correlation potential may be expressed as

$$\hat{\Sigma}^{(2)}(\varepsilon) = \begin{pmatrix} \Sigma_{\phi\phi} & \Sigma_{\phi\chi} \\ \Sigma_{\chi\phi} & \Sigma_{\chi\chi} \end{pmatrix}, \tag{3.10}$$

where ϕ and χ denote the "large" and "small" components of the Dirac spinor,

$$\psi = \begin{pmatrix} \phi \\ \chi \end{pmatrix}, \tag{3.11}$$

respectively (note that ϕ and χ are two-component spinors while ψ is a four-component spinor). These names come from the non-relativistic limit of the Dirac equation, known as the Pauli approximation, in which it can be shown that the two components of ψ satisfy [72],

$$\chi \approx \frac{\boldsymbol{\sigma} \cdot \boldsymbol{p}}{2mc}\phi. \tag{3.12}$$

In non-relativistic contexts, $mc \gg \boldsymbol{p}$ so the lower component of the Dirac spinor ψ is much smaller than the upper component. Furthermore, since $\chi \sim (1/c)\phi$, the lower right component of the correlation potential is of order $(1/c)^2$, and should therefore be of the same order as the Breit interaction [99, 100]. For this reason, it is often convenient in atomic calculations to only calculate the top left component of the correlation potential in Eq. (3.10) when calculating the second-order energy correction to valence states, with minimal loss of accuracy. However, since the Breit interaction is of the same order as the lower components of the correlation potential, it may be important to include all its components when including the Breit interaction into the calculation of atomic properties. Therefore, to test whether this is the case, I calculated the perturbative Breit corrections to the valence energies of caesium separately with just the top left component of the correlation potential and then with every component of the correlation potential. As Table 3.4 shows, there is almost no difference in the Breit corrections between these two versions of the correlation potential, meaning that there is no important contribution from the relativistic components of the potential and can be excluded from calculations in caesium with minimal loss of accuracy.

Table 3.4: One-body and two-body Breit contributions to the second order valence energy corrections in caesium in units of cm^{-1}, calculated using all of the spinor components of the correlation potential $\Sigma^{(2)}$ and only keeping the top left (ff) component $\Sigma^{(2)}_{ff}$. The column labelled error is the error between the corresponding correction calculated with the full correlation potential and the same correction calculated with only the top left component.

	$\delta^{(2)}E$, $B^{(1)}$			$\delta^{(2)}E$, $B^{(2)}$		
State	Full matrix	Top left only	Error	Full matrix	Top left only	Error
$6s_{1/2}$	5.735	5.727	−0.14%	−0.49	−0.30	39.09%
$7s_{1/2}$	0.97	0.969	−0.10%	−0.11	−0.07	38.94%
$6p_{1/2}$	6.958	6.953	−0.07%	−0.18	−0.38	−111.86%
$7p_{1/2}$	1.735	1.733	−0.12%	−0.06	−0.12	−96.61%
$6p_{3/2}$	4.11	4.11	−0.07%	−0.16	0.02	114.01%
$7p_{3/2}$	1.077	1.08	−0.09%	−0.05	0.00	109.43%
$5d_{3/2}$	−9.29	−9.29	0.02%	−0.37	−1.17	−216.76%
$5d_{5/2}$	−11.805	−11.80	0.02%	−0.35	0.35	198.87%

3.2 Breit corrections to matrix elements

In addition to testing the correction to valence energies in caesium, I have also calculated the Breit contributions to hyperfine-structure constants and to E1 transition matrix elements at various levels of perturbation theory and other effects. These are again compared to the results from Derevianko's paper.

3.2.1 Hyperfine structure constants

The interaction between an atomic electron with the magnetic moment of the nucleus gives rise to a one-body interaction known as the hyperfine interaction, described by,

$$h_{\rm hfs}(r) = e\boldsymbol{\alpha}\cdot\boldsymbol{A}(r) = \frac{e\boldsymbol{\alpha}\cdot(\boldsymbol{\mu}\times\boldsymbol{r})}{r^3}F(r), \tag{3.13}$$

where $\boldsymbol{A}(r)$ is the magnetic electric potential generated by the nucleus, $\mu = \mu_0\boldsymbol{I}/I$ is the nuclear magnetic moment, with $\boldsymbol{I}$ the nuclear spin, and $F(r)$ is the magnetic distribution inside the nucleus [19, 21, 101]. The interaction of the electrons with the nucleus leads to hyperfine level splitting of atomic energy levels and, due to the $1/r^3$ dependence of the operator, is useful for high-accuracy probes of wave functions close to the nucleus, where there is high sensitivity to changes in the Standard Model, and relativistic effects are expected to be significant [46, 47, 78, 102]. Derevianko calculated diagonal matrix elements of the magnetic hyperfine interaction operator, $A = \langle v|h_{\rm hfs}(\boldsymbol{r})|v\rangle$, with Breit corrections to this amplitude calculated at the level of the HF orbitals, at third order in the random phase approximation (RPA), and due to the use of Brueckner orbitals [orbitals satisfying Eq. (2.37)] in the summation over states.

The random phase approximation is a method by which corrections to the HF potential due to the interaction of the wave functions with an external electromagnetic field, and

Breit contributions to these corrections were carried out to the third order [103]. I have performed these same calculations using AMPSCI, and a comparison between my results and Derevianko's are shown in Table 3.5.

TABLE 3.5: Breit corrections to magnetic-dipole hyperfine structure constants for valence states of caesium in units of MHz.

	A_{CHF}		δA_{HF}		δA_{RPA}		$\delta A_{\mathrm{BO+RPA}}$	
State	This work	Derev.	This work	Derev.	This work	Derev.	This work	Derev.
$6s_{1/2}$	1421.17	1425.3	0.011	0.011	4.01	4.10	2.99	0.79
$7s_{1/2}$	390.50	391.6	−0.028	−0.029	1.09	1.10	0.29	0.08
$6p_{1/2}$	160.63	160.9	−0.678	−0.680	0.44	0.39	−0.66	−0.24
$7p_{1/2}$	57.51	57.62	−0.234	−0.230	0.16	0.14	−0.22	−0.059
$6p_{3/2}$	23.88	23.92	−0.062	−0.060	0.14	0.10	0.02	−0.008
$7p_{3/2}$	8.626	8.642	−0.022	−0.022	0.049	0.038	0.00	−0.002
$5d_{3/2}$	18.20	18.23	0.099	0.099	0.13	0.10	0.44	0.11

We can see that my results agree almost perfectly at the CHF level, and the Breit corrections at the level of HF basis shift and the RPA also agree very closely. There is some disagreement, however, between the corrections at the level of also including Breit into the Brueckner orbitals that are used in the summation over states. This could be due to the difference in how the Breit orbitals are calculated in AMPSCI compared to how Derevianko calculates them (as outlined in Sec. 3.1), which we saw led to comparable differences in the Breit corrections to valence energies at second order in perturbation theory. The corrections are of the same sign and comparable in terms of magnitude in most states, so it is likely that the numerical implementation of the second-order corrections are responsible for these differences.

Based on the discussion in Section 2.7, hyperfine structure constants are especially important to have good accuracy for in the context of construction of the first nuclear clock, as they provide an indirect way of probing the nuclear structure without any reference to the underlying nuclear theory. We can see that in this particular case, one-body Breit corrections at the level of Brueckner orbitals (second-order correlation effects) are comparable to the Breit corrections at the HF level, and so the effect of including Breit to higher orders of perturbation theory for highly relativistic systems is important for high-accuracy hyperfine structure constants.

3.2.2 Reduced electric-dipole matrix elements

Finally, in addition to calculating hyperfine structure constants, Derevianko calculates Breit corrections electric-dipole matrix elements for transitions between the valence states of caesium at various orders of perturbation theory (the same as those used to calculate the hyperfine structure constants). The electric-dipole operator is defined as

$$\boldsymbol{d} = e\boldsymbol{r}, \tag{3.14}$$

Table 3.6: Breit corrections to reduced E1 electric-dipole transition matrix elements for valence states of caesium in units of MHz.

	D_{CHF}		δD_{HF}		δD_{RPA}		δD_{BO}	
Transition	This work	Derev.	This work	Derev.	This work	Derev.	This work	Derev.
$6s_{1/2} - 6p_{1/2}$	5.278	5.278	0.000351	0.00035	−0.00035	−0.00022	−0.000221	−0.0011
$6s_{1/2} - 6p_{3/2}$	7.426	7.426	0.000777	0.00078	0.00014	−0.00045	−0.001366	−0.0014
$6s_{1/2} - 7p_{1/2}$	0.372	0.3717	0.0018109	0.0018	0.00161	−0.00013	−0.003544	0.00021
$6s_{1/2} - 7p_{3/2}$	0.695	0.6947	0.000603	0.00059	0.00031	−0.0002	−0.001096	0.00011
$7s_{1/2} - 6p_{1/2}$	4.413	4.413	0.004605	0.0046	0.00454	−0.000067	−0.009211	0.00038
$7s_{1/2} - 6p_{3/2}$	6.671	6.671	0.001841	0.0019	0.00185	−0.000011	−0.003762	−0.0003
$7s_{1/2} - 7p_{1/2}$	11.009	11.01	−0.00104	−0.0011	−0.00113	−0.00005	0.002180	−0.0018
$7s_{1/2} - 7p_{3/2}$	15.345	15.34	0.00076	0.0007	0.00057	−0.00013	−0.001400	−0.0019
$5d_{3/2} - 6p_{1/2}$	8.978	8.978	−0.004414	−0.0044	−0.00488	−0.00035	0.008934	−0.0082
$5d_{3/2} - 6p_{3/2}$	4.062	4.062	−0.002804	−0.0028	−0.00306	−0.00019	0.005667	−0.0035

and its matrix elements, $\langle\phi_a|\boldsymbol{d}|\phi_b\rangle$, are related to the amplitude of an electron transitioning from state a to state b due to its interaction with an external electromagnetic field [19]. The electric-dipole matrix element can be expressed, via the use of the Wigner-Eckhardt theorem [19], as

$$\langle\phi_a|d_z|\phi_b\rangle = (-1)^{j_a-m_a}\begin{pmatrix} j_a & 1 & j_b \\ -m_a & 0 & m_b \end{pmatrix}\langle n_a\kappa_a\|d_z\|n_b\kappa_b\rangle, \tag{3.15}$$

where j_i is the total angular momentum of the state ϕ_i, with projection onto the z-axis m_i, and with principal quantum number n_i and relativistic angular momentum quantum number $\kappa = (l-j)(2j+1)$, $(:::)$ is a Wigner 3-j symbol, and $\langle n_i\kappa_i\|d_z\|n_j\kappa_j\rangle$ is a number that does not depend on the angular momentum projections m_a and m_b, referred to as the reduced E1 electric-dipole matrix element [19, 104]. Since the reduced E1 matrix element is proportional to $\boldsymbol{r}$, comparing theoretical predictions of their value against experimental measurements provides a probe of the accuracy of electron wave functions far away from the nucleus, complementing hyperfine structure constants which probe distances close to the nucleus [46]. In addition to this, E1 amplitudes are subject to parity selection rules, an observed violation of which could indicate new physics beyond the Standard Model [105]. A comparison of my calculated E1 reduced matrix elements (using AMPSCI) with Derevianko's are shown in Table 3.6. In general, we can see that the Breit corrections at each column of this table are smaller than the correction in the same column in Table 3.5, which is what we'd physically expect since the Breit interaction is a relativistic effect and its inclusion should therefore result in a smaller modification to matrix elements that probe distances further away from the nucleus like the E1 amplitude, where relativistic effects are less important, compared to hyperfine structure constants which probe wave functions close to the nucleus.

Regarding the agreement between my own results and Derevianko's, we can see that, just like the hyperfine structure constants, the E1 amplitudes at the level of the CHF approximation and the HF level Breit corrections agree almost exactly with those in his paper.

However, whereas my corrections agreed with Derevianko's very closely at the RPA level for the hyperfine structure constants, they don't for the E1 amplitudes. In some cases, such as the $6s_{1/2} - 6p_{3/2}$ transition, the two corrections actually differ in sign but are of the same magnitude. Although this seems like this should be a problem, these corrections (and the ones at the level of the Brueckner orbitals) are so small that it is likely just numerical noise that we are observing in these corrections. It is unlikely that these corrections are numerically stable, and therefore the method by which these corrections are calculated is likely to have a very large effect on the correction itself, which is the likely explanation for the large discrepancies in the table. Regardless of these discrepancies, the agreement between my own calculations and those of Derevianko are close enough for me to move forward.

4 The Feynman method

Throughout my literature review, and also in the calculations I have presented in the previous chapter, when I have mentioned MBPT, almost all of the references I have cited use the standard approach, called the Goldstone method, which involves evaluating expressions like Eq. (2.35). In this chapter I will review an alternative approach to doing MBPT, called the Feynman method which involves evaluating integrals over frequencies, corresponding to Feynman diagrams, rather than sums over states. The benefit of this method is that the algebra of Green's functions allows us to sum certain series of Feynman diagrams to all orders in perturbation theory, thereby enabling us to include important quantum many-body effects non-perturbatively into atomic structure calculations.

4.1 Feynman Green's function

The Feynman CHF Green's function is defined, relative to a HF core state, $|0_c\rangle$ [17, 60, 106],

$$G(\boldsymbol{r}_1, \boldsymbol{r}_2; \varepsilon) = \lim_{\delta \to 0} \left[\sum_a^{\text{core}} \frac{\phi_a(\boldsymbol{r}_1)\phi_a^\dagger(\boldsymbol{r}_2)}{\varepsilon - \varepsilon_a - i\delta} + \sum_n^{\text{exc.}} \frac{\phi_n(\boldsymbol{r}_1)\phi_n^\dagger(\boldsymbol{r}_2)}{\varepsilon - \varepsilon_n + i\delta} \right], \tag{4.1}$$

where ϕ_i is an eigenstate of the CHF equation, the sum over a is over all core states, the sum over n is over all excited states. One can easily verify that this is a Green's function of the CHF equation,

$$(\varepsilon - h_0 - U^{\text{CHF}})G(\boldsymbol{r}_1, \boldsymbol{r}_2; \varepsilon) = \delta^3(\boldsymbol{r}_1 - \boldsymbol{r}_2). \tag{4.2}$$

The Feynman Green's function can be used to calculate perturbative corrections to energies of valence states as part of Feynman diagrams. In Appendices B and C I provide some more details on the Feynman method and how to extract energy corrections from the fundamental equations. For example, at second order in perturbation theory in the residual Coulomb

interaction, the correction to the energy of a valence state is represented diagrammatically by [14, 55, 106]

$\delta^{(2)}E_v =$

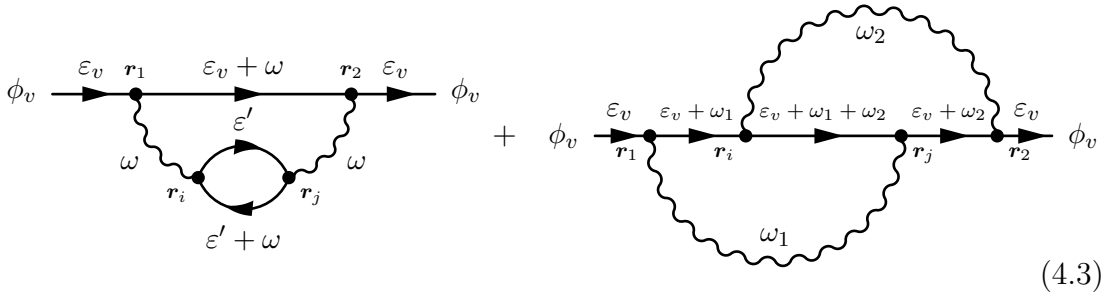

(4.3)

where straight, directed internal lines represent CHF Green's functions, wavy lines represent Coulomb operators and directed external lines represent valence wave functions. The first and second diagrams correspond respectively to the direct and exchange parts of the second-order energy correction. The rules for evaluating these diagrams can be found in e.g. Refs. [107, 108], with the first being equal to

$$\delta^{(2)}_{\text{dir}}E_v = \int d^3r_1\, d^3r_i\, d^3r_j\, d^3r_2 \int \frac{d\omega}{2\pi}\frac{d\varepsilon'}{2\pi}\, \phi_v^\dagger(\boldsymbol{r}_1)G_{12}(\varepsilon_v+\omega)Q_{1i}G_{ij}(\varepsilon')G_{ji}(\varepsilon'+\omega)Q_{j2}\,\phi_v(\boldsymbol{r}_2), \tag{4.4}$$

where I have used the shorthand notation $G_{ij}(\varepsilon) \equiv G(\boldsymbol{r}_i, \boldsymbol{r}_j; \varepsilon)$ and $Q_{ij} \equiv Q(\boldsymbol{r}_i, \boldsymbol{r}_j)$. It can be shown that evaluating Eq. (4.3) gives exactly Eq. (2.35) [60, 61]. Therefore, the Feynman method provides an alternative way of doing perturbation theory for atomic systems, often at the cost of reduced computational time and complexity, compared to the Goldstone method [61]. For example, while it can be shown that the Goldstone and Feynman methods are equivalent to every order in perturbation theory, each Feynman diagram contains multiple Goldstone diagrams due to the fact that the Feynman Green's function is time-ordered, and therefore contains all possible time-orderings of the vertices for a given scattering process [109, 110]. It also has the more important advantage that certain many-body effects, which would generally only be possible to include at low orders of perturbation theory in the Goldstone method, can be included exactly to all orders of perturbation theory in the Feynman method. Because very little is known from a first-principles point of view about the convergence of MBPT in atomic physics [6], summing many-body effects non-perturbatively entirely circumvents the problem of slow convergence at low orders of perturbation theory.

4.2 The Dyson equation

As an example of why the Feynman method is useful for including perturbative effects at all orders of perturbation theory, consider the CHF equation,

$$(\varepsilon - h_0 - V_{\text{dir}} - V_{\text{x}})\phi = 0 \tag{4.5}$$

where V_{dir} and V_{x} are the direct and exchange parts of the CHF potential, respectively. We know that the Green's function for this equation can be constructed as the summation in

Eq. (4.1), however, constructing it in this way is numerically unstable. Instead, if we neglect the exchange potential in Eq. (4.5), the Green's function for the resulting equation, known as the Hartree equation, can be calculated directly without the need for a basis as [111],

$$G_0(\boldsymbol{r}_1, \boldsymbol{r}_2) = \frac{\chi_0(r_<)\chi_\infty(r_>)}{w} \tag{4.6}$$

where $r_< = \min(r_1, r_2)$ and likewise for $r_>$, χ_0 and χ_∞ are the solutions of the Hartree equation that are regular as $r \to 0$ and $r \to \infty$, respectively, and $w = (f_0 g_\infty - f_\infty g_0)/\alpha$, with f and g the large and small radial components of χ, respectively, and α the fine structure constant. Note that the Green's function found in this way implicitly depends on ε through the fact that χ_0 and χ_∞ are found as solutions of the Hartree equation for a given energy, ε. The exchange potential cannot be included into the Green's function in this way since it is a non-local operator, and must instead be included perturbatively. To do so, the Hartree-Fock Green's function, including exchange, will satisfy the equation,

$$(\varepsilon - h_0 - V_{\text{dir}} - V_{\text{x}})G(\boldsymbol{r}_1, \boldsymbol{r}_2) = \delta^3(\boldsymbol{r}_1 - \boldsymbol{r}_2), \tag{4.7}$$

which we can solve order-by-order in V_{x}. At zeroth order in V_{x}, we simply have $G(\boldsymbol{r}_1, \boldsymbol{r}_2) = G_0(\boldsymbol{r}_1, \boldsymbol{r}_2)$. At first order in V_{x}, we write $G = G_0 + G_1$, where $G_1 = \mathcal{O}(V_{\text{x}})$, and substitute this into Eq. (4.7) to yield

$$\begin{aligned}
\delta^3(\boldsymbol{r}_1 - \boldsymbol{r}_2) &= (\varepsilon - h_0 - V_{\text{dir}} - V_{\text{x}})\left[G_0(\boldsymbol{r}_1, \boldsymbol{r}_2) + G_1(\boldsymbol{r}_1, \boldsymbol{r}_2)\right] && (4.8)\\
&= \underbrace{(\varepsilon - h_0 - V_{\text{dir}})G_0}_{=\delta^3(\boldsymbol{r}_1 - \boldsymbol{r}_2)} + (\varepsilon - h_0 - V_{\text{dir}})G_1 - V_{\text{x}}G_0 && (4.9)\\
V_{\text{x}}G_0(\boldsymbol{r}_1, \boldsymbol{r}_2) &= (\varepsilon - h_0 - V_{\text{dir}})G_1(\boldsymbol{r}_1, \boldsymbol{r}_2), && (4.10)
\end{aligned}$$

where we have discarded the $V_{\text{x}}G_1$ term since it is of order V_{x}^2. We see that this is just an inhomogeneous form of the Hartree equation with a source term $[V_{\text{x}}G_0](\boldsymbol{r}_1, \boldsymbol{r}_2)$. We can therefore write down an explicit solution for G_1 using the Green's function for the Hartree equation which, recall, is just G_0. Therefore,

$$G_1(\boldsymbol{r}_1, \boldsymbol{r}_2) = \int d^3r\, G_0(\boldsymbol{r}_1, \boldsymbol{r})[V_{\text{x}}G_0](\boldsymbol{r}, \boldsymbol{r}_2) \equiv \mathbf{G}_0\mathbf{V}_{\text{x}}\mathbf{G}_0 \tag{4.11}$$

where I have introduced the short-hand operator product notation in the final step, which implies integration over inner coordinates,

$$\mathbf{C} = \mathbf{AB} \iff C(\boldsymbol{r}_1, \boldsymbol{r}_2) = \int d^3r\, A(\boldsymbol{r}_1, \boldsymbol{r})B(\boldsymbol{r}, \boldsymbol{r}_2). \tag{4.12}$$

We can then keep up this perturbative expansion for G, and we would find the next term, for example, being $\mathbf{G}_2 = \mathbf{G}_0\mathbf{V}_{\text{x}}\mathbf{G}_0\mathbf{V}_{\text{x}}\mathbf{G}_0$. It can be shown that the rest of the terms continue in this pattern, leading to the infinite series,

$$\begin{aligned}
\mathbf{G} &= \mathbf{G}_0 + \mathbf{G}_1 + \mathbf{G}_2 + \dots && (4.13)\\
&= \mathbf{G}_0 + \mathbf{G}_0\mathbf{V}_{\text{x}}\mathbf{G}_0 + \mathbf{G}_0\mathbf{V}_{\text{x}}\mathbf{G}_0\mathbf{V}_{\text{x}}\mathbf{G}_0 + \dots && (4.14)
\end{aligned}$$

$$= \mathbf{G}_0 \left(\mathbf{1} + \mathbf{V}_\mathrm{x}\mathbf{G}_0 + \mathbf{V}_\mathrm{x}\mathbf{G}_0\mathbf{V}_\mathrm{x}\mathbf{G}_0 + \dots\right) \tag{4.15}$$

$$= \mathbf{G}_0 \left[\mathbf{1} + \mathbf{V}_\mathrm{x}\mathbf{G}_0 + (\mathbf{V}_\mathrm{x}\mathbf{G}_0)^2 + (\mathbf{V}_\mathrm{x}\mathbf{G}_0)^3 + \dots\right] \tag{4.16}$$

$$= \mathbf{G}_0(\mathbf{1} - \mathbf{V}_\mathrm{x}\mathbf{G}_0)^{-1}, \tag{4.17}$$

where the last line follows from the factorisation of the geometric series in square brackets in the previous line. Thus, exchange can be taken into account by solving the above equation, known as the Dyson equation [5, 106]. Note that although we started by solving perturbatively in V_x, the Dyson equation is *non-perturbative*, thereby allowing exchange to be included into the Green's function exactly. The Green's function G obtained in this way is therefore the Green's function for the full HF equation, including exchange.

4.3 The Breit interaction in the Feynman method

The Dyson equation will be useful for me since the aim of my project is to include the one-body part of the Breit interaction into the Green's function, which means that I want to replace all Green's functions in the diagrams in Eq. (4.3) with the BCHF Green's function, which is defined as

$$\bar{G}(\boldsymbol{r}_1, \boldsymbol{r}_2; \varepsilon) = \lim_{\delta\to 0}\left[\sum_a^{\text{core}} \frac{\bar{\phi}_a(\boldsymbol{r}_1)\bar{\phi}_a^\dagger(\boldsymbol{r}_2)}{\varepsilon - \bar{\varepsilon}_a - i\delta} + \sum_n^{\text{exc.}} \frac{\bar{\phi}_n(\boldsymbol{r}_1)\bar{\phi}_n^\dagger(\boldsymbol{r}_2)}{\varepsilon - \bar{\varepsilon}_n + i\delta}\right], \tag{4.18}$$

where recall that $\bar{\phi}_i$ is an eigenfunction of the Breit-Coulomb-HF equation with eigenvalue ε_i. But, as with the CHF Green's function, calculating it this way is numerically unstable, so we want to include the Breit interaction into the Green's function using the Dyson equation. Since the HF potential modifies only the exchange potential $\mathbf{V}_\mathrm{x} \to \mathbf{V}_\mathrm{x} + \mathbf{V}_\mathrm{Br}$ (the direct part of the Breit interaction is exactly zero in the closed-shell HF approximation [30]), I can include the Breit interaction into the Green's function by modifying the Dyson equation to be,

$$\bar{\mathbf{G}} = \mathbf{G}_0 \left[\mathbf{1} - (\mathbf{V}_\mathrm{x} + \mathbf{V}_\mathrm{Br})\mathbf{G}_0\right]^{-1}, \tag{4.19}$$

Including the one-body part of the Breit interaction into the Feynman method therefore requires calculating

$$\mathbf{V}_\mathrm{Br}\mathbf{G}_0 \equiv [V_\mathrm{Br}G_0](\boldsymbol{r}_1, \boldsymbol{r}_2) = \int V_\mathrm{Br}(\boldsymbol{r}_1, \boldsymbol{r}) G_0(\boldsymbol{r}, \boldsymbol{r}_2)\, d^3r. \tag{4.20}$$

If I can therefore construct the HF Breit operator as a coordinate operator (or through some other method of calculating $\mathbf{V}_\mathrm{Br}\mathbf{G}_0$), the Breit interaction can be included exactly into the Green's function and therefore into the Feynman method. Evaluating Eq. (4.3) with $\bar{G}$ instead of G, and with $\bar{\phi}_v$ instead of ϕ_v will therefore give the second-order energy correction to a valence state in Eq. (2.35), but with the one-body part of the Breit interaction included (i.e. replace each g_{ijkl} with $\bar{g}_{ijkl}$ and each ε_i with $\bar{\varepsilon}_i$). Diagrammatically, then, I aim to be able to calculate the diagrams,

$\bar{\delta}^{(2)}E_v =$ 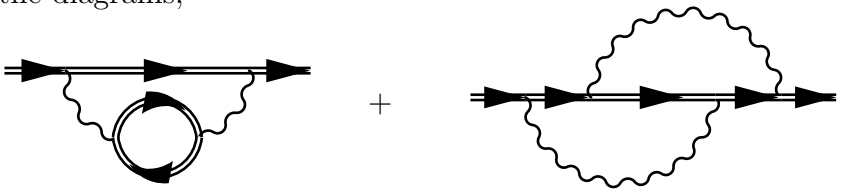 (4.21)

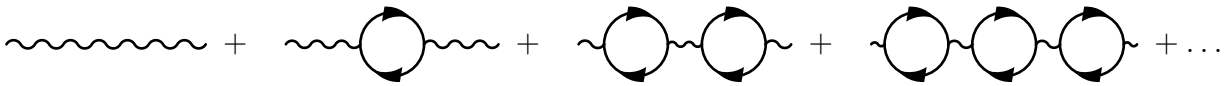

FIGURE 4.1: All-orders screening of the Coulomb interaction. The excitation of hole-particle pairs screen the electron-electron Coulomb interaction between valence and core electrons. This results in a renormalised electron-electron interaction which can be used in place of the normal Coulomb interaction in the evaluation of Feynman diagrams.

where the Green's function with the double line corresponds to the BCHF Green's function $\bar{G}(\boldsymbol{r}_1, \boldsymbol{r}_2)$ formed using the Dyson equation. The next chapter will be dedicated to discussing how the Breit interaction can be included into the Green's function.

4.4 All-orders correlation potential

As discussed in the previous sections, the Feynman method is powerful in that it lets us include certain perturbative effects that follow a geometric progression *exactly* into perturbation theory. The two most important many-body effects that can be included into the Feynman method are the all-orders screening of the Coulomb interaction, and the hole-particle interaction.

4.4.1 Screening of the Coulomb interaction

The electron loop in the first diagram in Eq. (4.3) corresponds to its own Feynman diagram, and forms an operator known as the polarisation operator,

$$\Pi(\boldsymbol{r}_1, \boldsymbol{r}_2, \omega) \equiv$$

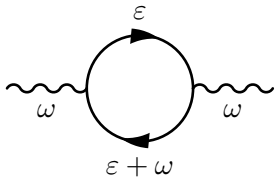

$$= \int \frac{d\varepsilon}{2\pi} G(\boldsymbol{r}_1, \boldsymbol{r}_2; \varepsilon) G(\boldsymbol{r}_2, \boldsymbol{r}_1; \varepsilon + \omega). \tag{4.22}$$

This corresponds physically to the screening of the Coulomb interaction between each pair of electrons by the presence of virtual-core pairs which form 'virtual dipoles' that polarise the atomic core [17, 108]. As we go to higher orders of perturbation theory, we will encounter diagrams that contain photon lines with a continued insertion of electron-hole loops, shown in Figure 4.1. This series of photon lines defines the renormalised Coulomb line,

$$\begin{aligned} \widetilde{\mathbf{Q}} &= \mathbf{Q} + (-i)\mathbf{Q}\mathbf{\Pi}\mathbf{Q} + (-i)^2\mathbf{Q}\mathbf{\Pi}\mathbf{Q}\mathbf{\Pi}\mathbf{Q}\mathbf{\Pi} + \dots && (4.23)\\ &= \mathbf{Q}\left[\mathbf{1} + (-i\mathbf{\Pi}\mathbf{Q}) + (-i\mathbf{\Pi}\mathbf{Q})^2 + (-i\mathbf{\Pi}\mathbf{Q})^3 + \dots\right] && (4.24)\\ &= \mathbf{Q}\left(\mathbf{1} + i\mathbf{\Pi}\mathbf{Q}\right)^{-1}. && (4.25) \end{aligned}$$

The same procedure can be carried out for the polarisation operator, which becomes,

$$\begin{aligned} \widetilde{\mathbf{\Pi}}(\omega) &= \mathbf{\Pi}(\omega) - i\mathbf{\Pi}(\omega)\mathbf{Q}\mathbf{\Pi}(\omega) + (-i)^2\mathbf{\Pi}(\omega)\mathbf{Q}\mathbf{\Pi}(\omega)\mathbf{Q}\mathbf{\Pi}(\omega) + \dots && (4.26)\\ &= \mathbf{\Pi}(\omega)\left[\mathbf{1} + i\mathbf{Q}\mathbf{\Pi}(\omega)\right]^{-1}, && (4.27) \end{aligned}$$

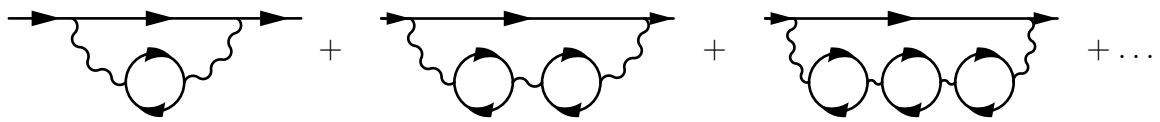

FIGURE 4.2: All-orders summation of the screened Coulomb interaction in the direct second order Feynman diagram.

FIGURE 4.3: Renormalised polarisation operator including the hole-particle interaction.

which includes screening to all orders. Mathematically, we can see that these diagrams indeed correspond to the screening of the Coulomb interaction since, in the limit of $\omega = 0$ and small momentum, it can be shown that Eq. (4.25) reduces to a screened Coulomb interaction [109]. There are higher order contributions to the Coulomb interaction, involving more complicated insertions into the loops, however, they are not considered in this approach, which only accounts for the lowest order, but most significant contributions, to the photon self-energy [108]. For example, it has been shown that the direct diagram with two polarisation loops – i.e. the second diagram in Figure 4.2 – gives the largest contribution to the energy correction of caesium at third order in perturbation theory out of all the third order diagrams [106, 112]. Therefore, including the insertion of polarisation loops to all orders captures the most important corrections to the Coulomb line. Including this screened Coulomb interaction into the second-order direct Feynman diagram thereby captures the infinite series of diagrams shown in Figure 4.2. This effect is enhanced by the number of electrons in the upper closed subshells in the core [106].

Note that although the screening diagrams in Figure 4.1 could in principle be calculated in the Goldstone method, with corresponding diagrams known as Goldstone diagrams [21], there is no algebraic manipulation that allows this to be done conveniently to all orders. In the Goldstone method, these diagrams must therefore be calculated order-by-order, which quickly becomes complicated. Furthermore, due to the fact that individual Goldstone diagrams need to be calculated for each possible time-ordering of a single diagram, while Feynman diagrams capture all possible time-orderings, the Goldstone diagram expansion will actually contain many more diagrams than the Feynman method at each order of perturbation theory. For example, at second order in perturbation theory there are four Goldstone diagrams, while we have seen that there are only two in the Feynman approach. What's more, a calculation of the energy corrections to the valence states of caesium in Ref. [112] included the third order screening diagrams for the Coulomb interaction, but they found that this made agreement with experiment worse, indicating that these diagrams do not converge at low orders of perturbation theory, and so the Goldstone method cannot reasonably be

Figure 4.4: All-orders screening of the Coulomb interaction with the hole-particle interaction included.

used to include screening corrections. This problem is solved by the Feynman method which permits the infinite chain of screening diagrams in Figure 4.2 to be summed exactly [14].

4.4.2 Hole-particle interaction

The other important correction to the photon line that can be included in the Feynman method is the hole-particle interaction, which to lowest order inserts a photon line into the electron loop in the polarisation operator. Including these diagrams to all orders results in the expansion shown in Figure 4.3. Although not as important as the screening diagrams, the third order hole-particle interaction diagram has been shown to be half as large as the third order screening diagram in caesium [14]. Therefore, including the hole-particle interaction is important for high accuracy calculations, and the Feynman method allows this class of diagrams to be included to all orders of perturbation theory. Physically, the hole-particle interaction corresponds to the alteration of the core potential due to the excitation of the particle from the core to the virtual intermediate state, i.e. the excited core particle (the backwards facing particle) in the polarisation loop moves in the field of $N-2$ core electrons, instead of the usual $N-1$ core electrons [61]. In the Hartree-Fock procedure, the self-energy of each core electron in the direct part of the potential is exactly cancelled by the exchange term, since the definition of the HF potential on the core orbital a is,

$$U^{\mathrm{CHF}}\phi_a(\boldsymbol{r}) = \sum_i^{\mathrm{core}} \left[\int \frac{\phi_i^\dagger(\boldsymbol{r'})\phi_i(\boldsymbol{r'})}{|\boldsymbol{r}-\boldsymbol{r'}|}\, d^3\boldsymbol{r'}\, \phi_a(\boldsymbol{r}) - \int \frac{\phi_i^\dagger(\boldsymbol{r'})\phi_a(\boldsymbol{r'})}{|\boldsymbol{r}-\boldsymbol{r'}|}\, d^3\boldsymbol{r'}\, \phi_i(\boldsymbol{r}) \right], \tag{4.28}$$

and so the term in the summation where $i = a$ gives exactly zero. However, in the particle-hole diagrams, no such cancellation occurs for the excited core electron, and so the self-energy part of each excited core electron should be subtracted from the HF potential. This means that the polarisation operator needs to be solved in the V^{N-2} potential, rather than the usual V^{N-1} potential. This is done by solving for the local Green's function in the potential,

$$\hat{V} = \hat{V}^{N-1} - (1-\hat{P})\hat{V}_{\mathrm{self}}(1-\hat{P}), \tag{4.29}$$

where $\hat{P}$ is the projection operator onto the core states,

$$\hat{P} = \sum_a^{\mathrm{core}} |a\rangle\langle a|, \tag{4.30}$$

and $\hat{V}_{\mathrm{self}}$ is the self-interaction part of the HF potential for the outgoing core electron. Although similar subtractions should occur for the higher order terms in the particle-hole interaction series of diagrams, these contributions are very small and are therefore not included [14]. In this way, the dominating hole-particle effects are included into the correlation

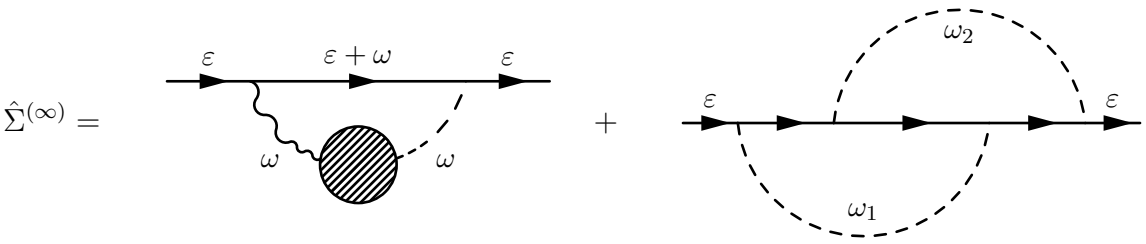

FIGURE 4.5: Feynman diagrams corresponding to the direct and exchange parts of the all-orders correlation potential in the Feynman method.

potential. The all-orders screened Coulomb interaction with the hole-particle interaction can be included into the Feynman diagrams by replacing the Coulomb lines and the polarisation operator in the Feynman diagrams in Eq. (4.3) with the renormalised Coulomb and polarisation operators shown in Figure 4.4.

Mathematically, the direct and exchange parts of the second-order correlation potential in the Feynman method are [c.f. Eq. (4.4)],

$$\Sigma^{(2)}_{\rm dir}(\boldsymbol{r}_1,\boldsymbol{r}_2;\varepsilon) = \int d^3r_i\, d^3r_j \int \frac{d\omega}{2\pi}\, G_{12}(\varepsilon+\omega) Q_{1i}\Pi_{ij}(\omega) Q_{j2} \tag{4.31}$$

$$\Sigma^{(2)}_{\rm x}(\boldsymbol{r}_1,\boldsymbol{r}_2;\varepsilon) = -\int d^3r_i\, d^3r_j \int \frac{d\omega_1}{2\pi} \int \frac{d\omega_2}{2\pi}\, G_{1i}(\varepsilon+\omega_1) Q_{1j} \times G_{ij}(\varepsilon+\omega_1+\omega_2) Q_{i2} G_{j2}(\varepsilon+\omega_2) \tag{4.32}$$

Including the all-orders screened Coulomb operator with the hole-particle interaction, and the polarisation operator into the second-order Feynman diagrams defines the all-orders correlation potential,

$$\Sigma^{(\infty)}_{\rm dir}(\boldsymbol{r}_1,\boldsymbol{r}_2;\varepsilon) = \int d^3r_i\, d^3r_j \int \frac{d\omega}{2\pi}\, G_{12}(\varepsilon_v+\omega) Q_{1i}\widetilde{\Pi}_{ij}(\omega) \widetilde{Q}_{j2} \tag{4.33}$$

$$\Sigma^{(\infty)}_{\rm x}(\boldsymbol{r}_1,\boldsymbol{r}_2;\varepsilon) = -\int d^3r_i\, d^3r_j \int \frac{d\omega_1}{2\pi} \int \frac{d\omega_2}{2\pi}\, G_{1i}(\varepsilon+\omega_1) \widetilde{Q}_{1j}(\omega_1) \times G_{ij}(\varepsilon+\omega_1+\omega_2) \widetilde{Q}_{i2}(\omega_2) G_{j2}(\varepsilon+\omega_2). \tag{4.34}$$

This is shown diagramatically in Figure 4.5. Note that the all-orders screened Coulomb interaction replaces only one of the Coulomb lines in the direct diagram but both in the exchange diagram. This is because replacing both of the Coulomb lines in the direct diagram would actually over-count the contribution from the infinite series of insertions into the $Q\Pi Q$ loop.

5

Theoretical implementation of the Breit interaction into the Feynman method

In this chapter I will show how the Breit interaction can be included into the Feynman method for perturbation theory, and in particular into the Green's function. I will first outline how the exchange potential is included into the Green's function in AMPSCI, and then describe how applying this to the Breit interaction is not straightforward, and instead a more generic formula is desirable. I will then proceed to explain two methods I have tried to include Breit into the Green's function that get around the complicated mathematical structure of the Breit interaction.

5.1 The exchange potential

In order to understand how the Breit interaction is to be constructed, I will first outline how the exchange matrix is normally constructed in AMPSCI so that the problems with applying the same method to the Breit interaction will be clear. The action of the exchange potential on a Dirac spinor is given by the second term of Eq. (2.33),

$$[\hat{V}_{\mathrm{x}}\phi_a](\boldsymbol{r}) = -\sum_{b\neq a}^{\mathrm{core}} \int \frac{\phi_b^\dagger(\boldsymbol{r}')\phi_a(\boldsymbol{r}')}{|\boldsymbol{r}-\boldsymbol{r}'|}\, d^3\boldsymbol{r}'\, \phi_b(\boldsymbol{r}). \tag{5.1}$$

In atomic physics calculations, a separable solution in the radial and angular coordinates is assumed for each single-particle Dirac spinor,

$$\phi_{n\kappa m}(\boldsymbol{r}) = \frac{1}{r}\begin{pmatrix} f_{n\kappa}(r)\Omega_{\kappa m}(\theta,\phi) \\ ig_{n\kappa}(r)\Omega_{-\kappa,m}(\theta,\phi)\end{pmatrix}, \tag{5.2}$$

where n is the principle quantum number, $\kappa = (l-j)(2j+1)$ is the Dirac relativistic quantum number, $m = j_z$ is the projection of $\boldsymbol{j} = \boldsymbol{l} + \boldsymbol{s}$ onto the z-axis, and Ω is a spherical spinor,

$$\Omega_{\kappa m}(\theta,\phi) = \begin{pmatrix}1\\0\end{pmatrix} Y_{l,m-1/2}(\theta,\phi)\langle l, m-\tfrac{1}{2};\tfrac{1}{2},\tfrac{1}{2}|jm\rangle + \begin{pmatrix}0\\1\end{pmatrix} Y_{l,m+1/2}(\theta,\phi)\langle l, m+\tfrac{1}{2};\tfrac{1}{2},-\tfrac{1}{2}|jm\rangle, \tag{5.3}$$

with Y_{lm} a spherical harmonic of degree l and order m, and $\langle j_1, m_1; j_2, m_2|J, M\rangle$ is a Clebsch-Gordon coefficient [19]. This can be substituted into Eq. (5.1), as well as the Laplace expansion of the Coulomb operator in terms of radial and angular variables,

$$\frac{1}{|\boldsymbol{r}-\boldsymbol{r}'|} = \sum_{k=0}^{\infty} \frac{4\pi}{2k+1} \frac{r_<^k}{r_>^{k+1}} \sum_{q=-k}^{k} Y_{kq}^*(\theta,\phi) Y_{kq}(\theta',\phi'), \tag{5.4}$$

where $r_<$ ($r_>$) is the lesser (greater) of r and r', to get a separable integral in the radial and angular coordinates. The angular integral and the summation over q can be done analytically to leave us with

$$[\hat{V}_{\mathrm{x}} F_a](r) = -\frac{1}{[j_a]} \sum_{b}^{\text{core}} \sum_{k=0}^{\infty} (C_{ba}^k)^2 y_{ba}^k(r) F_b(r), \tag{5.5}$$

where $F_a(r)$ is a radial Dirac spinor,

$$F_a(r) = \begin{pmatrix} f(r) \\ g(r) \end{pmatrix}, \tag{5.6}$$

C_{ba}^k is a standard angular coefficient proportional to a Clebsch-Gordon coefficient, and y_{ba}^k is the Hartree screening function, defined as

$$y_{ba}^k(r) = \int_0^\infty dr' \, \frac{r_<^k}{r_>^{k+1}} \left[f_b(r') f_a(r') + g_b(r') g_a(r') \right] = \int_0^\infty dr' \, \frac{r_<^k}{r_>^{k+1}} F_b^\dagger(r') F_a(r'). \tag{5.7}$$

In order to include the exchange interaction into the Green's function through the Dyson equation, as discussed in the previous chapter, we need an expression for the exchange potential as a coordinate operator $V_{\mathrm{x}}(r_1, r_2)$. This can be done by noting that, in terms of this coordinate operator, the action of the exchange potential on a radial Dirac spinor should be given by

$$[V_{\mathrm{x}} F_a](r) \equiv \int_0^\infty dr' \, V_{\mathrm{x}}(r, r') F_a(r). \tag{5.8}$$

If we expand out Eq. (5.5) in terms of the Hartree screening function in Eq. (5.7) then we can see that this equation is just equal to

$$[V_{\mathrm{x}} F_a](r) = -\frac{1}{[j_a]} \int_0^\infty dr' \sum_{b}^{\text{core}} \sum_{k=0}^{\infty} (C_{ba}^k)^2 \frac{r_<^k}{r_>^{k+1}} F_b^\dagger(r') F_a(r') F_b(r). \tag{5.9}$$

Comparing this to Eq. (5.8) reveals that the exchange potential coordinate matrix can be written as

$$V_{\mathrm{x}}(r,r') = -\frac{1}{[j_a]}\sum_{b}^{\mathrm{core}}\sum_{k=0}^{\infty}(C^k_{ba})^2\frac{r^k_<}{r^{k+1}_>}F_b(r)F^\dagger_b(r'), \tag{5.10}$$

which can easily be confirmed by multiplying this onto $F_a(r')$ from the left and integrating over r' and comparing to Eq. (5.5).

In principle, constructing the radial Breit operator would require the same process of extracting out the coordinate Breit operator from the known action of the Breit HF operator on a single-particle operator. However, the action of the Breit HF potential on a single-particle operator takes on the much more complicated form,

$$[V_{\mathrm{Br}}F_i](r) = -\frac{1}{[j_i]}\sum_{b}^{\mathrm{core}}\sum_{k}\left\{\left(C^k_{bi}\right)^2\left[m^{k(ib)}_{bi}+o^{k(ib)}_{bi}+p^{k(ib)}_{bi}\right]+\left(C^k_{-b,i}\right)^2 n^{k(ib)}_{bi}\right\}F_b(r). \tag{5.11}$$

Each term in this expression will be explained in detail in Section 7.2.1, but what is important is that each of the screening functions, m, n, o and p are not diagonal in spinor space, and so the Breit potential will have a much more complicated spinor structure compared to the exchange potential. Furthermore, although determining coordinate operators in the way outlined above for the exchange potential can be applied in general, in cases such as the Breit interaction, the corresponding equations can be very complicated. In this case, a more general way of including a potential into the Green's function through the Dyson equation is desirable. The rest of this chapter is devoted to determining such a method, with the aim of applying it to the Breit interaction.

5.2 Method 1: Approximate inclusion of the Breit interaction

The first attempt I have made at including the Breit interaction into the Green's function is to not try and construct V_{Br} as a coordinate matrix, but instead to use the fact that the expression for $[V_{\mathrm{Br}}F_a](r)$ is known [Eq. (5.11)] and can be calculated inside AMPSCI. This allows us to calculate $\mathbf{V}_{\mathrm{Br}}\mathbf{G}_0$ directly according to,

$$[V_{\mathrm{Br}}G_0](r_1,r_2;\varepsilon) = \hat{V}_{\mathrm{Br}}\sum_i\frac{F_i(r_1)F^\dagger_i(r_2)}{\varepsilon-\bar{\varepsilon}_i} = \sum_i\frac{[V_{\mathrm{Br}}F_i](r_1)F^\dagger_i(r_2)}{\varepsilon-\bar{\varepsilon}_i}, \tag{5.12}$$

where the F_i are radial eigenspinors of the local Hartree-Fock equation *without exchange* and the sum over i extend over the complete eigenbasis of the local HF equation. In practice, this sum must be truncated, so this becomes over a sum over a set of approximately complete eigenstates of the Hartree equation. This basis can be constructed in a number of ways, such as a spline basis, which is what I have employed here. Eq. (5.12) can therefore be used to calculate the one-body Breit contribution to the second order valence energies in singly-ionised radium, as shown in Table 5.1. This calculation has been done using a basis size of 80.

This ion was chosen because electrons in the francium-isoelectronic sequence demonstrate very large Breit corrections of f orbitals at second order in MBPT. Therefore, these ions will provide a good test ground for the implementation of the Breit interaction in the Feynman method. Also shown in this table are the one-body Breit corrections calculated using the standard (Goldstone) method of MBPT. If this (approximate) inclusion of the one-body part of the Breit interaction into the Feynman method is valid, then the Breit corrections between the two methods should agree.

TABLE 5.1: Comparison of the one-body Breit contribution to the second-order valence energy corrections of Ra^+ in units of cm^{-1} using the Goldstone method and the approximate inclusion into the Feynman method [Eq. (5.12)] using 80 basis states. The percentage error between the approximate Feynman method inclusion and the Goldstone method is shown in the last column.

			2nd order $B^{(1)}$ correction		
State	E_{CHF}	$\delta_{\mathrm{HF}}E$	Goldstone	Feyn., method 1	Error
$7s_{1/2}$	−75897.40	25.53	−12.36	−126.69	924.7%
$8s_{1/2}$	−36859.90	9.55	−2.88	−28.51	891.3%
$7p_{1/2}$	−56878.10	51.76	1.14	−93.66	−8330.6%
$8p_{1/2}$	−30052.87	20.13	−0.48	−28.54	5846.7%
$7p_{3/2}$	−52905.62	18.22	−7.17	−90.65	1164.3%
$8p_{3/2}$	−28502.15	7.44	−2.48	−28.92	1064.8%
$6d_{3/2}$	−62355.65	−52.67	−13.93	−139.62	902.4%
$7d_{5/2}$	−31203.54	−13.98	−2.82	−22.86	710.6%
$5f_{5/2}$	−28660.44	−20.43	−174.57	−166.41	−4.7%
$6f_{5/2}$	−18791.95	−25.45	−76.33	−66.24	−13.2%
$7f_{5/2}$	−13169.19	−21.80	−21.78	−16.37	−24.9%
$7f_{7/2}$	−13171.17	−22.19	−28.18	−17.91	−36.4%
$8f_{7/2}$	−9679.45	−16.71	−10.07	−3.96	−60.7%

We can see from the final column in Table 5.1 that the error between the inclusion of the Breit interaction into the Goldstone method and the inclusion of the Breit interaction into the Green's function in the Feynman method using method 1 is quite large, seeming to disagree much more for the s, p and d orbitals than the f orbitals. The error between the Breit corrections in the two approaches are quite large, and this may be due to the slow convergence of the summation in Eq. (5.12). Since the sum in this equation is over eigenstates of the particular ion we are interested in, this basis becomes numerically expensive to calculate for heavy ions, and while also becoming less complete. While this method of including Breit into the Green's function might prove effective, it will be convenient to develop a construction that can be applied more universally without worrying about the problem of convergence.

5.3 Method 2: Exact inclusion of the Breit interaction

Given the failure of the approximate method outlined above, I have tried a different method of including the Breit interaction into the Green's function. The radial HF Breit operator

that we are looking for is defined as

$$V_{\rm Br}(r_1, r_2) = \langle r_1 | \hat{V}_{\rm Br} | r_2 \rangle. \tag{5.13}$$

We can insert a resolution of the identity operator in terms of a complete set of orthonormal single-particle spinors into this expression

$$V_{\rm Br}(r_1, r_2) = \langle r_1 | \hat{V}_{\rm Br} \left(\sum_i |F_i\rangle\langle F_i| \right) |r_2\rangle = \sum_i \langle r_1 | \hat{V}_{\rm Br} | F_i \rangle F_i^\dagger(r_2) \tag{5.14}$$

and then the identity operator resolved in radial coordinate space

$$V_{\rm Br}(r_1, r_2) = \sum_i \langle r_1 | \hat{V}_{\rm Br} \left(\int dr\, |r\rangle\langle r| \right) |F_i\rangle\langle F_i | r_2\rangle = \sum_i \int dr\, V_{\rm Br}(r_1, r) F_i(r) F_i^\dagger(r_2). \tag{5.15}$$

The integral over r can be identified as the HF Breit operator acting on the radial spinor $F_i(r)$,

$$\int dr\, V_{\rm Br}(r_1, r) F_i(r) \equiv [\hat{V}_{\rm Br} F_i](r_1), \tag{5.16}$$

which can be calculated inside AMPSCI. Therefore, Eq. (5.15) can be rewritten as

$$V_{\rm Br}(r_1, r_2) = \sum_i [\hat{V}_{\rm Br} F_i](r_1) F_i^\dagger(r_2). \tag{5.17}$$

The benefits of this second method for the inclusion of Breit over the first method are firstly that the sum over i in this expression is over *any* complete set of orthonormal single-particle orbitals. Therefore, to calculate the radial HF Breit operator using Eq. (5.17), we can use, for example, the hydrogen wave functions as our basis, which are much more numerically efficient to calculate than Hartree eigenstates (they are in fact just the usual Dirac equation hydrogenic radial wave functions), and do not depend on the ion that we are studying. Since we can efficiently generate a large basis, the sum over states should in principle converge more quickly than the sum in the previous method. The second benefit of this method is that this simple formula can be applied to construct the coordinate representation of any operator $\mathbf{V}$, so long as the corresponding expression for $[VF_i](r)$ is known. As we will see later, however, this formula will not be sufficient for energy-dependent interactions.

In order to test that this method works numerically then, I have applied Eq. (5.17) to calculate the coordinate matrix of the exchange potential by replacing $V_{\rm Br}$ with $V_{\rm x}$. I used 90 hydrogenic wave functions constructed in a cavity of radius 90 a.u. and have compared the second order radium valence energy corrections (without any inclusion of Breit) from this method to the way that AMPSCI normally calculates the exchange matrix [using Eq. (5.10)], the results of which are shown in Table 5.2. Also included in this table is the result from not including the negative energy states in the summation in Eq. (5.17). Since the Dirac equation predicts both positive and negative energy ($\varepsilon < -mc^2$) states, a complete set of radial spinors should include both. However, since the Breit interaction has historically had

TABLE 5.2: Comparison of the second-order valence energies in Ra^+ using different methods of constructing the exchange matrix to be included in the Green's function, in units of cm^{-1}. The standard method is outlined in Ref. [61], while the alternative method uses Eq. (5.17) with 90 hydrogenic wave functions in a cavity size of 90 a.u. This method was performed once including negative energy states and once excluding negative energy states. The column labelled 'Error' gives the percentage error with respect to the standard method of constructing the exchange matrix.

		Method 2 for exchange matrix			
	Std. method	Negative energy states included		Negative energy states excluded	
State	$E + \delta^{(2)} E_C$	$E + \delta^{(2)} E_C$	Error	$E + \delta^{(2)} E_C$	Error
$7s_{1/2}$	−83881.692	−83936.304	0.065%	−83939.029	0.068%
$8s_{1/2}$	−38908.341	−38921.44	0.034%	−38922.762	0.037%
$7p_{1/2}$	−61440.475	−61442.965	0.004%	−61447.832	0.012%
$8p_{1/2}$	−31511.163	−31501.506	−0.031%	−31503.237	−0.025%
$7p_{3/2}$	−56284.93	−56292.457	0.013%	−56297.641	0.023%
$8p_{3/2}$	−29659.255	−29651.121	−0.027%	−29652.958	−0.021%
$6d_{3/2}$	−71380.138	−71494.608	0.160%	−71498.321	0.166%
$7d_{5/2}$	−32789.581	−32804.808	0.046%	−32806.905	0.053%
$5f_{5/2}$	−34453.783	−34474.874	0.061%	−34480.045	0.076%
$6f_{5/2}$	−23170.601	−23184.194	0.059%	−23187.548	0.073%
$7f_{5/2}$	−15670.042	−15673.775	0.024%	−15675.44	0.034%
$7f_{7/2}$	−15477.938	−15480.415	0.016%	−15482.384	0.029%
$8f_{7/2}$	−11058.892	−11059.282	0.004%	−11060.366	0.013%

fundamental difficulties with negative energy states, it may be interesting to test if including the negative energy states leads to any significant difference. The exchange matrix should not have any such fundamental conflict, so I have tested if excluding the negative energy states in this construction of V_x leads to any significant change. As Table 5.2 shows, this method of calculating the exchange matrix, regardless of whether we include or exclude the negative energy states leads to almost the same energies as the way that it is calculated in AMPSCI. Therefore, this method of constructing the exchange potential coordinate matrix does indeed work.

As such, I have subsequently constructed the Breit HF operator using this method and have calculated the (one-body) Breit corrections to the second-order valence energy corrections in the Feynman approach, and compared it to the same correction but calculated in the Goldstone method. This is shown in Table 5.3. We can see that the one-body Breit corrections to s, p and d valence energies still differ significantly between the Feynman and Goldstone methods, while the corrections to f states agree well. This may be because the corrections to these latter orbitals are so much larger than the former that we are encountering less numerical noise, and the Breit corrections therefore agree much more robustly. Furthermore, we see that the error is universally lower with this method of including Breit into the Green's function if we exclude the negative energy states than if we retain them.

This is interesting since it is the opposite trend to what we saw when we constructed the exchange matrix in this way. There may therefore be some fundamental problem with using negative energy states in this method of constructing the Breit HF operator, which may be related to the theoretical difficulties in the past involving the use of the Breit interaction with negative energy states.

Table 5.3: Comparison of the second-order, one-body Breit correction to the valence energies in Ra^+ between the Goldstone method and the Feynman method using Eq. (5.17) to include the Breit interaction into the Green's function. The Goldstone corrections were calculated using a basis size of 80, while the Feynman corrections were calculated using 90 hydrogenic wave functions in a cavity size of 90 a.u. If the inclusion of Breit into the Feynman method is correct then the Goldstone and Feynman corrections should agree, with the columns labelled "Error" giving the percentage error between the Feynman correction and the Goldstone correction.

			Goldstone	Feyn., Method 2, $-E$ states incl.		Feyn., Method 2, $-E$ states excl.	
State	E_{CHF}	$\delta_{\mathrm{HF}}E$	$\delta^{(2)}E,\ B^{(1)}$	$\delta^{(2)}E,\ B^{(1)}$	Error	$\delta^{(2)}E,\ B^{(1)}$	Error
$7s_{1/2}$	−75897.40	25.526	−12.363	−2.096	−83.05%	−4.06	−67.20%
$8s_{1/2}$	−36859.90	9.552	−2.876	1.979	−168.81%	0.92	−132.02%
$7p_{1/2}$	−56878.10	51.765	1.138	15.295	1244.02%	11.38	900.00%
$8p_{1/2}$	−30052.87	20.134	−0.48	4.814	−1102.92%	3.43	−813.75%
$7p_{3/2}$	−52905.62	18.222	−7.17	10.76	−250.07%	6.29	−187.80%
$8p_{3/2}$	−28502.15	7.44	−2.483	3.782	−252.32%	2.21	−188.88%
$6d_{3/2}$	−62355.65	−52.669	−13.929	−8.797	−36.84%	−13.56	−2.62%
$7d_{3/2}$	−31574.97	−8.314	−0.895	4.623	−616.54%	2.99	−433.74%
$8d_{3/2}$	−19450.60	−3.117	−0.456	2.73	−698.68%	1.87	−510.75%
$6d_{5/2}$	−61592.27	−69.59	−24.269	−6.217	−74.38%	−10.32	−57.46%
$7d_{5/2}$	−31203.54	−13.982	−2.82	4.03	−242.91%	2.40	−185.21%
$8d_{5/2}$	−19261.02	−5.898	−1.231	2.391	−294.23%	1.53	−224.05%
$5f_{5/2}$	−28660.44	−20.434	−174.568	−162.108	−7.14%	−167.40	−4.11%
$6f_{5/2}$	−18791.95	−25.45	−76.334	−65.616	−14.04%	−68.99	−9.62%
$7f_{5/2}$	−13169.19	−21.804	−21.785	−16.11	−26.05%	−17.74	−18.57%
$8f_{5/2}$	−9684.33	−16.528	−6.163	−2.948	−52.17%	−3.84	−37.73%
$5f_{7/2}$	−28704.99	−21.405	−166.244	−146.534	−11.86%	−149.71	−9.95%
$6f_{7/2}$	−18811.72	−26.24	−84.565	−69.412	−17.92%	−71.83	−15.05%
$7f_{7/2}$	−13171.17	−22.19	−28.185	−20.409	−27.59%	−21.69	−23.03%
$8f_{7/2}$	−9679.45	−16.706	−10.071	−5.748	−42.93%	−6.47	−35.74%

Although the error here is lower than it was using the first method (Table 5.1), the corrections here still do not agree closely enough to consider this implementation "equivalent" to the implementation of the Breit interaction into the Goldstone method. For example, we can see that in the case of a large number of states, the correction predicted by the Feynman method is opposite in sign to the Goldstone correction, as in the case of the $8s_{1/2}$, $8p_{1/2}$, $7p_{3/2}$, and $7d_{5/2}$ states. While it is expected that the Feynman and Goldstone corrections won't exactly match due to the numerical differences inherent in performing numerical integrations over frequency rather than a sum over states, we should at least expect the corrections to be the same sign (unless they are so small that numerical instability determines the correction).

This hints that there is some aspect of the code or the implementation of the Feynman

method itself that is causing this difference. The most obvious explanation is that because the Breit interaction has a complicated spinor structure, the spinor structure of the rest of the Feynman diagrams is causing these issues. Indeed, as there are several known problems regarding the spin structure of the Feynman diagrams as they are calculated inside AMPSCI, this is the most likely cause. The next chapter will be devoted to discussing and resolving these issues.

6 Structure of the Feynman method

Based on the results I have presented in the previous chapter, the way in which the Feynman method is implemented into AMPSCI needs to be resolved in order that the Breit interaction can be included into the Feynman method of perturbation theory. I will firstly start by discussing how the polarisation operator and Green's functions are constructed in the program, and why they are inadequate for including the Breit interaction into the Green's function. I will then correct the full spinor structure of the Green's function, and then derive the correct form of the polarisation operator to be used in the direct diagram.

6.1 Relativistic components of the correlation potential

One place that may be affecting the implementation of the Breit interaction is in how the non-relativistic components of the correlation potential are dealt with in the Feynman method. As discussed for the Goldstone method in Section 3.1.3, the correlation potential, in addition to having coordinate indices, is also a matrix in (radial) spinor space,

$$\Sigma^{(2)}(r_1, r_2; \varepsilon) = \begin{pmatrix} \Sigma^{(2)}_{ff}(r_1, r_2; \varepsilon) & \Sigma^{(2)}_{fg}(r_1, r_2; \varepsilon) \\ \Sigma^{(2)}_{gf}(r_1, r_2; \varepsilon) & \Sigma^{(2)}_{gg}(r_1, r_2; \varepsilon) \end{pmatrix}, \tag{6.1}$$

where f and g denote respectively the relativistic and non-relativistic components. In the Goldstone method, once the whole correlation potential has been constructed, only the ff component is kept to calculate the second-order correlation correction to the energy of a valence state. As we saw in Section 3.1.3, this only leads to a meaningful amount of error when calculating the very small two-body Breit corrections. A similar procedure is carried out in the Feynman method in which only the ff component of the correlation potential

is calculated and retained for calculations of the energy correction. However, unlike in the Goldstone method where the full potential is calculated exactly, and then the non-relativistic components are discarded at the end of the calculation, in the Feynman method, at no point is the full correlation potential constructed. In AMPSCI, only the ff component of the Green's function is calculated, which is then used to calculate the ff component of the correlation potential. However, only constructing the ff component of the Green's function leaves out information that would be required to calculate the exact ff component of the correlation potential. To see why, recall that the exchange and Breit interactions are included into the Green's function through the Dyson equation,

$$\mathbf{G} = \mathbf{G}_0(\mathbf{1} - \mathbf{V}\mathbf{G}_0)^{-1}. \tag{6.2}$$

Numerically speaking, the Green's function, exchange matrix, etc. are each constructed as 2×2 matrices in spinor space, each of whose components is an $N \times N$ coordinate matrix, where N is the number of grid points used to represent the coordinate space over which our operators are defined. Thus, an arbitrary operator in the Feynman method has the form

$$\mathbf{O} = \begin{bmatrix} \begin{pmatrix} O_{ff}(r_1,r_1) & O_{ff}(r_1,r_2) & \cdots \\ O_{ff}(r_2,r_1) & O_{ff}(r_2,r_2) & \cdots \\ \vdots & \vdots & \ddots \end{pmatrix} & \begin{pmatrix} O_{fg}(r_1,r_1) & O_{fg}(r_1,r_2) & \cdots \\ O_{fg}(r_2,r_1) & O_{fg}(r_2,r_2) & \cdots \\ \vdots & \vdots & \ddots \end{pmatrix} \\ \begin{pmatrix} O_{fg}(r_1,r_1) & O_{fg}(r_1,r_2) & \cdots \\ O_{fg}(r_2,r_1) & O_{fg}(r_2,r_2) & \cdots \\ \vdots & \vdots & \ddots \end{pmatrix} & \begin{pmatrix} O_{gg}(r_1,r_1) & O_{gg}(r_1,r_2) & \cdots \\ O_{gg}(r_2,r_1) & O_{gg}(r_2,r_2) & \cdots \\ \vdots & \vdots & \ddots \end{pmatrix} \end{bmatrix}, \tag{6.3}$$

and to invert this $2N \times 2N$ matrix, as required by the Dyson equation, we can use either of the two equivalent formulae [113],

$$\begin{pmatrix} A & B \\ C & D \end{pmatrix}^{-1} = \begin{pmatrix} A^{-1} + A^{-1}B(D - CA^{-1}B)^{-1}CA^{-1} & -A^{-1}B(D - CA^{-1}B)^{-1} \\ -(D - CA^{-1}B)^{-1}CA^{-1} & (D - CA^{-1}B)^{-1} \end{pmatrix} \tag{6.4}$$

$$= \begin{pmatrix} (A - BD^{-1}C)^{-1} & -(A - BD^{-1}C)^{-1}BD^{-1} \\ -D^{-1}C(A - BD^{-1}C)^{-1} & D^{-1} + D^{-1}C(A - BD^{-1}C)^{-1}BD^{-1} \end{pmatrix}. \tag{6.5}$$

Thus, even though in practice we only ever include the upper-left component of the correlation potential in calculations of energy corrections, we actually need to know *every* component of the Green's function in order to invert the Dyson equation exactly, and hence to calculate the 2nd order correlation potential in the Feynman method [c.f. Eq. (4.31)]. In the current way in which calculations are performed in the Feynman method, only the upper-left component of the Green's function is calculated, which means that the Dyson equation is not solved exactly.

6.2 The local Green's function

In order to construct the full Green's function, we consider the inhomogenous radial Hartree equation,

$$[\varepsilon - h_l(r)]F(r) = S(r), \tag{6.6}$$

where $h_l(r) = h_0(r) + V_{\text{dir}}(r)$ is the local part of the single-particle Dirac-Hartree-Fock equation, and $S(r)$ is some nonzero radial (spinor) source term. To find what $F(r)$ is, we can find the Green's function of this equation [Eq. (4.6)], satisfying,

$$[\varepsilon - h_l(r)]G_0(r_1, r_2) = \delta(r_1 - r_2), \tag{6.7}$$

from which $F(r)$ can be constructed as

$$F(r) = \int_0^\infty G_0(r, r')S(r')\,dr'. \tag{6.8}$$

Here there is an implicit contraction over the inner spin index of $G_0^{\alpha\beta}(r_1, r_2)$ and the spin index of $S_\beta(r_2)$. Since the solution of Eq. (6.6) will need to satisfy the boundary conditions $F(r) \to 0$ as $r \to 0$ and $r \to \infty$, variation of parameters can be used to find a solution for $F(r)$ that solves Eq. (6.6) subject to these boundary conditions. This has the integral representation [61, 111],

$$F(r) = \frac{1}{w}\chi_\infty(r)\int_0^r \chi_0^\dagger(r')S(r')\,dr' + \frac{1}{w}\chi_0(r)\int_r^\infty \chi_\infty^\dagger(r')S(r')\,dr'. \tag{6.9}$$

Here, χ_0 and χ_∞ are the solutions of the homogeneous form of Eq. (6.6) [$S(r) = 0$] that are finite at $r \to 0$ and $r \to \infty$, respectively, and $w = [\chi_0^f(r)\chi_\infty^g(r) - \chi_\infty^f(r)\chi_0^g(r)]/\alpha$ can be shown to be an r-independent constant. Equating Eqs. (6.8) and (6.9) reveals that the local Green's function can be written as

$$G_0(r_1, r_2) = \begin{cases} \chi_0(r_1)\chi_\infty^\dagger(r_2), & r_1 < r_2 \\ \chi_\infty(r_1)\chi_0^\dagger(r_2), & r_1 > r_2. \end{cases} \tag{6.10}$$

Explicitly showing the spinor components, this becomes,

$$G_0(r_1, r_2) = \begin{cases} \begin{pmatrix} \chi_0^f(r_1)\chi_\infty^f(r_2) & \chi_0^f(r_1)\chi_\infty^g(r_2) \\ \chi_0^g(r_1)\chi_\infty^f(r_2) & \chi_0^g(r_1)\chi_\infty^g(r_2) \end{pmatrix}, & r_1 < r_2 \\ \begin{pmatrix} \chi_\infty^f(r_1)\chi_0^f(r_2) & \chi_\infty^f(r_1)\chi_0^g(r_2) \\ \chi_\infty^g(r_1)\chi_0^f(r_2) & \chi_\infty^g(r_1)\chi_0^g(r_2) \end{pmatrix}, & r_1 > r_2. \end{cases} \tag{6.11}$$

Implementing this expression into AMPSCI to replace the existing form of the local Green's function (which just has the ff component) will therefore allow me to construct the full Green's function exactly.

6.3 The polarisation operator

Another operator that needs to be adjusted if I want to calcuate the correlation potential exactly in the Feynman method is the polarisation operator, which corresponds to the fermion loop in the first diagram of Eq. (4.3), and which has the form,

$$\Pi(r_1, r_2; \omega) = \int \frac{d\varepsilon}{2\pi} G(r_i, r_j; \varepsilon) G(r_j, r_i; \varepsilon + \omega). \tag{6.12}$$

Although the polarisation operator can be calculated according to this integral, it is expensive to do this frequency integral numerically in addition to the other one required to evaluate this diagram [see Eq. (4.4)]. Because of this it is convenient to perform the frequency integral in the polarisation operator analytically. Doing so gives

$$\mathbf{\Pi}(\omega) = i \sum_a |a\rangle \left[\mathbf{G}^{\mathrm{ex}}(\varepsilon_a + \omega) + \mathbf{G}^{\mathrm{ex}}(\varepsilon_a - \omega)\right] \langle a|, \tag{6.13}$$

where the sum over a is over the core orbitals and $\mathbf{G}^{\mathrm{ex}}(\varepsilon)$ is the Green's function restricted to only include the excited orbitals [61, 106, 114]. This formula is unclear in terms of the spin indices of each object, and different expressions exist in the literature for the implied spin structure of Eq. (6.13). In practice, this doesn't affect the calculations since only the ff component of each object in the expression for the polarisation operator is used to construct it (at least in AMPSCI), and this is insensitive to what the correct spin structure is. As I will show below, however, the polarisation operator should actually have no spinor indices.

Since I want to exactly calculate the correlation potential, so for this purpose it is necessary that I use the correct form of the polarisation operator. In Appendix C I provide my own derivation of the second-order direct Feynman diagram using time-dependent perturbation theory, from which the exact form of the polarisation operator can be deduced. Although this sort of calculation has been performed before in other quantum many-body contexts, as far as I know there is no resource in the atomic physics literature that derives these specific diagrams in the exact mathematical form in which they are evaluated here, e.g. with only the time-component of the electron propagator Fourier-transformed. The details of this calculation can be found in Appendix C, but the main result is Eq. (C.19), which gives the correct structure of the polarisation operator as

$$\Pi(\boldsymbol{x}, \boldsymbol{y}; \omega) = \int \frac{d\varepsilon}{2\pi} G_{\mu\nu}(\boldsymbol{y}, \boldsymbol{x}; \varepsilon) G^{\nu\mu}(\boldsymbol{x}, \boldsymbol{y}; \varepsilon + \omega) \tag{6.14}$$

$$= \int \frac{d\varepsilon}{2\pi} \mathrm{Tr}\left[G(\boldsymbol{y}, \boldsymbol{x}; \varepsilon) G(\boldsymbol{x}, \boldsymbol{y}; \varepsilon + \omega)\right], \tag{6.15}$$

where μ, ν are spinor indices that are being implicitly summed over. Performing the integration over ω analytically results in the expression in Eq. (C.32),

$$\Pi(\boldsymbol{x}, \boldsymbol{y}; \omega) = i \sum_a^{\mathrm{core}} \left[\phi_a^\dagger(\boldsymbol{x}) G^{\mathrm{ex}}(\boldsymbol{x}, \boldsymbol{y}; \varepsilon_a - \omega) \phi_a(\boldsymbol{y}) + \phi_a^\dagger(\boldsymbol{y}) G^{\mathrm{ex}}(\boldsymbol{y}, \boldsymbol{x}; \varepsilon_a + \omega) \phi_a(\boldsymbol{x})\right], \tag{6.16}$$

where I have suppressed the summation over the spinor indices implied in the product $\psi^\dagger G\psi$. The radial component of the polarisation operator is therefore given by

$$\Pi(r_1, r_2; \omega) = i \sum_a^{\text{core}} \left[F_a^\dagger(r_1) G^{\text{ex}}(r_1, r_2; \varepsilon_a - \omega) F_a(r_2) + F_a^\dagger(r_2) G^{\text{ex}}(r_2, r_1; \varepsilon_a + \omega) F_a(r_1) \right], \tag{6.17}$$

which can be simplified by noting that the radial CHF eigenspinors F_i are real, so this whole expression is symmetric in r_1 and r_2, meaning the polarisation operator can be written as

$$\Pi(r_1, r_2; \omega) = i \sum_a^{\text{core}} F_a^\dagger(r_1) \left[G^{\text{ex}}(r_1, r_2; \varepsilon_a - \omega) + G^{\text{ex}}(r_1, r_2; \varepsilon_a + \omega) \right] F_a(r_2). \tag{6.18}$$

I have calculated the Breit corrections to the valence energies of caesium using the complete form for the Green's function as well as the exact form of the polarisation operator, and the results are shown in the column labelled 'Full Π, G' in Table 6.1, from which we can see that the corrections agree with the Goldstone corrections much better now for every state compared to the 'Standard Π, G' column, and in every case resolves the issue in the sign of the correction. For example, the $8s_{1/2}$, $8p_{1/2}$ and $7p_{3/2}$ corrections are now all the same sign and the correct order of magnitude. However, there are still some states, namely the $p_{1/2}$ and $d_{3/2}$ states, for which the Goldstone and Feynman methods disagree quite prominently. This is an unexpected result since it's not just all p states that suffer this issue, but specifically the $p_{1/2}$, and similarly for the $d_{3/2}$ states. This is likely due to the fact that the $j = l - 1/2$ states (e.g. $p_{1/2}$ and $d_{3/2}$) are more relativistic than the $j = l + 1/2$ states [45], and so experience larger corrections due to the inclusion of the Breit interaction.

What is important to note, however, is that while there are still some states for which the Goldstone and Feynman method corrections don't agree, it is clear that using all of the components of the Green's function and the exact form of the polarisation operator is very important in establishing physical equivalence between the Goldstone and Feynman methods at second order in perturbation theory for the core-valence correlations. Although it has been conventional to only use the ff component of the Green's function in previous calculations using the Feynman method, with a minimal loss of accuracy, my calculations establish that this is not sufficient when attempting to include the one-body part of the Breit interaction into correlation corrections.

6.4 Choice of grid

At this stage, my implementation of the one-body part of the Breit interaction into the Feynman method – with my second method of constructing $V_{\text{Br}}(r_1, r_2)$, the full spinor matrix for the Green's function and the complete polarisation operator – should be theoretically equivalent to the implementation in the Goldstone method, as analytical integration of the expression for the direct diagram with the BCHF Green's function (obtained by solving the Dyson equation with V_{Br}) should give exactly the same second order energy with Breit

included as the first term on the right-hand side of Eq. (3.4). As there are still some states, however, whose energy corrections do not agree between the two methods, there is still some source of numerical difference that must be causing this. The most obvious possible cause is that in calculating the second-order energy correction, anytime the action of V_{Br} occurs on a state in the Goldstone method, this is done analytically by summing over core states using Eq. (5.11), whereas in the Feynman method, the equivalent action is being done using my form of the coordinate Breit operator as the integral,

$$[V_{\mathrm{Br}}F_i](r) = \int V_{\mathrm{Br}}(r,r')F_i(r')\,dr'. \tag{6.19}$$

Therefore, the only difference between the way that the HF Breit operator acts on orbitals between the Goldstone and Feynman methods is that the Feynman method involves an integration over coordinates, rather than a sum over states, as in the Goldstone method. The grid on which the HF Breit operator is defined, therefore, may be what's causing the difference in the Breit corrections between the two methods. By default, the code written in AMPSCI for the Feynman method defines the Green's functions and polarisation operators on a subgrid with 155 grid points from $10^{-4} \leq r \leq 29.4$, in atomic units. This is done as it is known that the correlation potential can be safely defined on a subgrid with minimal loss of accuracy. However, when including the Breit interaction into the Feynman method this may not be sufficient, and therefore could be the cause of the disagreement between the Breit corrections predicted by the two methods. Therefore, I have tried extending the range of the subgrid to be from $10^{-4} \leq r \leq 60$ with 132 points over the whole subgrid to see if this improves the agreement between the Breit corrections in the Feynman and Goldstone methods. The results of this are shown in the column labelled "Full Π, G, expanded grid" in Table 6.1.

We can see from this final column that indeed, the Feynman and Goldstone methods finally seem to agree relatively well, with agreement ranging between 0.1-20% for most states. The one exception is the correction to the energy of the $7d_{3/2}$ valence state, which has an error between the Goldstone correction of 69.66%. While this seems to be alarming, the correction to this state is actually much smaller than the corrections to the other states, and so we are likely just seeing numerical noise dominating this correction. Another thing to note is that while the agreement of the $p_{1/2}$ orbitals has increased, it is still markedly larger than the agreement between the corrections to most of the other states. Therefore, it seems that the problem with these particular orbitals is still present, but is greatly mitigated by this extension of the subgrid. Although the error for these states still seem to be quite large, with -15% and -21% for the $7p_{1/2}$ and $8p_{1/2}$ states, respectively, the actual corrections seem to agree closely; the Goldstone corrections for the $7p_{1/2}$ and $8p_{1/2}$ states are 1.142 and -0.358, respectively, while the corresponding Feynman corrections with the extended subgrid are 0.97 and -0.43, respectively, both of which are relatively close. Therefore, it seems that increasing the subgrid has greatly improved the results of my implementation of the Breit interaction into the Feynman method, and therefore permits us to apply this to calculations where Breit is included to all orders of perturbation theory.

An interesting observation is that increasing the maximum radius on which the subgrid is defined made a very large difference to the results, when it would be expected that this

Table 6.1: Comparison of one-body Breit corrections to valence removal energies in Ra^+ in the Goldstone method (second column) to the Feynman method corrections. The third column gives the corrections calculated in the Feynman method with the current implementation of the Green's function G and polarisation operator Π in AMPSCI (incorrect spinor structure for Π and incomplete G), the next column gives the corrections with my corrected versions of G and Π but on the default subgrid choice, and the final column gives the corrections with the corrected G, Π, and on an extended subgrid.

		Feynman					
	Goldstone	Standard Π, G		Full Π, G		Full Π, G, expanded grid	
State	$B^{(1)}$	$B^{(1)}$	Error	$B^{(1)}$	Error	$B^{(1)}$	Error
$7s_{1/2}$	−12.368	−4.055	67.21%	−13.663	−10.47%	−12.38	−0.11%
$8s_{1/2}$	−2.469	0.921	137.30%	−2.799	−13.37%	−2.48	−0.36%
$7p_{1/2}$	1.142	11.38	896.50%	−4.819	−521.98%	0.97	−15.32%
$8p_{1/2}$	−0.358	3.426	1056.98%	−1.954	−445.81%	−0.43	−20.95%
$7p_{3/2}$	−7.17	6.295	187.80%	−11.05	−54.11%	−7.21	−0.61%
$8p_{3/2}$	−2.197	2.207	200.46%	−3.414	−55.39%	−2.23	−1.37%
$6d_{3/2}$	−13.937	−13.564	2.68%	−19.421	−39.35%	−13.29	4.63%
$7d_{3/2}$	−0.145	2.987	2160.00%	−1.086	−648.97%	−0.04	69.66%
$6d_{5/2}$	−24.279	−10.323	57.48%	−30.828	−26.97%	−25.49	−4.99%
$7d_{5/2}$	−1.96	2.403	222.60%	−3.13	−59.69%	−2.05	−4.64%
$5f_{5/2}$	−174.834	−167.397	4.25%	−178.731	−2.23%	−172.56	1.30%
$6f_{5/2}$	−77.252	−68.987	10.70%	−77.53	−0.36%	−85.54	−10.73%
$5f_{7/2}$	−166.437	−149.71	10.05%	−171.241	−2.89%	−172.558	−3.68%
$6f_{7/2}$	−84.766	−71.834	15.26%	−85.786	−1.20%	−85.541	−0.91%

would actually not make a very large difference. The reason that you wouldn't expect the maximum radius of the subgrid to make a big difference to the Breit corrections is that the Breit interaction is a relativistic effect, and it should therefore be much larger at distances close to the nucleus than it is at large distances from the nucleus. In particular, you would expect that within 30 Bohr radii of the nucleus, which is the maximum radius on which the subgrid is defined by default in AMPSCI, would be sufficient for defining V_{Br}, and therefore extending the cavity radius to 60 Bohr radii would be negligible. However, this clearly does make a large difference in improving the accuracy of the Breit corrections to valence energies. A possible explanation for this is that we are not directly using the HF Breit operator in calculating the second-order Feynman diagrams. Instead, we include the Breit operator into the Green's function through the Dyson equation and this involves inverting $\hat{V}_{\mathrm{Br}}\hat{G}_0$ in coordinate and spinor space. This inversion will become more accurate as we extend r_{max}, as we are effectively truncating the numerical representation of numerical space at a higher term. We wouldn't expect such a big difference if we didn't invert $\hat{V}_{\mathrm{Br}}\hat{G}_0$ when calculating the Green's function, since $V_{\mathrm{Br}}(r_1, r_2)$ would be small for large distances away from the nucleus.

7 Frequency-dependent Breit interaction

In this chapter I will discuss a generalisation of the Breit interaction known as the frequency-dependent Breit interaction. Like the regular Breit interaction that I have discussed so far in this thesis, it arises from perturbation theory in quantum electrodynamics, but differs from the regular Breit interaction in that it accounts for retardation effects to all orders in v/c. From a field-theoretic point of view, this interaction arises out of a $e^-e^- \to e^-e^-$ scattering event in which the electrons exchange only a single transverse photon, and depends on the energy of the scattered electrons. I will firstly start by explaining its origin from second-order perturbation theory in QED in the Coulomb gauge, and then discuss the theory necessary to include it into atomic structure calculations. The main results in this chapter are that I have identified and resolved a mistake in the textbook by Johnson [19], one of the main references for atomic theory, and my inclusion of the frequency-dependent Breit interaction into the Hartree-Fock procedure, which has not been done before in the literature.

7.1 Origin of the frequency-dependent Breit interaction

In Section 2.1 I presented the outline of a derivation for the Breit interaction from the QED scattering amplitude of two electrons exchanging a single photon. This derivation was performed in the Feynman gauge and in this gauge the Breit interaction arises as the lowest order relativistic correction (of order $1/c^2$) to the instantaneous charge-charge interaction between two particles. Alternatively, when the electromagnetic field is quantised in the *Coulomb gauge*, the frequency-independent Breit interaction instead arises due to the exchange of a single *transverse photon* between two electrons. In the Coulomb gauge, the

amplitude corresponding to the first diagram in Figure 2.1 is given by Eq. (2.14),

$$S_{fi} = \frac{-e^2}{2}\int d^4x \int d^4y\, D^C_{\mu\nu}(x,y) e^{ix_0(\varepsilon_a-\varepsilon_c)} e^{iy_0(\varepsilon_b-\varepsilon_d)} \bar{\psi}_a(\boldsymbol{x})\gamma^\mu\psi_c(\boldsymbol{x})\bar{\psi}_b(\boldsymbol{y})\gamma^\nu\psi_d(\boldsymbol{y}), \tag{7.1}$$

but the Feynman gauge photon propagator is now replaced with the Coulomb gauge photon propagator,

$$D^C_{\mu\nu}(x,y) = i\int \frac{d^4k}{(2\pi)^4}\frac{\Delta_{\mu\nu}}{k^2+i\varepsilon}e^{-ik\cdot(x-y)}, \tag{7.2}$$

where

$$\Delta_{ij} = \delta_{ij} - \frac{k_ik_j}{\boldsymbol{k}^2}, \quad \Delta_{00} = \frac{k^2}{\boldsymbol{k}^2}, \quad \Delta_{0i} = \Delta_{i0} = 0, \tag{7.3}$$

and $k^2 = k_0^2 - \boldsymbol{k}^2$. Note that $D^C_{00}(x,y)$ is just the Fourier component of the Coulomb interaction [38], so in the Coulomb gauge keeping only the time components in the sums over μ and ν in the scattering amplitude corresponds to the electrons interacting through only the Coulomb interaction. With this choice of gauge, then, the Coulomb interaction and the transverse electron interactions are completely separated; the temporal part of the propagator gives rise to the instantaneous Coulomb interaction, while the spatial, or transverse, parts of the photon propagator become

$$D^C_{ij}(x,y) = i\int \frac{d^4k}{(2\pi)^4}\frac{\Delta_{ij}}{k^2+i\varepsilon}e^{-ik\cdot(x-y)} \tag{7.4}$$

$$= i\int \frac{d^4k}{(2\pi)^4}\frac{\delta_{ij}-k_ik_j/\boldsymbol{k}^2}{k^2+i\varepsilon}e^{-ik\cdot(x-y)} \tag{7.5}$$

$$= i\int \frac{d^4k}{(2\pi)^4}\frac{\delta_{ij}}{k^2+i\varepsilon}e^{-ik\cdot(x-y)} - \frac{\partial^2}{\partial x^i\partial y^j}\int\frac{d^4k}{(2\pi)^4}\frac{1}{\boldsymbol{k}^2\,(k^2+i\varepsilon)}e^{-ik\cdot(x-y)}, \tag{7.6}$$

where we have used the fact that

$$\frac{\partial e^{-ik\cdot(x-y)}}{\partial x^i} = -ik_ie^{-ik\cdot(x-y)} \quad \text{and} \quad \frac{\partial e^{-ik\cdot(x-y)}}{\partial y^i} = ik_ie^{-ik\cdot(x-y)}. \tag{7.7}$$

Upon performing the integrals over the spatial components of the momenta in Eq. (7.6), we get

$$D^C_{ij}(x,y) = \int\frac{dk_0}{2\pi}\left[\frac{\delta_{ij}e^{ik_0r}}{r} - \frac{\partial^2}{\partial x^i\partial y^j}\left(\frac{e^{ik_0r}-1}{k_0^2r}\right)\right]e^{-ik_0(x_0-y_0)}, \tag{7.8}$$

where $r = |\boldsymbol{x}-\boldsymbol{y}|$. When we insert this into Eq. (2.14), performing the time integrations will force k_0 to be equal to the energy difference of the two electrons a and b, $k_0 = \varepsilon_a - \varepsilon_c = \omega_{ac}$ (which by overall energy conservation is equal to ω_{bd}), and therefore the scattering amplitude will become,

$$\mathcal{A}_{fi} = e^2\int d^3x\int d^3y\,\psi^\dagger_a(\boldsymbol{x})\alpha^i\psi_c(\boldsymbol{x})\left[\frac{\delta_{ij}e^{i\omega_{ac}r}}{r} - \frac{\partial^2}{\partial x^i\partial y^j}\left(\frac{e^{i\omega_{ac}r}-1}{\omega_{ac}^2r}\right)\right]\psi^\dagger_b(\boldsymbol{y})\alpha^j\psi_d(\boldsymbol{y}), \tag{7.9}$$

which resembles the matrix element of a two-body operator in non-relativistic quantum mechanics. If we neglect the frequency-dependence by setting $\omega_{ac} \to 0$, which retains only the terms of order $(v/c)^2$ (remembering that the Dirac matrices are of order v/c), then this reduces to the conventional Breit interaction. Therefore, in the Coulomb gauge, the Breit interaction corresponds to the lowest order correction to the Coulomb interaction in powers of e^2, *appropriate for small electron velocities*, e.g. in light atoms. Without setting $\omega_{ac} = 0$, the term in square brackets defines a more general version of the Breit interaction that depends on the energy of the exchanged transverse photon. This is called the *frequency-dependent* Breit interaction, or simply the transverse interaction,

$$H'_{\mathrm{Br}}(\omega) \equiv \alpha^i \alpha^j \left\{ \frac{\delta_{ij} \cos(\omega r)}{r} + \frac{\partial^2}{\partial r^i \partial r^j} \left[\frac{\cos(\omega r) - 1}{\omega^2 r} \right] \right\}. \tag{7.10}$$

Here, only the real part has been taken since this is what physically contributes to energy shifts [23], and I have defined the separation vector $r^i = x^i - y^i$ so that $\partial_{y^i} f(r) = -\partial_{r^i} f(r)$. What is important to note is that Eq. (7.10) is a non-local operator, and corresponds to the lowest order correction to the Coulomb interaction in powers of e^2 appropriate for *all* electron velocities, unlike the frequency-independent Breit interaction, which only holds in the limit where $v/c \ll 1$ [30]. While in theory the frequency-dependent form of the Breit interaction is what should always be used in atomic physics calculations, as it captures retardation effects to all orders, the frequency-dependent effects become significant only at order $(v/c)^4$, so are suppressed for all but very heavy ions [45, 115]. A numerical study of the frequency-dependent Breit interaction by Mann and Johnson [30] showed that for a selected range of atoms, the *first-order* energy shift associated with the frequency-dependent Breit interaction agrees with the corresponding energy shift due to the frequency-independent Breit interaction to within 1 eV for atoms with atomic masses up to $Z = 48$, but for heavier atoms than this the difference between the two energy shifts is significant, and grows with Z. Others [115, 116] have found similar scaling laws.

The studies cited above above all included the frequency-dependent Breit interaction only when calculating perturbative corrections to the valence energies of the systems they were interested in, but they did not include the frequency-dependent Breit interaction into the self-consistent HF procedure, which would have allowed for the inclusion of core-relaxation effects, since the core orbitals would have been solved for in the mean field generated by the frequency-dependent Breit interaction. As far as I am aware, no one has done this before, and while it is expected that the deviation of the frequency-dependent Breit interaction from the frequency-independent Breit interaction to the HF eigenvalues is small [45], it would provide a more complete and accurate inclusion of the Breit interaction into the study of atomic systems if we were to do so.

7.2 Inclusion into the Hartree-Fock procedure

In order to include the frequency-dependent Breit interaction into the Hartree-Fock procedure, the action of the frequency-dependent Breit HF operator on a single-particle orbital must be known. The derivation for this is very similar to that of the ordinary HF potential

and has been worked out by Lindroth et al. [45]. To first understand this, however, we note that the Coulomb and the frequency-independent Breit interactions can be included into the many-body Hamiltonian straightforwardly, since they are two-body operators dependent only on the coordinates of each pair of electrons. However, as Eq. (7.9) makes clear, the two-particle matrix element of the frequency-dependent Breit operator depends on the energies of either the incident or final electrons that are exchanging the transverse photon. In a $e^-e^- \to e^-e^-$ QED scattering amplitude, these energy differences are equal to each other due to conservation of 4-momentum for during scattering processes. However, when we include the frequency-dependent Breit interaction as an effective two-body operator into the full many-body Hamiltonian, we will have to evaluate matrix elements that are off-shell, i.e. where the total energy is not guaranteed to be conserved. It has been shown by Brown [117] and Mittleman [118–120] that the matrix element that should be used in this case is

$$\langle ab|H'_{\mathrm{Br}}|cd\rangle = \langle ab|\frac{1}{2}\left[H'_{\mathrm{Br}}(\omega_{ac}) + H'_{\mathrm{Br}}(\omega_{bd})\right]|cd\rangle, \tag{7.11}$$

where $\omega_{ij} = |\varepsilon_i - \varepsilon_j|/c$. It can be seen that if the electron pairs a and c, and b and d, satisfy the on-shell condition, $\omega_{ac} = \omega_{bd}$, then this reduces to what we would expect from the QED scattering amplitude. Therefore, when included into the full many-body Hamiltonian, a matrix element of the frequency-dependent Breit interaction takes on the expression in Eq. (7.11). In practice, this means that in second-quantised form, the operator that should be added to the many-body Hamiltonian is

$$\hat{H}'_{\mathrm{Br}} = \frac{1}{2}\sum_{ijkl}\langle ij|H'_{\mathrm{Br}}|kl\rangle\, a_i^\dagger a_j^\dagger a_l a_k = \frac{1}{2}\sum_{ijkl}\langle ij|\frac{1}{2}\left[H'_{\mathrm{Br}}(\omega_{ik}) + H'_{\mathrm{Br}}(\omega_{jl})\right]|kl\rangle\, a_i^\dagger a_j^\dagger a_l a_k. \tag{7.12}$$

It can then be shown, by minimising the expectation value of the full many-body Hamiltonian assuming a Slater determinant wave function (or in the language of second-quantisation, by normal-ordering the above expression with respect to the HF core), that this leads to an addition to the Hartree-Fock potential of the form [45]

$$V'_{\mathrm{Br}}|a\rangle = \frac{1}{2}\sum_{b}^{\mathrm{core}}\sum_{i}\left\{|i\rangle\langle ib|\left[H_{\mathrm{Br}} + H'_{\mathrm{Br}}(\omega_{ia})\right]|ab\rangle - |i\rangle\langle ib|\left[H'_{\mathrm{Br}}(\omega_{ab}) + H'_{\mathrm{Br}}(\omega_{ib})\right]|ba\rangle\right\}, \tag{7.13}$$

where the sum over i is over a complete set of orthonormal states. In contrast to the modification of the HF potential that comes from the frequency-independent Breit interaction, computing this expression requires a numerically expensive double summation.

Since the frequency-dependent Breit interaction is expected only to depend weakly on the frequency at which it is evaluated, it would therefore be advantageous to seek out a less computationally demanding potential to use instead of the one stated above. Eq. (7.13) was derived by demanding that the expectation value of the many-body Hamiltonian be minimised with respect to single substitutions in the Slater determinant wave function, but if we instead just minimise the expectation value of the Hamiltonian with respect to variations in the single-particle orbitals, then we would obtain a correction to the HF potential of the

form [45],

$$V''_{\mathrm{Br}}|a\rangle = -\sum_{b}^{\mathrm{core}}\langle b|H'_{\mathrm{Br}}(\omega_{ab})|a\rangle|b\rangle \tag{7.14}$$

which is just shorthand for the explicit coordinate space representation [cf. the exchange term in Eq. (2.33)],

$$[V''_{\mathrm{Br}}\phi_a](\boldsymbol{r}) = -\sum_{b}^{\mathrm{core}}\int d^3r'\,\phi_b^\dagger(\boldsymbol{r}')H'_{\mathrm{Br}}(\omega_{ab})\phi_a(\boldsymbol{r}')\phi_b(\boldsymbol{r}). \tag{7.15}$$

Note here that the direct contribution vanishes identically for closed-shell systems [30], which are the focus of this thesis. Note that this also means that the first term on the right-hand side of Eq. (7.13) vanishes. The spinor indices in Eq. (7.15) are being contracted as

$$\begin{aligned}\phi_i^\dagger(\boldsymbol{r}_1)H'_{\mathrm{Br}}(\omega_{ik})\phi_j(\boldsymbol{r}_1)\phi_k(\boldsymbol{r}_2) \equiv{}& \phi_i^{\dagger\mu}(\boldsymbol{r}_1)\boldsymbol{\alpha}_{\mu\nu}\phi_j^\nu(\boldsymbol{r}_1)\cdot\boldsymbol{\alpha}_{\rho\sigma}\phi_k^\sigma(\boldsymbol{r}_2)\frac{\cos(\omega_{ik}r)}{r}\\ &+\phi_i^{\dagger\mu}(\boldsymbol{r}_1)\boldsymbol{\alpha}_{\mu\nu}\phi_j^\nu(\boldsymbol{r}_1)\cdot\nabla_1\left\{\nabla_1\cdot\boldsymbol{\alpha}_{\rho\sigma}\phi_k^\sigma(\boldsymbol{r}_2)\left[\frac{\cos(\omega_{ik}r)-1}{\omega^2 r}\right]\right\},\end{aligned} \tag{7.16}$$

where $r = |\boldsymbol{r}_1 - \boldsymbol{r}_2|$ and ∇_1 denotes the gradient vector for the coordinates $\boldsymbol{r}_1$. It can easily be seen that the potential defined in Eq. (7.15) is non-Hermitian as

$$\langle\phi_j|V''_{\mathrm{Br}}|\phi_i\rangle = -\sum_{b}^{\mathrm{core}}\langle jb|H'_{\mathrm{Br}}(\omega_{ib})|bi\rangle, \tag{7.17}$$

while the transposed matrix element is

$$\langle\phi_i|V''_{\mathrm{Br}}|\phi_j\rangle = -\sum_{b}^{\mathrm{core}}\langle ib|H'_{\mathrm{Br}}(\omega_{jb})|bj\rangle, \tag{7.18}$$

which are clearly not equal (up to complex conjugation) due to the differing energy arguments [45]. This means that if the Hamiltonian were diagonalised over a set of basis states then its matrix representation would be non-hermitian, which would result in a non-orthogonal basis. This means that the usual formulas from second order perturbation theory could not be applied. However, if we only wish to include this potential into the self-consistent procedure for the core and valence states, then we do not need a representation of the complete basis, and this shouldn't be a problem we explicitly encounter. This will still mean we are solving a single-particle Dirac equation with a non-Hermitian potential, but the non-Hermiticity induced by the energy dependence is expected to be of relatively small order, and so should not spoil the convergence of the Hartree-Fock procedure. This will be done while also avoiding the numerical cost associated with a sum over a complete set of states that would be required in the Hermitian expression, Eq. (7.13).

7.2.1 Frequency-dependent Breit radial integrals

Having determined the form of the contribution to the frequency-dependent Breit operator to the HF potential to implement [Eq. (7.15)], we need to determine an explicit expression for the effective one-body matrix element $\langle b|H'_{\mathrm{Br}}(\omega_{ab})|a\rangle$. This matrix element is analogous to the effective one-body matrix element that is commonly defined for the exchange part of the HF potential [see Eq. (5.5)], and can generally be found by considering the complete two-body matrix element $\langle ib|H'_{\mathrm{Br}}(\omega_{ab})|aj\rangle$, and then undoing the integration over one of the pairs of coordinates. Since atomic physics calculations are commonly done by separating out the angular and radial dependence of the matrix elements, the matrix element $\langle ab|H'_{\mathrm{Br}}(\omega)|cd\rangle$ is expressed as a product of an angular part A^k_{abcd}, and a radial part $B^k_{abcd}(\omega)$, each with multipolarity k, such that

$$\begin{aligned}\langle ab|H'_{\mathrm{Br}}(\omega)|cd\rangle = &\iint d^3r_1\, d^3r_2\, \phi^\dagger_a(\boldsymbol{r}_1)\alpha^i\phi_c(\boldsymbol{r}_1) \\ &\times\left\{\frac{\delta_{ij}\cos(\omega r)}{r} + \frac{\partial^2}{\partial r^i \partial r^j}\left[\frac{\cos(\omega r)-1}{\omega^2 r}\right]\right\}\phi^\dagger_b(\boldsymbol{r}_2)\alpha^j\phi_d(\boldsymbol{r}_2)\end{aligned} \tag{7.19}$$

$$= \sum_{k=0}^{\infty} A^k_{abcd} B^k_{abcd}(\omega). \tag{7.20}$$

Details of the angular reduction can be found in Refs. [30] and [40]. The angular coefficient can be found in several resources, e.g. Ref. [19], and is just equivalent to a number. The radial integral $B^k_{abcd}(\omega)$ is given by

$$B^k_{abcd}(\omega) = (-1)^{k+|j_a-j_b|}\left\{C^k_{ac}C^k_{bd}\left[m^k_{abcd}(\omega)+o^k_{abcd}(\omega)+p^k_{abcd}(\omega)\right] + C^k_{-a,c}C^k_{-b,d}n^k_{abcd}(\omega)\right\}, \tag{7.21}$$

where I have adapted the notation of Ref. [61] used for the frequency-*independent* Breit radial integrals. The m and n terms are due to the Gaunt part of the frequency-dependent Breit interaction, while the o and p terms are due to the retardation interaction. Here C^k_{ij} is a standard angular coefficient that is not of interest to us. To understand where these frequency-dependent Breit radial integrals come from, it is instructive to first consider the equations that are used for the frequency-independent Breit interaction angular decomposition, equivalent to taking the limit as $\omega \to 0$ in all the above equations. In this limit, we define [19, 40],

$$s^k_{abcd} = \int_0^\infty dr_1 \int_0^\infty dr_2\, \frac{r^{k+1}_<}{r^{k+2}_>} Q^k_{ac}(r_1)P^k_{bd}(r_2) \tag{7.22}$$

$$t^k_{abcd} = \int_0^\infty dr_1 \int_0^\infty dr_2\, \frac{r^{k-1}_<}{r^{k}_>} P^k_{ac}(r_1)Q^k_{bd}(r_2) \tag{7.23}$$

$$u^k_{abcd} = \int_0^\infty dr_1 \int_0^\infty dr_2\, \frac{r^{k}_<}{r^{k+1}_>} X^k_{ac}(r_1)X^k_{bd}(r_2) \tag{7.24}$$

$$\begin{aligned}v^k_{abcd} = &\int_0^\infty dr_1 \int_0^{r_1} dr_2 \left(\frac{r^{k-1}_<}{r^{k}_>} - \frac{r^{k+1}_<}{r^{k+2}_>}\right) Q^k_{ac}(r_1)P^k_{bd}(r_2) \\ &+ \int_0^\infty dr_1 \int_{r_1}^\infty dr_2 \left(\frac{r^{k-1}_<}{r^{k}_>} - \frac{r^{k+1}_<}{r^{k+2}_>}\right) P^k_{ac}(r_1)Q^k_{bd}(r_2),\end{aligned} \tag{7.25}$$

where we have defined for convenience,

$$P^k_{ij}(r) = \frac{\kappa_i - \kappa_j}{k} X_{ij}(r) - Y_{ij}(r) \quad \text{and} \quad Q^k_{ij}(r) = \frac{\kappa_i - \kappa_j}{k+1} X_{ij}(r) + Y_{ij}(r), \tag{7.26}$$

where

$$X_{ij}(r) = F^\dagger_i(r)\theta_x F_j(r) = f_i(r)g_j(r) + g_i(r)f_j(r), \tag{7.27}$$

$$Y_{ij}(r) = F^\dagger_i(r)\theta_y F_j(r) = f_i(r)g_j(r) - g_i(r)f_j(r), \tag{7.28}$$

and where the radial spin matrices θ_x and θ_y are defined as

$$\theta_x = \begin{pmatrix} 0 & 1 \\ 1 & 0 \end{pmatrix} \quad \text{and} \quad \theta_y = \begin{pmatrix} 0 & 1 \\ -1 & 0 \end{pmatrix}. \tag{7.29}$$

Then, the frequency-independent form of the radial integrals defined in Eq. (7.21) are given by

$$m^k_{abcd} = \frac{k+1}{2k+3} s^k_{abcd} + \frac{k}{2k-1} t^k_{abcd} \tag{7.30}$$

$$n^k_{abcd} = -\frac{(\kappa_a + \kappa_c)(\kappa_b + \kappa_d)}{k(k+1)} u^k_{abcd} \tag{7.31}$$

$$o^k_{abcd} = -\frac{(k+1)^2}{(2k+1)(2k+3)} s^k_{abcd} - \frac{k^2}{(2k+1)(2k-1)} t^k_{abcd} \tag{7.32}$$

$$p^k_{abcd} = -\frac{k(k+1)}{2(2k+1)} v^k_{abcd}. \tag{7.33}$$

Johnson [19] says that to obtain the frequency-dependent Breit integrals in Eq. (7.21), the formulas (7.30)-(7.33) still hold, provided that in Eqs. (7.22)-(7.24) we make the replacement

$$\frac{r^k_<}{r^{k+1}_>} \to -\omega(2k+1) j_k(\omega r_<) y_k(\omega r_>), \tag{7.34}$$

where $j_k(x)$ and $y_k(x)$ are spherical Bessel functions of the first and second kind, respectively, and we replace the entirety of Eq. (7.25) by

$$\begin{aligned} -2 \int_0^\infty dr_1 \int_0^{r_1} dr_2 \Bigg\{ & \left[\omega j_{k-1}(\omega r_<) y_{k+1}(\omega r_>) + \frac{2k+1}{\omega^2} \frac{r^{k-1}_<}{r^{k+2}_>} \right] Q^k_{ac}(r_1) P^k_{bd}(r_2) \\ & + \omega j_{k+1}(\omega r_<) y_{k-1}(\omega r_>) P^k_{ac}(r_1) Q^k_{bd}(r_2) \Bigg\}. \end{aligned} \tag{7.35}$$

It is clear that the replacement stated in Eq. (7.34) will recover the correct limit since [30]

$$\lim_{\omega \to 0^+} -\omega(2k+1) j_k(\omega r_<) y_k(\omega r_>) = \frac{r^k_<}{r^{k+1}_>}. \tag{7.36}$$

However, the replacement recommended in Eq. (7.35) clearly cannot be correct as this replacement should recover Eq. (7.25) in the frequency-independent limit. But the second line of v^k_{abcd} has an integral over r_2 from r_1 up to ∞, which clearly cannot be recovered from the single integral in Eq. (7.35) in the limit that $\omega \to 0$. This indicates that the expression recommended by Johnson cannot be correct. Finding the correct formula to replace Eq. (7.34) would in principle require either performing the angular reduction of Eq. (7.19) or by seeking the correct formula from an alternative resource. While the angular reduction could be done, it is in practice very lengthy, requiring the expansion of $\cos(\omega r)$ and $\phi_i^\dagger \boldsymbol{\alpha} \phi_j$ in terms of scalar and vector spherical harmonics and spherical Bessel functions. Furthermore, although there exist other papers that outline the angular reduction [121–123], the former two references perform the expansion using different normalisation conventions, and the latter performs the reduction using a technique known as the Racah algebra, which results in a much more complicated final expression. Instead, a more straightforward way to determine what the correct equations should be is to determine the limiting behaviour of Eq. (7.35), and then make an educated guess at the correct expression. The reason that this seems like a valid course of action is that the equations stated in Ref. [19] come from a previous paper written by the same author [30], in which the exchange matrix element $\langle ab|H'_{\mathrm{Br}}|ba\rangle$ is evaluated. Their expression for this matrix element is correct, and is predicted correctly by Eq. (7.35). Therefore, the generic two-body matrix element $\langle ab|H'_{\mathrm{Br}}|cd\rangle$ is likely to be close to Eq. (7.35).

In order to determine the correct expression, it is first necessary to evaluate the limiting behaviour of Eq. (7.35). To do so, we can expand the spherical Bessel functions of the first and second kind in powers of ω,

$$j_k(\omega r) = \omega^k \left[\frac{r^k}{(2k+1)!!} - \frac{r^{k+2}\omega^2}{2(2k+3)!!} + \mathcal{O}(\omega)^3 \right] \tag{7.37}$$

$$y_k(\omega r) = -\omega^{-k} \left[\frac{r^{-k-1}(2k-1)!!}{\omega} + \frac{r^{-k+1}(2k-3)!!\omega}{2} + \mathcal{O}(\omega)^2 \right], \tag{7.38}$$

where the double factorial $(2x+1)!!$ denotes the product of all odd numbers less than or equal to $2x+1$. Using these definitions we can find the series expansion for the first term in the square brackets in Eq. (7.35),

$$\begin{aligned} \omega j_{k-1}(\omega r_<) y_{k+1}(\omega r_>) = \omega \cdot \omega^{k-1} &\left\{ \frac{r_<^{k-1}}{[2(k-1)+1]!!} - \frac{r_<^{k-1+2}\omega^2}{2[2(k-1)+3]!!} + \mathcal{O}(\omega)^3 \right\} \\ &\times -\omega^{-(k+1)} \left\{ \frac{r_>^{-(k+1)-1}[2(k+1)-1]!!}{\omega} \right. \\ &\left. + \frac{r_>^{-(k+1)+1}[2(k+1)-3]!!\omega}{2} + \mathcal{O}(\omega)^2 \right\} \end{aligned} \tag{7.39}$$

$$= -\frac{2k+1}{\omega^2}\frac{r_<^{k-1}}{r_>^k} - \frac{1}{2}\frac{r_<^{k-1}}{r_>^{k+2}} + \frac{1}{2}\frac{r_<^{k+1}}{r_>^{k+2}} - \frac{\omega^2}{4}\frac{r_<^{k+1}}{r_>^k} + \mathcal{O}(\omega)^4. \tag{7.40}$$

In the limit that $\omega \to 0$ the final two terms go to zero, and so the first integral in Eq. (7.35),

in the frequency-independent limit, reduces to

$$-2\int_0^\infty dr_1\int_0^{r_1} dr_2\left[-\frac{2k+1}{\omega^2}\frac{r_<^{k-1}}{r_>^{k+2}}-\frac{1}{2}\frac{r_<^{k-1}}{r_>^{k}}+\frac{1}{2}\frac{r_<^{k+1}}{r_>^{k+2}}+\frac{2k+1}{\omega^2}\frac{r_<^{k-1}}{r_>^{k+2}}\right]Q^k_{ac}(r_1)P^k_{bd}(r_2)$$
$$=\int_0^\infty dr_1\int_0^{r_1} dr_2\left(\frac{r_<^{k-1}}{r_>^{k}}-\frac{r_<^{k+1}}{r_>^{k+2}}\right)Q^k_{ac}(r_1)P^k_{bd}(r_2), \tag{7.41}$$

which is exactly just the first line of Eq. (7.25). Therefore, the first part of the replacement recommended by Johnson indeed reduces to the correct expression in the limit of zero frequency. Following the same procedure as carried out above, the second term in the recommended replacement has the series expansion,

$$\omega j_{k+1}(\omega r_<)y_{k-1}(\omega r_>)=-\omega^3\left[\frac{r_<^{k+1}}{(2k+3)!!}-\frac{r_<^{k+3}\omega^2}{2(2k+5)!!}+\mathcal{O}(\omega)^3\right]$$
$$\times\left[\frac{r_>^{-k}(2k-3)!!}{\omega}+\frac{r_>^{-k+2}(2k-5)!!\omega}{2}+\mathcal{O}(\omega)^2\right]. \tag{7.42}$$

It is clear that every term in this expansion will be of order ω^2 or higher, so this entire term reduces to zero in the limit that $\omega\to 0$, and so Eq. (7.35) reduces only to the first line of Eq. (7.25) in the frequency-independent limit. Therefore, the correct expression that should replace both lines of Eq. (7.25) should be Eq. (7.35) but with an extra term containing an r_2 integral that goes from r_1 up to infinity, which in the $\omega\to 0$ limit gives the second line of Eq. (7.25). But since the integrand in both lines of Eq. (7.25) are the same, with the exception that $Q^k\leftrightarrow P^k$, one candidate for the correct expression would be the one recommended by Johnson, with an additional integral of the exact same form, except with the r_2 integral now going from r_1 up to infinity, and with $P^k\leftrightarrow Q^k$ This would make the full frequency-dependent expression,

$$-2\int_0^\infty dr_1\int_0^{r_1} dr_2\left\{\left[\omega j_{k-1}(\omega r_<)y_{k+1}(\omega r_>)+\frac{2k+1}{\omega^2}\frac{r_<^{k-1}}{r_>^{k+2}}\right]Q^k_{ac}(r_1)P^k_{bd}(r_2)\right.$$
$$\left.+\,\omega j_{k+1}(\omega r_<)y_{k-1}(\omega r_>)P^k_{ac}(r_1)Q^k_{bd}(r_2)\right\}$$
$$-2\int_0^\infty dr_1\int_{r_1}^\infty dr_2\left\{\left[\omega j_{k-1}(\omega r_<)y_{k+1}(\omega r_>)+\frac{2k+1}{\omega^2}\frac{r_<^{k-1}}{r_>^{k+2}}\right]P^k_{ac}(r_1)Q^k_{bd}(r_2)\right. \tag{7.43}$$
$$\left.+\,\omega j_{k+1}(\omega r_<)y_{k-1}(\omega r_>)Q^k_{ac}(r_1)P^k_{bd}(r_2)\right\}.$$

Because of the fact that the second and fourth lines in this equation vanish as $\omega\to 0$, it is possible that there should be other terms in this expression that also go to zero in the frequency-independent limit that are being missed. However, this choice seems more symmetric with regards to the two r_2 integrals. Furthermore, this formula reproduces the correct exchange matrix element given in Ref. [30]. Therefore, this expression will be taken to be

the appropriate one to replace Eq. (7.25) for the frequency-dependent Breit matrix element.

Now that I have defined the frequency-dependent Breit radial integrals, the frequency-dependent Breit potential can be explicitly constructed. This can be done in analogy with the frequency-independent case [61], by 'undoing' the integration over r_1 in the four frequency-dependent radial integrals. This defines four additional one-body Breit radial operators. For example, the frequency-*dependent* form of s^k_{abcd} in Eq. (7.22) is given by

$$s^k_{abcd}(\omega) = -\omega(2k+3)\int_0^\infty dr_1 \int_0^\infty dr_2\, j_{k+1}(\omega r_<) y_{k+1}(\omega r_>) Q^k_{ac}(r_1) P^k_{bd}(r_2) \tag{7.44}$$

$$= -\omega(2k+3)\int_0^\infty dr_1 \int_0^\infty dr_2\, j_{k+1}(\omega r_<) y_{k+1}(\omega r_>) P^k_{bd}(r_2) \times F^\dagger_a(r_1)\left(\frac{\kappa_a-\kappa_c}{k+1}\theta_x + \theta_y\right) F_c(r_1), \tag{7.45}$$

which can be written as the matrix element of an effective one-body operator $s^{k(ac)}_{bd}(\omega)$,

$$\langle F_a | s^{k(ac)}_{bd}(\omega) | F_c\rangle \equiv \int_0^\infty dr_1\, F^\dagger_a(r_1) s^{k(ac)}_{bd}(r_1;\omega) F_c(r_1) = s^k_{abcd}(\omega), \tag{7.46}$$

where

$$s^{k(ac)}_{bd}(r_1;\omega) = -\omega(2k+3)\int_0^\infty dr_2\, j_{k+1}(\omega r_<) y_{k+1}(\omega r_>) P^k_{bd}(r_2)\left(\frac{\kappa_a-\kappa_c}{k+1}\theta_x + \theta_y\right). \tag{7.47}$$

This means, for example, that the frequency-dependent operator corresponding to Eq. (7.30) is given by

$$m^{k(ac)}_{bd}(r_1;\omega) = \frac{k+1}{2k+3} s^{k(ac)}_{bd}(r_1;\omega) + \frac{k}{2k-1} t^{k(ac)}_{bd}(r_1;\omega). \tag{7.48}$$

Similar expressions can be derived for the other Breit radial operators. The action of the frequency-dependent Breit potential on a single-particle orbital is therefore given by

$$[V''_{\rm Br}F_i](r) = -\frac{1}{[j_i]}\sum_b^{\rm core}\sum_k \Big\{ (C_{ib})^2 \left[m^{k(ib)}_{bi}(r;\omega_{ib}) + o^{k(ib)}_{bi}(r;\omega_{ib}) + p^{k(ib)}_{bi}(r;\omega_{ib})\right] + \left(C^k_{-b,i}\right)^2 n^{k(ib)}_{bi}(r;\omega_{ib})\Big\} F_b(r). \tag{7.49}$$

Note that the matrix element $\langle F_j | V''_{\rm Br} | F_i\rangle$ is zero unless $|F_i\rangle$ and $|F_j\rangle$ have the same Dirac quantum number κ.

7.2.2 Numerical application to the Hartree-Fock approximation

Having determined the equations to include into the Hartree-Fock method, we can now apply the frequency-dependent Breit interaction to the study of atomic systems. We can firstly test how the frequency-dependence at the Hartree-Fock level affects ions as a function of their

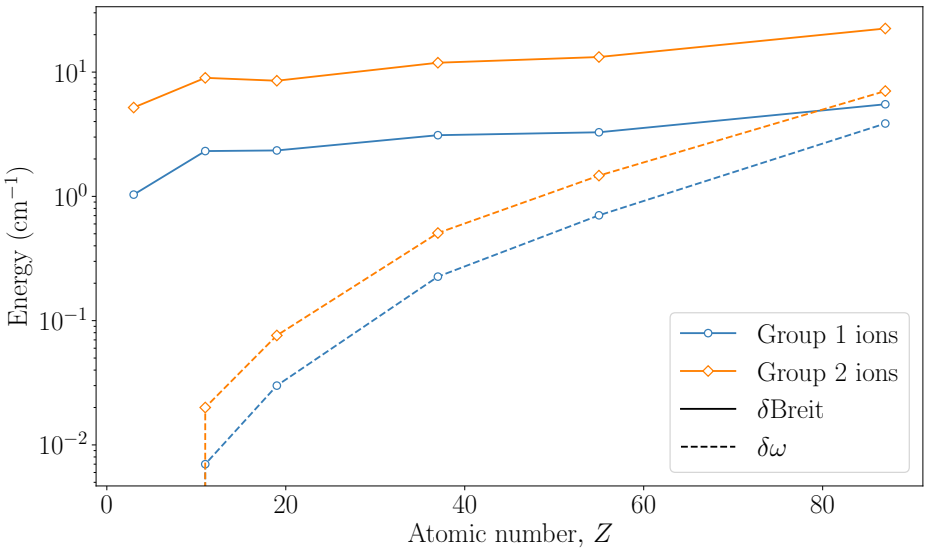

Figure 7.1: Scaling behaviour of the Breit and frequency-dependent corrections to the HF energy of the ground state for group-1 and group-2 atoms (cm^{-1}). The blue lines with hollow circles correspond to the group-1 atoms, while the blue lines correspond to the group-2 atoms. The correction to the CHF energy of the ground state due to the frequency-independent Breit interaction is denoted by the solid lines, while the correction to the Breit interaction after including frequency-dependence is denoted by the dashed lines. The total HF energy of each state is given by $\varepsilon_{\text{tot}} = \varepsilon_{\text{CHF}} + \delta\text{Breit} + \delta\omega$.

atomic number Z. I have done this calculation for the group-1 and the (singly-ionised) group-2 atoms, and this is shown in Figure 7.1. The solid line represents the size of the regular frequency-independent Breit correction to the HF energy, while the dashed line represents the frequency-dependent correction to the frequency-independent Breit energy. This means that the total correction to the energy due to the transverse interaction (frequency-dependent Breit interaction) is given by

$$\delta\varepsilon_{\text{tr}} = \delta\text{Breit} + \delta\omega. \tag{7.50}$$

As we can see from this figure, the scaling behaviour is almost identical for the two classes of ions, with the frequency-dependence being zero for the lightest atoms, and becomingly increasingly important for larger Z. One difference between the two groups of atoms, however, is that the Breit and frequency corrections to the HF energies of the group-1 ions (the blue solid and dashed lines, respectively) are for all values of Z smaller than the corresponding corrections to the group-2 ions (the orange solid and dashed lines, respectively). This is what we would expect since the group-2 ions are more highly charged as single valence systems, meaning the electrons are more relativistic, and so the frequency-dependence should be more important.

One other difference that we can see is that for almost all atoms, the frequency-dependent corrections are an order of magnitude smaller than the much larger frequency-independent Breit correction. However, for the heaviest group-1 ion, francium, the frequency-dependent correction is the same order of magnitude as the regular Breit correction. This is a particularly important result as it implies that the frequency-dependence plays a significant

role in the transverse electron-electron interactions at the level of the HF approximation for the ground state of this particular ion. Indeed, we see that although the similarity isn't as close for the group-2 ions, a similar trend can be seen for the heaviest ions. However, we need to keep in mind that the Breit correction to the ground $7s$ state in francium is not very large by itself, and so although the frequency-dependent correction to the Breit interaction is comparable in size to the Breit correction, the total correction due to the transverse electron-electron interactions is still not particularly large. However, for the highest accuracy, this frequency-dependence may need to be accounted for in the HF procedure.

7.3 Inclusion into perturbation theory

In the previous section, we determined the equations required to include the frequency-dependent Breit interaction into the Hartree-Fock procedure, and found that the frequency-dependence became more important for heavier, and more highly charged systems, which is to be expected for a small relativistic correction to the regular, frequency-independent Breit interaction.

In principle, the next step would be to try and include the frequency-dependent Breit interaction into perturbative calculations. If we tried, however, to apply the frequency-dependent Breit interaction into perturbation theory, we would encounter numerical difficulties. The main problem is that if we wish to include the one-body part of the frequency-dependent Breit interaction into the correlation potential, this would require generating a basis of HF eigenstates by diagonalising the HF Hamiltonian using a spline basis. But this will not work using the potential in Eq. (7.14), since this is not Hermitian. The correct prescription would be to use the potential defined in Eq. (7.13) in the diagonalisation procedure, however, as we have mentioned previously, this requires a numerically expensive double sum. For heavy ions, where a relatively large basis of $\gtrsim 50$ states is required, this would be impractical to calculate. Because the frequency-dependence is expected to lead to only small modifications at the level of the HF approximation, however, and since the frequency-dependence can reasonably be expected to be smaller still at second order in perturbation theory, we could simply neglect the frequency-dependence beyond the HF approximation. Although this will mean that the frequency-dependence can't be included into the all-orders calculations, for example, this will aid in the computational efficiency of the calculations, and I expect that this will capture the most important frequency-dependent effects, although this should be checked at some stage in the future. This treatment is similar to that of Johnson et al. [124] in calculating energy levels along the sodium isoelectronic sequence. There, the authors use the frequency-dependent Breit interaction in calculating *first-order* energy shifts, and then the frequency-independent form when calculating second- and third-order perturbative corrections. The treatment here would differ in the fact that I am including the frequency-dependent Breit interaction into the self-consistent field process, and so we would be accounting for an additional effect known as core relaxation that is missed by just treating it as a first order perturbation. Note that the reason that the authors in [124] have to calculate first-order Breit corrections, but I never do, is because they do not include the Breit interaction into the construction of the HF potential, and so first-order corrections due

to the Breit interaction do not identically vanish.

To summarise, the frequency-dependent Breit interaction can be included into the HF frozen-core potential using Eq. (7.14), and then the perturbative corrections can be calculated with the inclusion of the frequency-independent Breit interaction. Since the frequency-dependence is only of order $(v/c)^4$, its inclusion only at the level of the HF approximation is expected to capture the most important frequency-dependence as we go to higher orders of perturbation theory.

In practice, trying to include the frequency-dependent Breit interaction at the level of the HF approximation for the core and valence states, and then calculating perturbative corrections by only including the frequency-independent Breit interaction into the basis is numerically unstable, and leads to nonphysically large corrections. From the point of view of the Feynman method, this has to do with the fact that the Green's function is highly sensitive to the orthogonality of the HF core states to the core states that are used to construct the Green's function. Since we are calculating the HF core states in the mean potential that is constructed from the frequency-dependent Breit interaction, while we are only including the frequency-independent Breit interaction into the Green's function, these states are not orthogonal, and so regular perturbation theory can't be applied.

One way to proceed from here would be to assume that the additional correction to energy levels, matrix elements, etc. in perturbation theory from including the one-body part of the frequency-dependent Breit interaction into these calculations would be negligible compared to the lowest-order correction at the HF approximation. If I were to assume this, then I could simply add the corrections at the level of the HF approximation due to the frequency-dependence of the Breit interaction into calculations that just used the frequency-independent Breit interaction. However, such a procedure would need to be validated by actually including the frequency-dependent Breit interaction into perturbation theory, and then checking that the higher order corrections indeed are small enough to be neglected. For the purposes of the all-orders calculations I will perform in the next chapter, however, I will not assume this and will omit the frequency-dependent Breit interaction from the calculations. Of course, this opens up the possibility of building on the work done in this chapter to determine some way of including the one-body part of the frequency-dependent Breit interaction into perturbative calculations.

8

Application to the francium isoelectronic sequence

In the preceding chapters, I have included the (one-body) Breit interaction into the Feynman method, and checked that the resulting corrections to valence energies at the second order of perturbation theory agree with those predicted by the Goldstone method. In this chapter, I will use the Feynman method to include the Breit interaction into the all-orders correlation potential and apply this to the calculation of the atomic properties of ions along the francium-isoelectronic sequence. In order to check the numerical impact that including the Breit interaction has to all-orders, I will first start by calculating the Breit correction to energies at the all-orders level, and compare this to the corrections at second order in perturbation theory. This analysis will be particularly important as it will allow us to check whether the very large Breit corrections to f states for these ions at second order are changed when we include the Breit interaction to all-orders in perturbation theory. Then, to determine whether including the Breit interaction into the all-orders calculations improves the *accuracy* of atomic structure calculations, I will calculate energy levels along the Fr-isoelectronic sequence, and compare my calculated values to experiment. Finally, I will calculate the fine structure intervals for these same ions, with the purpose of determining the impact of the Breit interaction on the accuracy of this more relativistic quantity.

To reiterate, calculations at the level of the HF approximation and second order in perturbation theory, with and without the one-body part of the Breit interaction, could already be done before this thesis. However, calculating the all-orders Feynman diagrams with the one-body part of the Breit interaction was not possible. Because I have included the Breit interaction into the Green's function, the all-orders correlation potential diagrams can now be calculated with the BCHF Green's function, thereby including the one-body part of the Breit interaction into all orders of perturbation theory.

8.1 All-orders Breit corrections to energy levels

TABLE 8.1: Breit corrections to energy levels of ions along the Fr-isoelectronic sequence (cm^{-1}). $\delta^{(2)}B$ gives the (one-body) Breit correction to the second-order energy correction while $\delta^{(\infty)}B$ gives the (one-body) Breit correction to the all-orders energy correction to the energy.

Fr			Ra^+			Ac^{2+}			Th^{3+}		
State	$\delta^{(2)}B$	$\delta^{(\infty)}B$	State	$\delta^{(2)}B$	$\delta^{(\infty)}B$	State	$\delta^{(2)}B$	$\delta^{(\infty)}B$	State	$\delta^{(2)}B$	$\delta^{(\infty)}B$
$7s_{1/2}$	-3.6	1.2	$7s_{1/2}$	13.4	19.3	$7s_{1/2}$	39.5	46.1	$5f_{5/2}$	-762.8	-748.4
$7p_{1/2}$	15.0	556.7*	$6d_{3/2}$	-65.6	-63.8	$6d_{3/2}$	-64.3	-64.1	$5f_{7/2}$	-904.3	-880.9
$7p_{3/2}$	0.8	2.3	$6d_{5/2}$	-94.8	-90.1	$6d_{5/2}$	-121.3	-117.1	$6d_{3/2}$	-48.1	-49.5
$6d_{3/2}$	-33.3	-29.5	$7p_{1/2}$	53.0	54.8	$5f_{5/2}$	-615.9	-587.7	$6d_{5/2}$	-134.1	-130.8
$6d_{5/2}$	-37.2	-33.0	$7p_{3/2}$	11.2	14.1	$5f_{7/2}$	-699.4	-661.1	$7s_{1/2}$	73.0	79.8
$8s_{1/2}$	0.6	1.3	$8s_{1/2}$	7.1	8.3	$7p_{1/2}$	103.4	105.8	$7p_{1/2}$	164.5	166.7
$8p_{1/2}$	5.1	155.6*	$5f_{5/2}$	-202.6	-131.0	$7p_{3/2}$	29.3	33.2	$7p_{3/2}$	54.0	57.7
$8p_{3/2}$	0.6	1.0	$5f_{7/2}$	-195.3	-128.1	$8s_{1/2}$	18.3	19.8	$8s_{1/2}$	33.6	35.2
$5f_{7/2}$	-0.5	-0.4	$8p_{1/2}$	19.8	20.4	$8p_{1/2}$	41.7	42.5	$8p_{1/2}$	69.9	70.8
$5f_{5/2}$	-0.5	-0.3	$8p_{3/2}$	5.3	6.2	$8p_{3/2}$	13.8	15.1	$8p_{3/2}$	26.0	27.3

* These values are likely caused by a numerical error in the calculation of $\Sigma_x^{(\infty)}$. See discussion in-text.

As a first test of the all-orders correlation potential method with the inclusion of the Breit interaction, I have calculated in Table 8.1 the one-body Breit correction at second order in perturbation theory, and at all orders in perturbation theory, to the lowest-lying valence states of the ions along the francium-isoelectronic sequence. We already know that the Breit interaction leads to a large correction to the d and f states for these ions, and so I can now determine whether the jump from second order to "all orders" makes a large difference. If we look at Table 8.1, we can see that for most states (except the $p_{1/2}$ states in francium, see below), the all-orders correction is very close to the second-order correction. This indicates that most of the Breit correction that we get from including Breit into the all-orders diagrams actually comes from its effect at second order, and we do not get much of an additional correction from the higher-order diagrams. Indeed, for all states but the $7s$ state in Fr, the all-orders correction is the same sign and order of magnitude as the second-order correction, being particularly close for the p and d states. The largest difference between the second-order corrections and the all-orders corrections are in the ground state of each ion, and in the f states of the two most relativistic ions Ac^{2+} and Th^{3+}. The difference is especially stark in the $7s$ ground state of Fr, where the all-orders Breit correction is half as large as the second-order correction but opposite in sign, indicating that the latter is actually completely cancelled due to the contributions from the higher order diagrams.

In terms of the f states, we can see that in Ra^+, Ac^{2+} and Th^{3+} the second-order Breit correction is very large, which is a known occurrence. The hope was that including the Breit interaction into the all-orders diagrams would lead to a significant modification of this correction, and this is partially true. For example, for the $5f_{5/2}$ state in Ra^+, the second-order Breit correction is $-202.6\,cm^{-1}$, while the all-orders Breit correction is reduced to $-131.1\,cm^{-1}$. While this is still an order of magnitude larger than the HF level Breit correction of $-20.4\,cm^{-1}$ (see Table 5.1), the perturbative correction is almost halved. Thus, although we are still left with a large Breit correction at the all-orders level, this shows that

the very large second-order correction is not a valid representation of how large the contribution from Breit is to these states in perturbation theory, with this large correction being significantly decreased when the higher order diagrams are taken into account. Although the difference is not as large for the f states of Ac^{2+} and Th^{3+}, we do still see meaningful differences between the second-order and all-orders Breit corrections.

If we look now to the Breit corrections to the $p_{1/2}$ states in Fr, the all-orders corrections to these orbitals, $556.7\,\mathrm{cm}^{-1}$ and $155.6\,\mathrm{cm}^{-1}$, respectively, are huge compared to the corresponding corrections at second order, which are $15\,\mathrm{cm}^{-1}$ and $5.1\,\mathrm{cm}^{-1}$, respectively. While it may seem that the jump from including Breit at second-order to all orders is leading to a large correction, this is actually due to a numerical error in evaluating the Feynman diagrams. From inspecting the individual contributions due to the direct and exchange diagrams in the code output, the exchange diagrams are actually contributing in a nonphysically large way to these states. To understand the source of this error, it is important to know that in AMPSCI, the all-orders exchange Feynman diagrams are not actually directly calculated, and instead are calculated by introducing an effective screening factor f for the Coulomb operator in the exchange diagram,

$$\widetilde{Q}_{ij} \approx f Q_{ij}. \tag{8.1}$$

Here, f is the ratio of the second-order direct diagram with the all-orders screened Coulomb interaction and the normal, second-order direct diagram (without the all-orders screening). Upon doing the analytical frequency integrations with this effective screening factor, the approximate all-orders exchange diagram can just be evaluated using the Goldstone method with the Coulomb operators in Eq. (8.1). Note this only approximates the all-orders exchange diagram, but this should in practice not be an issue since the contribution from the exchange diagram is known to be much smaller than the direct diagram. In most cases, these effective screening factors are sufficient to calculate the all-orders exchange diagram, however, when I try to calculate this diagram including Breit for the $p_{1/2}$ states in francium, these screening factors are orders of magnitude too large. This is what leads to the huge Breit corrections that we can see for francium in Table 8.1. For all the other states, the screening factors evaluate to what we would expect, so these Breit corrections are well-behaved. Although we could in principle avoid this source of numerical error by calculating the all-orders exchange diagrams directly, rather than using the effective screening factors in the Goldstone method, the attempts to do so inside AMPSCI have been unsuccessful. We suspect that this is due to the previously incorrect spinor structure of the Feynman diagrams. Now that I have corrected this, the possibility of including the full exchange diagrams in AMPSCI will be discussed more at the end of this chapter.

To summarise, including the Breit interaction into the all-orders Feynman diagram calculations does not in most cases lead to a significantly different correction compared to when we include Breit at only second order. This tells us that for most states the correction that the one-body part of the Breit interaction makes to energies in perturbation theory is mostly captured by its inclusion at second-order, and including it into the all-orders diagrams only leads to a small additional correction. The states for which including the Breit interaction

to all orders *does* have a large impact are the ground states of each ion, and also in the f states, where in some cases the contribution from the Breit interaction at second-order is almost halved from its contribution in the higher order diagrams taken into account in the all-orders Feynman diagram technique.

8.2 Energy levels

Having determined the impact that including the Breit interaction has at the all-orders level compared to second order, I have calculated the energy levels of Fr-like ions at the level of the Hartree-Fock approximation, second-order perturbation theory $\Sigma^{(2)}$, and the all-orders correlation potential $\Sigma^{(\infty)}$, with each of these being calculated with and without the inclusion of the one-body part of the Breit interaction. These results are shown in Tables 8.2-8.5. In addition to including the Breit interaction into the all-orders energy levels, I have also included radiative corrections from quantum electrodynamics. This was done using the QED radiative potential method [125], in which a local potential is added to the Hartree-Fock Hamiltonian that approximates the one-loop vacuum polarisation and self-energy corrections to the electron propagator,

$$V_{\rm rad}(\boldsymbol{r}) = V_{\rm Ueh}(r) + V_{\rm SE}^{\rm h}(r) + V_{\rm SE}^{\rm l}(r) + V_{\rm SE}^{\rm mag}(r), \tag{8.2}$$

where the first term represents the (finite-size) Uehling potential, the lowest-order correction to the Coulomb interaction due to vacuum polarisation [110], and the second, third and fourth terms represent, respectively, the high-frequency, low-frequency, and magnetic contributions to the electron self-energy. Including this potential into the Hartree-Fock equations leads to a large correction, particularly for states with $l > 0$, known as core relaxation, that would be missed if it was instead treated as a perturbation [126, 127]. The corrections to energy levels and matrix elements due to the QED radiative potential are important in relativistic systems, and including it at the same time as the Breit interaction has been shown to lead to important cancellations, so for high-accuracy calculations they should be included together. I have only included the QED radiative effects into the all-orders calculations, and not into the HF and second-order calculations, since corrections due to the inclusion of the QED radiative potential are known to be linear, and so the correction due to the radiative potential at the level of the HF approximation for the energy is essentially the same as the correction at the all-orders level. Furthermore, I have also verified that the QED correction at the all-orders level is the same regardless of whether we include Breit at the same time or not, indicating that the QED effects are still linear with the Breit interaction included into the all-orders correlation potential.

The first point to notice about each of these tables is that at the level of the Hartree-Fock approximation the agreement with experiment is relatively good, but there is a large jump in accuracy in going from HF to the level of second-order perturbation theory, where the deviation from experiment gets a lot smaller. This is particularly noticeable in the case of Th^{3+} where the HF approximation actually predicts the ground (valence) state as being $6d_{3/2}$, which is incorrect. This is corrected as we go to second order in perturbation theory,

Table 8.2: Calculated energy levels of Fr and comparison with experiment, in units of cm^{-1}. The calculated energy level is calculated at the Hartree-Fock (HF), second-order $\Sigma^{(2)}$, and all-orders levels $\Sigma^{(\infty)}$, with each level of calculation done with and without the inclusion of the one-body part of the Breit interaction. The all-orders calculations are also performed with the inclusion of the QED radiative potential in the $\Sigma^{(\infty)}$ + QED column. Experimental data from [128, 129].

	HF		$\Sigma^{(2)}$		$\Sigma^{(\infty)}$		$\Sigma^{(\infty)}$ + QED		
State	No Breit	Breit	No Breit	Breit	No Breit	Breit	No Breit	Breit	Expt.
$7s_{1/2}$	0	0	0	0	0	0	0	0	0
$7p_{1/2}$	9912	9920	13140	13159	11914	12469	11969	12491	12237
$7p_{3/2}$	11112	11110	14967	14971	13990	13991	13944	13946	13924
$6d_{3/2}$	14942	14923	16952	16923	16226	16196	16169	16138	16230
$6d_{5/2}$	14843	14822	17293	17260	16414	16380	16360	16325	16430
$8s_{1/2}$	16486	16481	20857	20861	19868	19868	19832	19833	19740
$8p_{1/2}$	19527	19526	24331	24340	23111	23265	23093	23239	23113
$8p_{3/2}$	19956	19951	24900	24904	23754	23753	23708	23708	23658
$7d_{3/2}$	21043	21030	25422	25418	24323	24314	24274	24265	24244
$7d_{5/2}$	21020	21008	25545	25539	24409	24398	24360	24350	24333
$9s_{1/2}$	21909	21904	26910	26914	25780	25780	25739	25738	25671
$5f_{7/2}$	21900	21894	27178	27181	25979	25978	25934	25932	
$5f_{5/2}$	21901	21894	27179	27182	25980	25979	25935	25933	
$6f_{7/2}$	24370	24364	29692	29695	28486	28484	28440	28439	
$6f_{5/2}$	24371	24365	29692	29696	28487	28485	28441	28440	

where the energy of the $5f_{5/2}$ state, the actual ground state, falls below $6d_{3/2}$. Furthermore, the agreement with experiment once again generally improves once we go to the all-orders correlation level, although the jump isn't as large. Therefore, as we go to higher orders of perturbation theory, the Breit and QED corrections start to play a more important role in reducing the deviation from experiment. Therefore, I will only discuss the last two columns of each table, which give the $\Sigma^{(\infty)}$ + QED corrections with and without the Breit interaction.

We see that in francium, the inclusion of the Breit interaction at the same time as the QED radiative potential does not generally make the agreement with experiment better or worse, particularly for the highly excited valence states, where its contribution at the all-orders level is essentially zero. Looking at the first few excited states, recall that the $7p_{1/2}$ and $8p_{1/2}$ states in Fr had nonphysically large Breit corrections at all-orders (see Section 8.1). Indeed, we can see that for the $7p_{1/2}$ valence state, including the Breit interaction into $\Sigma^{(\infty)}$ leads to a large correction of $522\,cm^{-1}$, but the deviation from experiment before and after its inclusion is roughly the same, with the deviation being -2.2% without Breit and $+2.1\%$ with Breit. It is interesting that although the all-orders calculation with Breit is almost certainly a spurious result, it doesn't actually make the agreement with experiment worse, although this is likely just a coincidence.

TABLE 8.3: Calculated energy levels of Ra^+ and comparison to experiment. For an explanation of each column, see Table 8.2.

	HF		$\Sigma^{(2)}$		$\Sigma^{(\infty)}$		$\Sigma^{(\infty)}$ + QED		
State	No Breit	Breit	No Breit	Breit	No Breit	Breit	No Breit	Breit	Expt.
$7s_{1/2}$	0	0	0	0	0	0	0	0	0
$6d_{3/2}$	13542	13464	12502	12422	11759	11676	11629	11547	12084
$6d_{5/2}$	14305	14210	14554	14447	13459	13350	13339	13230	13743
$7p_{1/2}$	19019	19046	22443	22483	21392	21428	21303	21339	21351
$7p_{3/2}$	22992	22984	27600	27598	26341	26336	26256	26251	26209
$8s_{1/2}$	39038	39022	45163	45157	43776	43765	43714	43703	43405
$7d_{3/2}$	44322	44289	50721	50700	49109	49082	49014	48987	48744
$5f_{5/2}$	47237	47191	49426	49217	49446	49296	49329	49178	48988
$7d_{5/2}$	44694	44654	51255	51226	49598	49564	49505	49471	49240
$5f_{7/2}$	47192	47145	49983	49782	49685	49537	49573	49425	49272
$8p_{1/2}$	45845	45839	52494	52500	50912	50913	50824	50826	50606
$8p_{3/2}$	47395	47377	54315	54307	52680	52667	52594	52581	52392
$9s_{1/2}$	53893	53872	61114	61105	59473	59458	59397	59382	59165
$6f_{5/2}$	57105	57054	60838	60722	60075	59958	59965	59848	59517
$6f_{7/2}$	57086	57034	61229	61104	60339	60220	60232	60113	59814

For Ra^+, we see again that beyond the $7p_{1/2}$ valence state, the Breit correction at the all-orders + QED level does not make a particularly large difference to the energy levels. In most cases it is interesting to note that the inclusion of Breit does make the agreement with experiment better, but the corrections are quite small in relation to how close the deviation from experiment at the all-orders level already was. The largest deviation from experiment occurs for the $5f$ and d states, and these are the problematic states for which we know including the Breit interaction at second order is not sufficient to reach good agreement with experiment, so we can now inspect the contribution that including the Breit interaction into $\Sigma^{(\infty)}$ makes.

The $5f$ states undergo the largest modification with the inclusion of the Breit interaction at the all-orders level, and in both cases quite meaningfully narrows the deviation from experiment. However, even after adding these all-orders Breit corrections, the predicted energies are still overestimated compared to the experimental values. If we recall that the $\Sigma^{(2)}$ Breit corrections to the f states in Ra^+ are actually larger than the corresponding $\Sigma^{(\infty)}$ corrections, this means that we would actually have gotten *closer* to experiment if we had added the $\Sigma^{(2)}$ Breit correction to the all-orders + QED energy, rather than the Breit correction to $\Sigma^{(\infty)}$. Because the $5f$ states have the largest deviation from experiment out of all the states in Ra^+, we can see that the known problem with the f states has not been solved with the inclusion of the Breit interaction into the all-orders Feynman diagrams. A similar trend can be seen for the $6d$ and $7d$ states.

Table 8.4: Calculated energy levels of Ac^{2+} and comparison to experiment. For an explanation of each column, see Table 8.2.

	HF		$\Sigma^{(2)}$		$\Sigma^{(\infty)}$		$\Sigma^{(\infty)}$ + QED		
State	No Breit	Breit	No Breit	Breit	No Breit	Breit	No Breit	Breit	Expt.
$7s_{1/2}$	0	0	0	0	0	0	0	0	0
$6d_{3/2}$	2943	2832	1383	1278	440	330	242	132	801
$6d_{5/2}$	5318	5167	5283	5123	3911	3748	3729	3566	4204
$5f_{5/2}$	37972	37433	20539	19887	23648	23014	23360	22726	23454
$5f_{7/2}$	39480	38896	23738	23004	26333	25626	26063	25356	26080
$7p_{1/2}$	27311	27360	30628	30693	29512	29572	29379	29439	29466
$7p_{3/2}$	34772	34758	39660	39650	38257	38244	38130	38118	38063
$8s_{1/2}$	64045	64013	71350	71329	69694	69667	69606	69580	
$7d_{3/2}$	67870	67814	75519	75474	73588	73538	73444	73394	
$7d_{5/2}$	68795	68726	76606	76546	74630	74565	74490	74425	
$8p_{1/2}$	74722	74711	82559	82562	80683	80679	80551	80548	
$6f_{5/2}$	78281	78158	84891	84797	83195	83094	83049	82948	
$6f_{7/2}$	78653	78514	85247	85139	83543	83427	83398	83283	
$8p_{3/2}$	77818	77782	86025	86000	84070	84039	83941	83911	
$9s_{1/2}$	90494	90451	99268	99238	97269	97233	97158	97123	

Table 8.5: Calculated energy levels of Th^{3+} and comparison to experiment. For an explanation of each column, see Table 8.2.

	HF		$\Sigma^{(2)}$		$\Sigma^{(\infty)}$		$\Sigma^{(\infty)}$ + QED		
State	No Breit	Breit	No Breit	Breit	No Breit	Breit	No Breit	Breit	Expt.
$5f_{5/2}$	0	0	0	0	0	0	0	0	0
$5f_{7/2}$	3427	3316	4905	4764	4436	4304	4460	4328	4325
$6d_{3/2}$	-5189	-4534	13132	13844	8709	9408	8835	9534	9193
$6d_{5/2}$	-964	-377	18997	19626	14096	14714	14244	14861	14486
$7s_{1/2}$	6339	7126	26232	27067	22966	23795	23360	24187	23131
$7p_{1/2}$	41515	42377	64534	65460	60141	61056	60354	61269	60239
$7p_{3/2}$	53038	53802	77926	78742	73172	73978	73394	74200	73056
$8s_{1/2}$	97410	98146	125539	126336	120417	121201	120697	121480	119622
$7d_{3/2}$	97971	98675	126394	127159	120984	121736	121180	121932	119685
$7d_{5/2}$	99578	100260	128162	128902	122709	123437	122910	123638	121427
$6f_{5/2}$	106689	107326	133873	134567	128790	129474	128986	129670	
$6f_{7/2}$	107129	107747	134362	135038	129258	129923	129456	130121	
$8p_{1/2}$	112013	112783	140648	141480	135301	136120	135516	136335	134517
$8p_{3/2}$	117015	117743	146097	146886	140647	141423	140866	141641	139871
$9s_{1/2}$	137155	137873	167070	167850	161534	162301	161781	162548	160728

In Table 8.4, if we look at the lowest-lying valence states of Ac^{2+}, we can see that including the Breit interaction at the all-orders + QED level does meaningfully make the agreement with experiment worse. Firstly, the $6d_{3/2}$ state can be ignored due to its removal energy of only 801 cm^{-1}. This is so small that it is very difficult to obtain a good agreement with experiment from a purely first-principles calculation. The agreement with experiment is meaningfully worse, however, for the $6d_{5/2}$, $5f_{5/2}$ and $5f_{7/2}$ states, as the inclusion of the Breit interaction for the f states in particular leads to very large corrections that take the $\Sigma^{(\infty)}$ + QED predictions significantly further away from experiment. The fact that this is occurring for the f states is telling, as again it is the f states that are known to lead to such large Breit corrections at second order. This is again another sign that including the Breit interaction into the all-orders correlation potential actually doesn't seem to be the solution to this problem.

Finally, Table 8.5 shows my calculations for the energy levels of Th^{3+}, and we see that unlike the other ions we have considered, including the Breit interaction into the all-orders correlation potential at the same time as the QED radiative potential actually meaningfully narrows the disagreement with experiment for the $5f_{5/2}$ ground state, while for the higher energy states the disagreement becomes worse with the inclusion of the Breit interaction.

In addition to the problems stated above in determining whether the inclusion of Breit into the all-orders calculations makes the accuracy of the predicted values better, there is also the problem that energy levels are subject to a wide variety of different many-body effects outside of just relativistic effects such as the Breit interaction. This can be seen clearly from the HF and $\Sigma^{(2)}$ of the above tables, as increasing the order of perturbation theory had a much larger impact on the agreement with experiment than the Breit interaction or the QED radiative corrections. This means that although the Breit interaction does play a role in determining the accuracy of atomic theory calculations, there may be other effects that we are not taking into account that would play a more important role. This may explain why in some cases including the Breit interaction into the all-orders correlation potential improves the accuracy of the calculations while in other cases it does not make the agreement better. In order to have a better understanding of the impact of including the Breit interaction into the all-orders calculations, we can instead look at more relativistic quantities, such as fine structure intervals.

8.3 Fine structure intervals

Fine structure intervals are the energy splitting that occurs between each subshell corresponding to the same principal quantum number n and orbital angular momentum quantum number l but different total angular momentum j, such as the $6p_{1/2}$ and $6p_{3/2}$ states. In the non-relativistic limit, these two states are predicted to have the exact same energy. However, relativistic effects lift this degeneracy, thereby resulting in the energies of these subshells to have an energy difference known as the fine structure interval [19, 130–134]. Because fine structure splitting is a highly relativistic effect, as we increase the order of perturbation theory at which we include the Breit interaction we should in principle get closer to experiment, without having to worry about the neglect of other many-body effects. However, even

though it is a relativistic effect, correlation corrections do still play a role in the accuracy of fine structure intervals, and we generally reach the best agreement at the $\Sigma^{(\infty)}$ level. It is for this reason that we will just add the Breit correction at each level to the all-orders interval with QED radiative effects, but *without* Breit. In principle the Breit interaction and the QED radiative corrections should constitute the most important relativistic corrections to fine structure intervals. The calculated intervals for the four ions I considered in the previous section are shown in Figure 8.1.

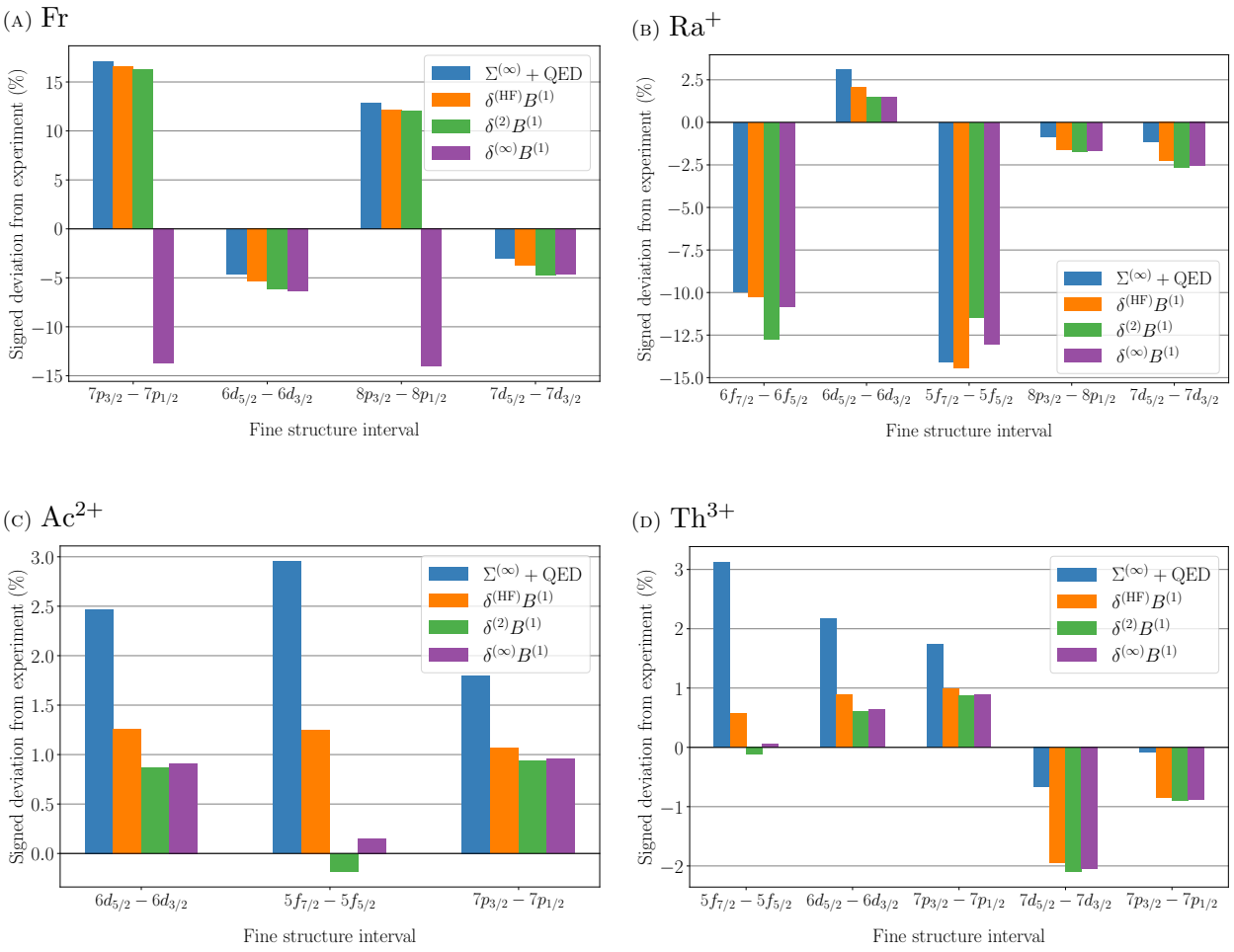

Figure 8.1: Signed percentage deviation from experiment for the fine structure intervals of ions along the francium-isoelectronic sequence. $\Sigma^{(\infty)}$ + QED shows the deviation from experiment at the all-orders correlation potential level as well as with QED radiative corrections. The bars $\delta^{(\mathrm{HF})}B^{(1)}$, $\delta^{(2)}B^{(1)}$, and $\delta^{(\infty)}B^{(1)}$ denote the $\Sigma^{(\infty)}$ + QED fine structure interval with the addition of the one-body Breit correction at the Hartree-Fock, second-order, and all-orders levels of perturbation theory, respectively.

From these figures, it is again hard to tell the effect that including the Breit interaction to all-orders is having on the accuracy of the calculations. In some cases, including the Breit interaction correction does not improve the agreement with experiment, such as the $6f$ interval in Ra^{2+}, or the $7d$ interval in Th^{3+}. We can see that this is typically happening for the d and f intervals, which we know are problematic with the inclusion of the Breit interaction.

What is important to note for these intervals is that including the Breit interaction at the level of the HF approximation makes the agreement worse, and including it to higher orders further worsens it. For these intervals then, it seems that including the Breit interaction to higher orders of perturbation theory only widens the deviation from experiment. As with the energy levels, this might be due to the fact that there is some other effect that I am not including into these calculations.

Although in a lot of cases it seems as though including the Breit interaction to all orders doesn't necessarily make the agreement with experiment better or worse, there are some cases where it noticeably does improve the agreement with experiment. The most prominent intervals where this occurs are the $5f$ intervals in Ac^{2+} and Th^{3+}. In both cases, the interval from the $\Sigma^{(\infty)} + \text{QED}$ level becomes noticeably better upon including the all-orders Breit correction, leading to a sub-0.5% deviation from experiment. What is important to note in these cases, however, is that the deviation from experiment is already quite good, in both cases being about 3%; this level of deviation from experiment for a fine structure interval is already very accurate. Nonetheless, the $5f$ intervals becoming better indicates that including the Breit interaction to all orders does improve the accuracy of the calculations, at least in some cases.

Therefore, rather than looking for the intervals where Breit noticeably makes the agreement with experiment better or worse, we can look for the intervals that have the largest deviation from experiment with just QED radiative effects and no Breit. In francium, this is the case for the $7p$ and $8p$ intervals, where the deviations from experiment without the Breit interaction are 17.1% and 12.8%, respectively. We see in these cases that including the Breit interaction at the HF, and then the $\Sigma^{(2)}$ level, makes the agreement with experiment increasingly better, but still leaves us with over 10% deviations. The ideal scenario would then be that including the all-orders Breit correction resolves this by a substantial amount; but including our spurious corrections just reverses the sign of the deviation. Again, given the numerical problems already discussed for the francium $p_{1/2}$ states, this is likely just a coincidence, and is not a physically meaningful result. Given the relatively large disagreement between theory and experiment for the $p_{1/2}$ intervals without the Breit interaction, they may actually provide a valuable testing ground for the impact in accuracy that including the Breit interaction to all-orders has to atomic structure calculations. As mentioned previously, however, this is not currently possible given the limitations in evaluating the all-orders Feynman diagram in AMPSCI.

In Ra^{2+}, the largest deviation from experiment occurs for the $6f$ and $5f$ intervals. This is a known problem and, again, it would be ideal if including the Breit interaction into the all-orders correlation potential resolves this problem. For the former interval, however, the agreement with experiment is worsened upon including the HF correction and then the $\Sigma^{(2)}$ correction, but from here is improved with the $\Sigma^{(2)}$ correction. Conversely, for the $5f$ interval, the agreement *improves* when we include the second order Breit correction, but is *worsened* when we include the all-orders correction. Again, it is hard to discern from this whether including the Breit interaction into the all-orders calculations improves the accuracy of our calculations, but the fact that the deviation from experiment is still greater than 10%

in both cases, with or without taking into account Breit corrections, is a sign that there is some other problem that is resulting in these significant disagreements.

8.4 Summary

In this chapter I have presented calculations for the energy levels of ions along the Fr-isoelectronic sequence at the HF, second-order, and all-orders levels of perturbation theory. The previously known second-order Breit corrections are compared to the corrections at the all-orders level evaluated with the method I have developed throughout Chapters 5 and 6. I have shown that the additional correction due to including the Breit interaction at the all-orders level is in most cases small compared to the existing correction at second order in perturbation theory. When applied to a detailed study of energy levels, we find that including the Breit interaction into the all-orders calculations does not unequivocally make the agreement with experiment worse or better, and in the case of the fine structure intervals, the known problem with certain of the d and f intervals is not improved with the inclusion of the Breit interaction into the all-orders method. This indicates that there is likely some other effect that we are not accounting for that would play a role in resolving this disagreement. Where including the Breit interaction into the all-orders correlation potential did make the largest difference was in reducing the large second-order Breit corrections to the f states of Ra^+ by almost half, indicating that the higher-order diagrams do play a large role with the exact inclusion of the Breit interaction, and also in the f states of Th^{3+}. This latter point is especially encouraging, since $5f_{5/2}$ is the ground valence state of Th^{3+}, and so obtaining a close agreement with experiment here is pivotal to having a good understanding of the rest of the atomic structure.

Finally, we also found that including the Breit interaction into the all-orders correlation potential is numerically unstable for the $p_{1/2}$ states of francium, and we found that this was due to the approximate way in which the exchange Feynman diagram is calculated inside AMPSCI. Because I have now corrected the spin structure of the Green's function and polarisation operator, the path is now open to exactly calculate the second-order exchange Feynman diagram and its all-orders counterpart. This will likely resolve the issue we have found with the $p_{1/2}$ states in francium, but may also modify the contribution that the Breit interaction makes in the all-orders calculations. However, given that the all-orders Breit corrections were so close to the second-order corrections, it's likely that for all the other states the exchange diagram is well-behaved. This would likely mean that calculating the exact all-orders exchange diagram would only lead to a small modification of the results presented here, since the exchange diagram only contributes a small amount to the full correlation potential, and the modification to this from including the all-orders screening even less so.

9 Conclusion

The aim of this thesis was to include the Breit interaction into the Feynman method of perturbation theory in atomic physics. The purpose of doing this was to include the Breit interaction into the so-called all-orders correlation potential method, which includes dominating corrections to the atomic properties of atomic states by summing an infinite series of diagrams in the Coulomb interaction. In order to do this, I first had to resolve several problems with the implementation of the Feynman method into AMPSCI. The first of these was the full spin structure of the Feynman Green's function, which was previously being calculated in such a way that missed out on some numerical information upon solving the Dyson equation. The other main issue that had to be resolved was the structure of the polarisation operator; by deriving myself the second-order Feynman diagrams, I was able to construct the correct polarisation operator, and doing so allowed for the inclusion of the Breit interaction into the Feynman method. This now allows us to construct the direct part of the correlation potential with the one-body part of the Breit interaction purely using the Feynman method, without needing any recourse to the much less numerically desirable Goldstone method.

It also then allowed me to include the Breit interaction into the calculation of energy levels and fine structure intervals for ions along the Fr-isoelectronic sequence with the one-body part of the Breit interaction now included to all orders of perturbation theory. I showed that the effect of including the Breit interaction into the all-orders correlation potential is comparable to the effect of including it only at second order for most atomic states; for the f states of certain ions, however, it did lead to a meaningful difference compared to its impact at second order, demonstrating that the large Breit corrections that arise at second order for these states are actually renormalised by a meaningful amount when the higher order are taken into account. While I showed that including the Breit interaction into the all-orders correlation potential did not resolve the known issues with the d and f states for ions along the Fr-sequence, this demonstrates that the issue is most likely coming from some

other many-body effect that we have not accounted for in this thesis.

I also found, however, that there are certain states, such as the $p_{1/2}$ orbitals of francium, which are numerically unstable to calculate in the all-orders correlation potential method. I suspect that this isn't due to the code I have written for the Breit interaction, or any other change I made in the Feynman method, but in the approximate way that the exchange diagram is calculated in AMPSCI, and this should be addressed in the future. Now that I have corrected the spin structure of the Feynman diagrams, one obvious direction for future work would be to attempt to include the exact form of the exchange diagram into this program, and to this end I have presented a derivation of the exchange Feynman diagram in Section C.2 with the complete spinor indexing. Although implementing this numerically would make the Feynman method code in AMPSCI completely self-contained, allowing us to calculate both the direct *and exchange* parts of the correlation potential without any need for the Goldstone method, it would likely only lead to a small correction to the all-orders Breit corrections calculated in Chapter 8 that were numerically stable. It would also fix the unstable $7p_{1/2}$ corrections in francium, although it is not expected that these would be very different from the second-order corrections upon making this modification to the code.

Another direction for future work would be to work on including the frequency-dependent Breit interaction into the correlation potential method in a numerically stable way. In Chapter 7 I showed that including the frequency-dependent Breit interaction into the Hartree-Fock procedure leads to large corrections to the standard Breit interaction for heavy and highly-charged ions, and so it would be worthwhile to try to include it into perturbative calculations. Some extra thought would have to be put into how to include it into perturbation theory in a way that is consistent physically, and also that is numerically efficient and stable. This might potentially open the possibility of including the frequency-dependent Breit interaction also into the all-orders correlation potential method. Given the effect that the Breit interaction plays at second and higher-orders in perturbation theory, it would be interesting to determine whether the frequency-dependence will resolve the issues surrounding the d and f states and fine structure intervals discussed in this thesis.

Another possible future project could be to include the two-body part of the Breit interaction into the Feynman method. This would make the Goldstone and Feynman methods equivalent in AMPSCI in terms of how the Breit interaction can be included inside them, and would involve making the replacement $Q_{ij} \to Q_{ij} + (H_{\mathrm{Br}})_{ij}$ in the second-order Feynman diagrams. The difficulty with this is that the angular reduction of the Breit interaction is so complicated, and its resulting spinor structure so non-trivial, that the equations would be involved and tedious. Although the theory is actually not too difficult, it would require representing the radial Breit operator as a tensor product of spinor matrices, and making sure that the spinor indices are all being contracted in the right way inside the diagrams. While it was shown in Chapter 3 that the two-body Breit corrections are much less important than the one-body corrections at second order in caesium, it may be more important for more relativistic systems. After including it into the second-order Feynman diagrams, we could also try to include it into the all-orders screening and hole-particle diagrams. This would be a much harder problem still, as the spinor structure of the polarisation operator

and the Coulomb interaction would need to be entirely rewritten to accommodate the non-trivial spinor structure of the Breit interaction. Doing so would allow the two-body part of the Breit interaction to be calculated exactly to all-orders in the series of diagrams that are included in the all-orders correlation potential method. Again, however, the two-body contribution is so small at second order, so it is unlikely that including it in the all-orders diagrams would make much of a difference, although this would ideally need to be checked and, like the inclusion of the one-body part into the all-orders correlation potential, this would definitely be a novel result.

The final avenue for future investigation would be to try to calculate the next higher-order correction to the Coulomb interaction in powers of e^2. We have seen that the Breit interaction, which is the lowest-order correction in powers of $1/c^2$ to the Coulomb interaction leads to large corrections to many-body effects at second-order in perturbation theory. We have also seen that the frequency-dependent Breit interaction captures the retardation effects that the frequency-independent Breit interaction misses out on to all orders in $1/c^2$. We could in principle go further than this to calculate higher-order corrections to the Coulomb interaction, corresponding to the exchange of more than one photon between the two electrons. The next highest order correction to the Coulomb interaction would come from every possible Feynman diagram where two photons are exchanged between two electrons. Determining this correction would likely be a novel result, and then including it into atomic structure calculations would likely allow for the most accurate inclusion of relativistic effects to date. Furthermore, since the issue with including the Breit interaction into the fine structure intervals for the d and f states of the Fr-isoelectronic sequence ions is not resolved based on the work done in this thesis, including the next relativistic correction to the Coulomb interaction into the atomic structure calculations might either resolve this, or shed new light on the source of the problem.

A

Derivation of secular equation for Breit-Coulomb-HF orbitals

In this appendix I will derive Eq. (2.19) of Ref. [16], as well as how to convert this equation into a tractable form for calculation.

In order to derive a basis of single-particle electron wave functions satisfying the Breit-Coulomb-HF equation, Derevianko constructs a basis of CHF orbitals using B-splines, and then finds the BCHF orbitals by expanding them as linear combinations of the CHF orbitals,

$$\bar{\phi}_i(\boldsymbol{r}) = \sum_j c_{ij}\phi_j(\boldsymbol{r}), \tag{A.1}$$

where the $c_{ij} = \langle\phi_j|\bar{\phi}_i\rangle$ are the matrix elements of the unitary transformation relating the BCHF basis to the CHF basis. We note that the BCHF orbitals will satisfy

$$\left(h_0 + U^{\mathrm{BCHF}}\right)\bar{\phi}_i(\boldsymbol{r}) = \left(h_0 + U^{\mathrm{CHF}} + V_{\mathrm{Br}}\right)\bar{\phi}_i(\boldsymbol{r}) = \bar{\varepsilon}_i\bar{\phi}_i(\boldsymbol{r}), \tag{A.2}$$

where $(U^{\mathrm{CHF}})_{ij} = g_{ij}$, $(U^{\mathrm{BCHF}})_{ij} = b_{ij}$, and $(V_{\mathrm{Br}})_{ij} = b_{ij}$ is the one-body part of the Breit interaction, i.e. the HF Breit operator. We then insert the expansion Eq. (A.1) into this expression to get

$$\bar{\varepsilon}_i \sum_j d_{ij}\phi_j(\boldsymbol{r}) = \left(h_0 + U^{\mathrm{CHF}} + V_{\mathrm{Br}}\right)\sum_j d_{ij}\phi_j(\boldsymbol{r}) \tag{A.3}$$

$$\sum_j d_{ij}\bar{\varepsilon}_i\phi_j(\boldsymbol{r}) = \sum_j d_{ij}\underbrace{\left(h_0 + U^{\mathrm{CHF}}\right)\phi_j(\boldsymbol{r})}_{=\varepsilon_j\phi_j(\boldsymbol{r})} + \sum_j d_{ij}V_{\mathrm{Br}}\phi_j(\boldsymbol{r}) \tag{A.4}$$

$$= \sum_j d_{ij}\varepsilon_j\phi_j(\boldsymbol{r}) + \sum_j d_{ij}V_{\mathrm{Br}}\phi_j(\boldsymbol{r}). \tag{A.5}$$

We can then multiply both sides of the above equation by $\phi_k(\boldsymbol{r})$ and integrate with respect to $\boldsymbol{r}$ to get

$$\sum_j d_{ij}\bar{\varepsilon}_i\langle\phi_k|\phi_j\rangle = \sum_j d_{ij}\varepsilon_j\langle\phi_k|\phi_j\rangle + \sum_j d_{ij}\langle\phi_k|V_{\mathrm{Br}}|\phi_j\rangle. \tag{A.6}$$

Then, using the orthonormality of the CHF orbitals, $\langle\phi_i|\phi_j\rangle = \delta_{ij}$, this becomes

$$\sum_j d_{ij}\bar{\varepsilon}_i\delta_{kj} = \sum_j d_{ij}\varepsilon_j\delta_{kj} + \sum_j d_{ij}(V_{\mathrm{Br}})_{kj} \tag{A.7}$$

$$d_{ik}\bar{\varepsilon}_i = d_{ik}\varepsilon_k + \sum_j (V_{\mathrm{Br}})_{kj}d_{ij}. \tag{A.8}$$

Note that if we fix i, then this is a vector equation with the index k denoting the vector components. This can be seen more clearly if we omit the index i, to write the above as,

$$d_k\bar{\varepsilon} = d_k\varepsilon_k + \sum_j (V_{\mathrm{Br}})_{kj}d_j. \tag{A.9}$$

The second term on the right-hand side is just a matrix multiplication, but it isn't obvious that the first term is. To see this, we can trivially insert a summation over j with the introduction of a Kronecker delta, to give us

$$\bar{\varepsilon}d_k = \sum_j d_j\varepsilon_j\delta_{kj} + \sum_j (V_{\mathrm{Br}})_{kj}d_j \tag{A.10}$$

$$= \sum_j \left[\varepsilon_j\delta_{kj} + (V_{\mathrm{Br}})_{kj}\right] d_j. \tag{A.11}$$

We can therefore write this as the matrix equation,

$$\bar{\varepsilon}\begin{pmatrix} d_1 \\ d_2 \\ d_3 \\ \vdots \end{pmatrix} = \begin{pmatrix} (V_{\mathrm{Br}})_{11}+\varepsilon_1 & (V_{\mathrm{Br}})_{12} & (V_{\mathrm{Br}})_{13} & \cdots \\ (V_{\mathrm{Br}})_{21} & (V_{\mathrm{Br}})_{22}+\varepsilon_2 & (V_{\mathrm{Br}})_{23} & \cdots \\ (V_{\mathrm{Br}})_{31} & (V_{\mathrm{Br}})_{32} & (V_{\mathrm{Br}})_{33}+\varepsilon_3 & \cdots \\ \vdots & \vdots & \vdots & \ddots \end{pmatrix}\begin{pmatrix} d_1 \\ d_2 \\ d_3 \\ \vdots \end{pmatrix}. \tag{A.12}$$

This then becomes matrix equation for the eigenvalue $\bar{\varepsilon}$ and eigenvector $(d_1, d_2, \dots)$. We can confirm this indeed gives back Eq. (A.9) by considering what both sides are equal to for an arbitrary k. Reading off the above matrix equation, this will be equal to

$$\bar{\varepsilon}d_k = \sum_j (V_{\mathrm{Br}})_{kj}d_j + \varepsilon_k d_k, \tag{A.13}$$

which is indeed the desired expression. If we put the index i back into this equation,

$$\bar{\varepsilon}_i\begin{pmatrix} d_{i1} \\ d_{i2} \\ d_{i3} \\ \vdots \end{pmatrix} = \begin{pmatrix} (V_{\mathrm{Br}})_{11}+\varepsilon_1 & (V_{\mathrm{Br}})_{12} & (V_{\mathrm{Br}})_{13} & \cdots \\ (V_{\mathrm{Br}})_{21} & (V_{\mathrm{Br}})_{22}+\varepsilon_2 & (V_{\mathrm{Br}})_{23} & \cdots \\ (V_{\mathrm{Br}})_{31} & (V_{\mathrm{Br}})_{32} & (V_{\mathrm{Br}})_{33}+\varepsilon_3 & \cdots \\ \vdots & \vdots & \vdots & \ddots \end{pmatrix}\begin{pmatrix} d_{i1} \\ d_{i2} \\ d_{i3} \\ \vdots \end{pmatrix}, \tag{A.14}$$

then the matrix whose eigenvalues and eigenvectors we are trying to solve for doesn't change. This makes it clear, therefore, that the N eigenvalues we get from this equation correspond to the N BCHF orbitals that this solution will generate, with the index i just serving as a label for these N solutions. For example, the first eigenvalue of Eq. (A.14) corresponds to the energy $\bar{\varepsilon}_i$ of the 'first' BCHF orbital, $\bar{\phi}_1$, with the eigenvector $(d_{i1}, d_{i2}, d_{i3}, \dots)$ corresponding to the expansion coefficients of the CHF orbitals required to construct the orbital $\bar{\phi}_i$ from Eq. (A.1).

B

Details of the Feynman method

In this appendix I will discuss the Feynman method in atomic physics using quantum field theory and the particle-hole formalism. This chapter is not necessary to follow the discussion of the Feynman method in my code, it is just here for the interested reader. More details can be found in Refs. [36, 67, 135–141].

The starting point for these calculations is the Furry picture [142], in which the electron quantum field is decomposed into a sum of bound state spinor solutions of some single-particle Hamiltonian, rather than free space solutions, as in normal QED [60, 135, 143, 144]. This has the benefit that the zeroth order approximation to the wave functions include the lowest order (mean field) corrections due to the Coulomb interaction. In units in which $e^2 = 4\pi\alpha$, where α is the fine structure constant, the Hamiltonian of QED is

$$H = \int d^3x\, \psi^\dagger(\boldsymbol{x}) \left(\boldsymbol{\alpha}\cdot\boldsymbol{p} + \beta m - \frac{Z\alpha}{r} \right) \psi(\boldsymbol{x}) - e \int d^3x\, \psi^\dagger(\boldsymbol{x}) \boldsymbol{\alpha}\cdot\boldsymbol{A}(\boldsymbol{x}) \psi(\boldsymbol{x}) + \frac{\alpha}{2} \int \frac{d^3x\, d^3y}{|\boldsymbol{x}-\boldsymbol{y}|} \psi^\dagger(\boldsymbol{x})\psi(\boldsymbol{x})\psi^\dagger(\boldsymbol{y})\psi(\boldsymbol{y}). \tag{B.1}$$

To make the connection with the way that MBPT is typically done in atomic physics, in which a mean field potential is used to generate the lowest order wave functions, we can add and subtract a single-particle potential $U(x)$ from the Hamiltonian to get

$$H = \int d^3x\, \psi^\dagger(\boldsymbol{x}) \left[\boldsymbol{\alpha}\cdot\boldsymbol{p} + \beta m + U(\boldsymbol{x}) \right] \psi(\boldsymbol{x}) - \int d^3x\, \psi^\dagger(\boldsymbol{x}) \left[\frac{\alpha Z}{r} + U(\boldsymbol{x}) \right] \psi(\boldsymbol{x}) - e \int d^3x\, \psi^\dagger(\boldsymbol{x}) \boldsymbol{\alpha}\cdot\boldsymbol{A}(\boldsymbol{x}) \psi(\boldsymbol{x}) + \frac{\alpha}{2} \int \frac{d^3x\, d^3y}{|\boldsymbol{x}-\boldsymbol{y}|} \psi^\dagger(\boldsymbol{x})\psi(\boldsymbol{x})\psi^\dagger(\boldsymbol{y})\psi(\boldsymbol{y}). \tag{B.2}$$

For the purposes of deriving the same energy corrections as those from the Goldstone method/traditional perturbation theory, we will take this mean field to be the Hartree-Fock

potential, $U_{ij} = U_{ij}^{\mathrm{HF}}$. We will split up the Hamiltonian into a "free" part,

$$H_0 = \int d^3x\, \psi^\dagger(\boldsymbol{x}) \left[\boldsymbol{\alpha}\cdot\boldsymbol{p} + \beta m + U(\boldsymbol{x})\right] \psi(\boldsymbol{x}), \tag{B.3}$$

and an interaction part,

$$\begin{aligned} H_I = \; -\int d^3x\, \psi^\dagger(\boldsymbol{x}) \left[\frac{\alpha Z}{r} + U(\boldsymbol{x})\right] \psi(\boldsymbol{x}) - e\int d^3x\, \psi^\dagger(\boldsymbol{x}) \boldsymbol{\alpha}\cdot\boldsymbol{A}(\boldsymbol{x})\psi(\boldsymbol{x}) \\ + \frac{\alpha}{2}\int \frac{d^3x\, d^3y}{|\boldsymbol{x}-\boldsymbol{y}|} \psi^\dagger(\boldsymbol{x})\psi(\boldsymbol{x})\psi^\dagger(\boldsymbol{y})\psi(\boldsymbol{y}), \end{aligned} \tag{B.4}$$

which will be treated perturbatively. Here, ψ and $\psi^\dagger$ are second-quantised field operators with the expansions (in the particle-hole formalism),

$$\bar{\psi}(x) = \psi^\dagger(x)\gamma^0 = \sum_a^{\text{core}} b_a e^{-i\varepsilon_a t}\bar{\phi}_a(\boldsymbol{x}) + \sum_n^{\text{exc.}} c_n^\dagger e^{i\varepsilon_n t}\bar{\phi}_n(\boldsymbol{x}) \tag{B.5}$$

$$\text{and} \quad \psi(x) = \sum_a^{\text{core}} b_a^\dagger e^{i\varepsilon_a t}\phi_a(\boldsymbol{x}) + \sum_n^{\text{exc.}} c_n e^{-i\varepsilon_n t}\phi_n(\boldsymbol{x}). \tag{B.6}$$

Here, $\hat{b}$ and c are particle-hole operators satisfying the anti-commutation relations,

$$\{b_i, b_j^\dagger\} = \{c_i, c_j^\dagger\} = \delta_{ij}, \tag{B.7}$$

with all other commutation relations being zero. We are working in the particle-hole formalism so $b^\dagger$ creates an electron in the core (a hole), $c^\dagger$ creates an electron in a virtual orbital (a particle), etc. [21, 108, 109]. The basis spinors ϕ_i in the field operator expansions in Eqs. (B.5) and (B.6) are exactly the eigenfunctions of the single-particle Hartree-Fock equation in the V^{N-1} approximation,

$$\left[-i\hbar\boldsymbol{\alpha}\cdot\nabla + \beta m + U^{\mathrm{HF}}(\boldsymbol{x})\right]\phi_i(\boldsymbol{x}) = \varepsilon_i\phi(\boldsymbol{x}). \tag{B.8}$$

Note that in the particle-hole picture energies are defined relative to the Fermi energy (i.e. the energy of the highest core orbital) so the hole (core) wave functions (as well as the negative energy states) have negative energy, while the particle (excited) states have positive energy. The mode expansion for the electromagnetic 3-potential is

$$\boldsymbol{A}(x) = \sum_{\lambda=1}^{2}\int \frac{d^3k}{\sqrt{2\omega(2\pi)^3}}\boldsymbol{\varepsilon}(\boldsymbol{k},\lambda)\left[a(\boldsymbol{k},\lambda)e^{-ik\cdot x} + a^\dagger(\boldsymbol{k},\lambda)e^{ik\cdot x}\right], \tag{B.9}$$

where λ describes the two polarisations, $\boldsymbol{\varepsilon}(\boldsymbol{k},\lambda)$ is a basis polarisation vector with polarisation λ and momentum $\boldsymbol{k}$, and $a(\boldsymbol{k},\lambda)$ and $a^\dagger(\boldsymbol{k},\lambda)$ destroy and create photons with momentum $\boldsymbol{k}$ and polarisation λ, respectively (assuming real polarisations) [38]. The electron propagator is defined as

$$S_F^{\alpha\beta}(x,y) = -i\langle 0_c|T\{\psi^\alpha(x)\bar{\psi}^\beta(y)\}|0_c\rangle = -i\left[\psi^\alpha(x)\bar{\psi}^\beta(y)\theta(x_0-y_0) - \bar{\psi}^\beta(y)\psi^\alpha(x)\theta(y_0-x_0)\right] \tag{B.10}$$

where $|0_c\rangle$ is the Hartree-Fock closed core 'vacuum' introduced in Section 2.4, T denotes the time-ordering of two operators, α and β are spinor indices, and $\theta(x)$ is the Heaviside step function. Since we assume that the electrons are moving in a time-independent field it is useful to introduce a propagator that is Fourier-transformed just in the time domain, so that

$$S_F^{\alpha\beta}(x,y) = \int \frac{d\omega}{2\pi}\, e^{-i\omega(x_0-y_0)} S_F^{\alpha\beta}(\boldsymbol{x},\boldsymbol{y};\omega). \tag{B.11}$$

One can show using the Fourier representation of the Heaviside step function that the Fourier-transformed propagator is given by [108, 109]

$$S_F^{\alpha\beta}(\boldsymbol{x},\boldsymbol{y};E) = \lim_{\delta\to 0}\left[\sum_a^{\text{core}} \frac{\phi_a^\alpha(\boldsymbol{x})\bar{\phi}_a^\beta(\boldsymbol{y})}{E-\varepsilon_a-i\delta} + \sum_n^{\text{exc.}} \frac{\phi_n^\alpha(\boldsymbol{x})\bar{\phi}_n^\beta(\boldsymbol{y})}{E-\varepsilon_n+i\delta}\right]. \tag{B.12}$$

We can now turn to calculating energy corrections, which can be rigorously done using the Gell-Mann and Low formalism [55], or alternatively Sucher's generalisation in terms of the S-matrix (Feynman diagrams) [145], but also in a simpler way that is discussed in [60], which is what I will use here. Although the rigorous definition and the one I discuss here are equivalent at the level of the diagrams I am using in my project, the rigorous procedure becomes important for renormalising certain interactions, such as in cancelling the contribution from disconnected diagrams [135].

For systems of a single valence electron, we assume that the electrons, before the interaction is switched on, propagate according to H_0. In this picture, the state of the core and single valence electrons can be described, in the frozen-core approximation, by the state

$$|i\rangle = c_v^\dagger|0_c\rangle = c_v^\dagger \prod_a^{\text{core}} b_a^\dagger|0\rangle, \tag{B.13}$$

where $|0\rangle$ is the state which has no photons or electrons. Then, H_I is turned on for some interval of time $-t/2 \le t \le t/2$, during which the state propagates with the true ground state of the interacting theory, $E = E_0 + \Delta E$, and after H_I is turned off, the state must evolve back into $|i\rangle$ up to a phase determined by

$$|f\rangle = e^{-i\Delta E t}|i\rangle = \left[1 - i\Delta E t + \mathcal{O}(t^2)\right]|i\rangle. \tag{B.14}$$

The operator that evolves $|i\rangle$ to $|f\rangle$ is the interaction-picture time-evolution operator, solved formally by the Dyson series [146] ,

$$U(T/2,-T/2) = T\left\{\exp\left[-i\int_{-t/2}^{t/2} dt \int d^3x\, \mathcal{H}_I(x)\right]\right\}, \tag{B.15}$$

where $\mathcal{H}_I(x)$ is the interaction-picture interaction Hamiltonian. Therefore, if we know what $|f\rangle$ is, we can take the inner product of $|f\rangle$ with $|i\rangle$ (denoting the HF vacuum as $|0\rangle$ for conciseness), to get

$$\langle i|f\rangle = \langle i|U(-t/2,t/2)|i\rangle \tag{B.16}$$

$$= \langle 0_c | c_v T \left\{ \exp\left[-i \int_{-t/2}^{t/2} \int d^3x \, \mathcal{H}_I(x) \right] \right\} c_v^\dagger |0\rangle \tag{B.17}$$

$$= 1 - i \int d^4x \, \langle 0 | c_v T \{ \mathcal{H}_I(x) \} c_v^\dagger | 0 \rangle + \frac{(-i)^2}{2} \int d^4x \, d^4y \, \langle 0 | c_v T \{ \mathcal{H}_I(x) \mathcal{H}_I(y) \} c_v^\dagger | 0 \rangle + \ldots, \tag{B.18}$$

and identify the coefficients of t with the correction to the energy at that order [60]. From Eq. (B.4), the Hamiltonian density due to the interaction of the electrons with transverse photons (corresponding to the second term in H_I) can be read off from under the integral sign as

$$\mathcal{H}_T(x) = -e\psi^\dagger(x)\boldsymbol{\alpha} \cdot \boldsymbol{A}(x)\psi(x), \tag{B.19}$$

while the Hamiltonian density that generates the final term in H_I, corresponding to the Coulomb interaction, can be shown to be

$$\mathcal{H}_C(x) = \frac{\alpha}{2} \int d^4y \frac{\delta(x_0 - y_0)}{4\pi|\boldsymbol{x} - \boldsymbol{y}|} \psi^\dagger(x)\psi(x)\psi^\dagger(y)\psi(y). \tag{B.20}$$

Now we can start allowing the time-evolution operator to act order-by-order. To understand the connection between the Coulomb and the transverse parts of the interaction Hamiltonian, we note that since there are no photons in the initial or final state, $\mathcal{H}_T$ does not contribute at first order (since $\boldsymbol{A}$ will consist of photon creation and annihilation operators which will kill the HF vacuum in the time-ordered product), and contributes first at second order, when both of the photon fields are contracted, while the Coulomb part of the interaction Hamiltonian will act at first order. The two contributions are given respectively by,

$$S_T = -\frac{e^2}{2} \int d^4x \int d^4y \, \langle 0 | c_v T \{ \psi^\dagger(x)\boldsymbol{\alpha} \cdot \overbrace{\boldsymbol{A}(x)\psi(x)\psi^\dagger(y)\boldsymbol{\alpha} \cdot \boldsymbol{A}}(y)\psi(y) \} c_v^\dagger | 0 \rangle \tag{B.21}$$

$$= -\frac{e^2}{2} \int d^4x \int d^4y \, iD_F^{\mathrm{Tr}}(x,y)_{ij} \langle 0 | c_v T \left\{ \psi^\dagger(x)\alpha^i\psi(x)\psi^\dagger(y)\alpha^j\psi(y) \right\} c_v^\dagger | 0 \rangle \tag{B.22}$$

$$S_C = -i\frac{e^2}{2} \int d^4x \int d^4y \, \frac{\delta(x_0 - y_0)}{4\pi|\boldsymbol{x} - \boldsymbol{y}|} \langle 0 | c_v T \left\{ \psi^\dagger(x)\psi(x)\psi^\dagger(y)\psi(y) \right\} c_v^\dagger | 0 \rangle, \tag{B.23}$$

where in the second line we have contracted the two transverse photon fields to give the propagator for transverse photons,

$$iD^{\mathrm{Tr}}(x,y)_{ij} = \langle 0 | T\{ \hat{A}_i(x)\hat{A}_j(y) \} | 0 \rangle = i \int \frac{d^4k}{(2\pi)^4} \frac{e^{-ik\cdot(x-y)}}{k^2 + i\varepsilon} \left(\delta_{ij} - \frac{k_i k_j}{|\boldsymbol{k}|^2} \right), \tag{B.24}$$

which are exactly just the spatial components of the Coulomb gauge propagator (see below). We can also see that Eq. (B.23) contains the time component of the Coulomb gauge propagator,

$$D_C(x,y)_{00} = i \int \frac{d^4k}{(2\pi)^4} \frac{e^{-ik\cdot(x-y)}}{|\boldsymbol{k}|^2} = \frac{i\delta(x_0 - y_0)}{4\pi|\boldsymbol{x} - \boldsymbol{y}|} \quad \text{and} \quad D_C(x,y)_{0i} = D_C(x,y)_{i0} = 0, \tag{B.25}$$

meaning that Eqs. (B.22) and (B.23) are actually just describing the exact same scattering event, corresponding to the exchange of a single photon. In order to see this more clearly, we can introduce the Coulomb gauge photon propagator,

$$D_C(x,y)_{\mu\nu} = \langle 0|T\{A_\mu(x)A_\nu(y)\}|0\rangle \tag{B.26}$$

$$= i\int \frac{d^4k}{(2\pi)^4}\frac{\Delta_{\mu\nu}}{k^2+i\varepsilon}e^{-ik\cdot(x-y)}, \tag{B.27}$$

where

$$\Delta_{ij} = \delta_{ij} - \frac{k_i k_j}{|\boldsymbol{k}|^2}, \quad \Delta_{00} = \frac{k^2}{|\boldsymbol{k}|^2}, \quad \text{and} \quad \Delta_{0i} = \Delta_{i0} = 0, \tag{B.28}$$

using which S_T and S_C can be identified as belonging to the single expression,

$$\begin{aligned} S_{T+C} &= -\frac{e^2}{2}\int d^4x \int d^4y\, \langle i|T\big\{\bar\psi(x)\gamma^\mu\psi(x)\overbrace{A_\mu(x)\bar\psi(y)\gamma^\nu\psi(y)A_\nu(y)}\big\}|f\rangle \\ &= -i\frac{e^2}{2}\int d^4x \int d^4y\, D_C(x,y)_{\mu\nu}\langle i|T\big\{\bar\psi(x)\gamma^\mu\psi(x)(x)\bar\psi(y)\gamma^\nu\psi(y)\big\}|f\rangle \end{aligned} \tag{B.29}$$

$$\begin{aligned} &= -i\frac{e^2}{2}\int d^4x \int d^4y\, D_C(x,y)_{00}\langle i|T\left\{\bar\psi(x)\gamma^0\psi(x)\bar\psi(y)\gamma^0\psi(y)\right\}|f\rangle \\ &\quad - i\frac{e^2}{2}\int d^4x \int d^4y\, D_C(x,y)_{ij}\langle i|T\left\{\bar\psi(x)\gamma^i\psi(x)\bar\psi(y)\gamma^j\psi(y)\right\}|f\rangle. \end{aligned} \tag{B.30}$$

This can be seen more clearly by using the Dirac matrices, defined to be $\alpha^i = \gamma^0\gamma^i$ and the fact that $\bar\psi = \psi^\dagger\gamma^0$ (the overbar here denotes the Dirac adjoint of ψ, rather than a BCHF orbital), so that the above becomes

$$\begin{aligned} S_{T+C} &= -\frac{e^2}{2}\int d^4x \int d^4y\, \langle i|T\big\{\bar\psi(x)\gamma^\mu\psi(x)\overbrace{A_\mu(x)\bar\psi(y)\gamma^\nu\psi(y)A_\nu(y)}\big\}|f\rangle \\ &= -i\frac{e^2}{2}\int d^4x \int d^4y\, D_C(x,y)_{00}\langle i|T\left\{\psi^\dagger(x)(\gamma^0)^2\psi(x)\psi^\dagger(y)(\gamma^0)^2\psi(y)\right\}|f\rangle \\ &\quad - i\frac{e^2}{2}\int d^4x \int d^4y\, D_C(x,y)_{ij}\langle i|T\left\{\psi^\dagger(x)\gamma^0\gamma^i\psi(x)\psi^\dagger(y)\gamma^0\gamma^j\psi(y)\right\}|f\rangle \end{aligned} \tag{B.31}$$

$$\begin{aligned} &= -i\frac{e^2}{2}\int d^4x \int d^4y\, D_C(x,y)_{00}\langle i|T\left\{\psi^\dagger(x)\psi(x)\psi^\dagger(y)\psi(y)\right\}|f\rangle \\ &\quad - i\frac{e^2}{2}\int d^4x \int d^4y\, D_C(x,y)_{ij}\langle i|T\left\{\psi^\dagger(x)\alpha^i\psi(x)\psi^\dagger(y)\alpha^j\psi(y)\right\}|f\rangle, \end{aligned} \tag{B.32}$$

where we have used $(\gamma^0)^2 = 1_{4\times4}$. We see that this final expression corresponds exactly to the sum of S_T and S_C defined in Eqs. (B.22) and (B.23). Since this corresponds to a scattering event with two pairs of electromagnetic fields contracted, this scattering event corresponds to the exchange of a single photon between two electrons. Therefore, it is clear that from the QED Hamiltonian, splitting up the Hamiltonian into a perturbative part corresponding

to the Coulomb interaction, and an interaction with an external transverse electromagnetic field $\boldsymbol{A}$, really just describes a single interaction, corresponding to the Hamiltonian density,

$$\mathcal{H}_{\mathrm{QED}}(x) = -e\bar{\psi}(x)\gamma^{\mu}\psi(x)A_{\mu}(x), \tag{B.33}$$

which is just the typical QED interaction Hamiltonian. Note that this means that the electromagnetic interactions considered at the beginning of this appendix naturally contain both the Coulomb interaction in the time component of the photon propagator, and the Breit interaction in the lowest order transverse components (see Ref. [60] for more details). Note that since there are no photons in the final or initial states, any terms in the Dyson series of an odd power in $\mathcal{H}_{\mathrm{QED}}$, which will in turn be of odd order in e, will be exactly zero. In atomic physics, however, we perform perturbative expansions in powers of α, with $\alpha = e^2/4\pi$, so we only ever consider the equivalent of even terms in the Dyson series, which are strictly non-vanishing.

As a final note, note in these calculations that using the HF core as the ground state we calculate matrix elements with respect to means that we are implicitly allowing the core electrons to propagate unaffected by the interaction. This is exactly the same approach that is typically used in the frozen core approximation of old-fashioned MBPT, where the core and valence electrons are solved for self-consistently using the HF procedure, and then many-body corrections beyond the HF approximation are considered only for the valence electrons.

C

Derivation of second-order Feynman diagrams

In this appendix I will derive the second-order Feynman diagrams I state in Eq. (4.3) as well as their analytical expressions, following on from the theoretical aspects of the Feynman method I outlined in Appendix B. The main result of interest will be the final result for the direct correction to the energy where I derive the exact form of the polarisation operator.

C.1 Direct diagram

To arrive at the appropriate Feynman diagrams, we need to find the energy correction for a process in which two photon propagators are present, which means that we need to consider the fourth order term in the time evolution operator (of order e^4 or α^2). The fourth order term in the Dyson series is

$$S_{vv}^{(4)} = \frac{(-ie)^4}{4!}\int d^4x\, d^4y\, d^4z\, d^4w\, \langle 0|c_v T\left\{\bar{\psi}(x)\gamma^\mu\psi(x)A_\mu(x)\bar{\psi}(y)\gamma^\nu\psi(y)A_\nu(y) \times\bar{\psi}(z)\gamma^\alpha\psi(z)A_\alpha(z)\bar{\psi}(w)\gamma^\beta\psi(w)A_\beta(w)\right\}c_v^\dagger|0\rangle. \tag{C.1}$$

Wick's theorem [147, 148] can be used to evaluate the time-ordered product, and hence the inner product under the integral sign, as a sum of fully contracted terms. Firstly, all of the photon fields A_μ must be contracted in order for the inner product to be nonzero, and there are two ways to do this. I will first start by deriving the direct diagram, and the combination of photon contractions that gives this diagram is one in which the fields at x and y are contracted and the ones at z and w are contracted, leading to

$$S_{vv}^{(4)} = \frac{(-ie)^4}{4!}\int d^4x\, d^4y\, d^4z\, d^4w\, D_C(x,y)_{\mu\nu}D_C(z,w)_{\alpha\beta} \times \langle 0|c_v T\left\{\bar{\psi}(x)\gamma^\mu\psi(x)\bar{\psi}(y)\gamma^\nu\psi(y)\bar{\psi}(z)\gamma^\alpha\psi(z)\bar{\psi}(w)\gamma^\beta\psi(w)\right\}c_v^\dagger|0\rangle. \tag{C.2}$$

Next, we will neglect interactions with the transverse photons (i.e. Breit photons, to lowest order), so that we only retain the Coulomb (D_{00}) components of each of the photon propagators, leading to

$$S_{vv}^{(4)} = -\frac{e^4}{4!}\int d^4x\, d^4y\, d^4z\, d^4w\, \frac{\delta(x_0-y_0)\delta(z_0-w_0)}{(4\pi)^2|\boldsymbol{x}-\boldsymbol{y}||\boldsymbol{z}-\boldsymbol{w}|} \times \langle 0|c_v T\left\{\bar{\psi}(x)\gamma^0\psi(x)\bar{\psi}(y)\gamma^0\psi(y)\bar{\psi}(z)\gamma^0\psi(z)\bar{\psi}(w)\gamma^0\psi(w)\right\}c_v^\dagger|0\rangle. \tag{C.3}$$

The direct diagram then corresponds to one of the terms in the Wick expansion with contractions such as,

$$S_{vv}^{(4)} = -\frac{e^4}{4!}\int d^4x\, d^4y\, d^4z\, d^4w\, \frac{\delta(x_0-y_0)\delta(z_0-w_0)}{(4\pi)^2|\boldsymbol{x}-\boldsymbol{y}||\boldsymbol{z}-\boldsymbol{w}|} \times \langle 0|\overbrace{c_v T\left\{\bar{\psi}(x)\gamma^0\psi(x)\bar{\psi}(y)\gamma^0\psi(y)\bar{\psi}(z)\gamma^0\psi(z)\bar{\psi}(w)\gamma^0\psi(w)\right\}c_v^\dagger}|0\rangle. \tag{C.4}$$

Note here that contractions with external creation/annihilation operators simply denote swapping the order of the field and the creation/annihilation operator, and then applying this onto the vacuum state, so that, using Eq. (B.6),

$$\overbrace{\psi(w)c_v^\dagger} = \sum_a^{\text{core}}\big(\underbrace{\{b_a^\dagger, c_v^\dagger\}}_{=0} - c_v^\dagger b_a^\dagger\big)e^{i\varepsilon_a w_0}\phi_a(\boldsymbol{w}) + \sum_n^{\text{exc.}}\big(\underbrace{\{c_n, c_v^\dagger\}}_{=\delta_{nv}} - c_v^\dagger c_n\big)e^{-i\varepsilon_n w_0}\phi_n(\boldsymbol{w}) \tag{C.5}$$

$$= -\sum_a^{\text{core}} c_v^\dagger b_a^\dagger e^{i\varepsilon_a w_0}\phi_a(\boldsymbol{w}) + e^{i\varepsilon_v w_0}\phi_v(\boldsymbol{w}) - \sum_n^{\text{exc.}} c_v^\dagger c_n e^{-i\varepsilon_n w_0}\phi_n(\boldsymbol{w}). \tag{C.6}$$

When this acts on the frozen core vacuum state, only the second term will survive since an application of $b_a^\dagger$ (i.e. creating an additional electron in a core state) or c_n (destroying a particle in a state not in the core) will give zero. Therefore,

$$\overbrace{\psi(w)c_v^\dagger} = e^{-i\varepsilon_v w_0}\phi_v(\boldsymbol{w}) \quad \text{and} \quad \overbrace{c_v\bar{\psi}}(x) = \bar{\phi}_v(\boldsymbol{x})e^{i\varepsilon_v x_0}. \tag{C.7}$$

Substituting this back into Eq. (C.4), using Eq. (B.10), and keeping track of the minus signs, we get

$$S_{vv}^{(4)} = -\frac{e^4}{4!}\int d^4x\, d^4y\, d^4z\, d^4w\, \frac{\delta(x_0-y_0)\delta(z_0-w_0)e^{-i\varepsilon_v(w_0-x_0)}}{(4\pi)^2|\boldsymbol{x}-\boldsymbol{y}||\boldsymbol{z}-\boldsymbol{w}|} \times \bar{\phi}_v^\alpha(\boldsymbol{x})\gamma^0_{\alpha\beta}S_F^{\beta\rho}(x,w)S_F^{\nu\kappa}(z,y)\gamma^0_{\kappa\lambda}S_F^{\lambda\mu}(y,z)\gamma^0_{\mu\nu}\gamma^0_{\rho\sigma}\phi_v^\sigma(\boldsymbol{w}), \tag{C.8}$$

where I have explicitly included the spinor indices, and where the overall negative sign comes from anti-commuting the electron field operators to get the electron propagator in the correct order. Each electron propagator can then be written in terms of the Fourier transformed propagator as defined in Eq. (B.12), giving

$$S_{vv}^{(4)} = -\frac{e^4}{4!}\int d^4x\, d^4y\, d^4z\, d^4w\, \frac{\delta(x_0-y_0)\delta(z_0-w_0)e^{-i\varepsilon_v(w_0-x_0)}}{(4\pi)^2|\boldsymbol{x}-\boldsymbol{y}||\boldsymbol{z}-\boldsymbol{w}|}\bar{\phi}_v^\alpha(\boldsymbol{x})\gamma^0_{\alpha\beta}\gamma^0_{\kappa\lambda}\gamma^0_{\mu\nu}\gamma^0_{\rho\sigma}\phi_v^\sigma(\boldsymbol{w})$$
$$\times \int \frac{dE_1}{2\pi}\frac{dE_2}{2\pi}\frac{dE_3}{2\pi}e^{-iE_1(x_0-w_0)}S_F^{\beta\rho}(\boldsymbol{x},\boldsymbol{w};E_1)S_F^{\nu\kappa}(\boldsymbol{z},\boldsymbol{y};E_2)e^{-iE_2(z_0-y_0)}S_F^{\lambda\mu}(\boldsymbol{y},\boldsymbol{z};E_3)e^{-iE_3(y_0-z_0)}. \tag{C.9}$$

We can perform the time integrations over y_0 and w_0 (from $-t/2$ to $t/2$), with the use of the delta functions to get

$$\begin{aligned} S_{vv}^{(4)} = &-\frac{e^4}{4!}\int \frac{d^4x\, d^3y\, d^4z\, d^3w}{(4\pi)^2|\boldsymbol{x}-\boldsymbol{y}||\boldsymbol{z}-\boldsymbol{w}|}\bar{\phi}_v^\alpha(\boldsymbol{x})\gamma^0_{\alpha\beta}\gamma^0_{\kappa\lambda}\gamma^0_{\mu\nu}\gamma^0_{\rho\sigma}\phi_v^\sigma(\boldsymbol{w}) \\ &\times\int \frac{dE_1}{2\pi}\frac{dE_2}{2\pi}\frac{dE_3}{2\pi}S_F^{\beta\rho}(\boldsymbol{x},\boldsymbol{w};E_1)S_F^{\nu\kappa}(\boldsymbol{z},\boldsymbol{y};E_2)S_F^{\lambda\mu}(\boldsymbol{y},\boldsymbol{z};E_3)e^{-i(x_0-z_0)(E_1-\varepsilon_v+E_3-E_2)}. \end{aligned} \tag{C.10}$$

Then, performing the x_0 and z_0 integrations gives a factor of $2\pi t\delta(E_1-\varepsilon_v+E_3-E_2)$, leading to

$$\begin{aligned} S_{vv}^{(4)} = &-2\pi t\frac{e^4}{4!}\int \frac{d^3x\, d^3y\, d^3z\, d^3w}{(4\pi)^2|\boldsymbol{x}-\boldsymbol{y}||\boldsymbol{z}-\boldsymbol{w}|}\bar{\phi}_v^\alpha(\boldsymbol{x})\gamma^0_{\alpha\beta}\gamma^0_{\kappa\lambda}\gamma^0_{\mu\nu}\gamma^0_{\rho\sigma}\phi_v^\sigma(\boldsymbol{w}) \\ &\times\int \frac{dE_1}{2\pi}\frac{dE_2}{2\pi}\frac{dE_3}{2\pi}S_F^{\beta\rho}(\boldsymbol{x},\boldsymbol{w};E_1)S_F^{\nu\kappa}(\boldsymbol{z},\boldsymbol{y};E_2)S_F^{\lambda\mu}(\boldsymbol{y},\boldsymbol{z};E_3)\delta(E_1-\varepsilon_v+E_3-E_2), \end{aligned} \tag{C.11}$$

and then performing the integration over E_2 gives

$$\begin{aligned} S_{vv}^{(4)} = &-t\frac{e^4}{4!}\int \frac{d^3x\, d^3y\, d^3z\, d^3w}{(4\pi)^2|\boldsymbol{x}-\boldsymbol{y}||\boldsymbol{z}-\boldsymbol{w}|}\bar{\phi}_v^\alpha(\boldsymbol{x})\gamma^0_{\alpha\beta}\gamma^0_{\kappa\lambda}\gamma^0_{\mu\nu}\gamma^0_{\rho\sigma}\phi_v^\sigma(\boldsymbol{w}) \\ &\times\int \frac{dE_1}{2\pi}\frac{dE_3}{2\pi}S_F^{\beta\rho}(\boldsymbol{x},\boldsymbol{w};E_1)S_F^{\nu\kappa}(\boldsymbol{z},\boldsymbol{y};E_1+E_3-\varepsilon_v)S_F^{\lambda\mu}(\boldsymbol{y},\boldsymbol{z};E_3). \end{aligned} \tag{C.12}$$

Finally, to sort out the spinor indices, note that from Eq. (B.12),

$$S_F^{\alpha\beta}(\boldsymbol{x},\boldsymbol{y};E)\gamma^0_{\beta\lambda} = \lim_{\delta\to0}\left[\sum_a^{\text{core}}\frac{\phi_a^\alpha(\boldsymbol{x})\bar{\phi}_a^\beta(\boldsymbol{y})\gamma^0_{\beta\lambda}}{E-\varepsilon_a-i\delta}+\sum_n^{\text{exc.}}\frac{\phi_n^\alpha(\boldsymbol{x})\bar{\phi}_n^\beta(\boldsymbol{y})\gamma^0_{\beta\lambda}}{E-\varepsilon_n+i\delta}\right] \tag{C.13}$$

$$= \lim_{\delta\to0}\left[\sum_a^{\text{core}}\frac{\phi_a^\alpha(\boldsymbol{x})\phi_a^{\dagger\beta}(\boldsymbol{y})}{E-\varepsilon_a-i\delta}+\sum_n^{\text{exc.}}\frac{\phi_n^\alpha(\boldsymbol{x})\phi_n^{\dagger\beta}(\boldsymbol{y})}{E-\varepsilon_n+i\delta}\right] \tag{C.14}$$

$$= G^{\alpha\beta}(\boldsymbol{x},\boldsymbol{y};E), \tag{C.15}$$

where we have again used $\bar{\phi}\gamma^0 = \phi^\dagger$ and where $G(\boldsymbol{x},\boldsymbol{y};E)$ is the CHF Green's function, defined in Eq. (4.4). As a side note, since S_F is a time-ordered propagator, this means that the CHF Green's function $G = S_F\gamma^0$ is also time-ordered. Therefore, the Green's functions in the Feynman method contain all possible time-orderings of electron propagation, whereas in the traditional method of perturbation theory, each time-ordering must separately be accounted for, and this is one reason that the Feynman method is more numerically appealing than the Goldstone method.

Using Eq. (C.15), we find that Eq. (C.12) becomes

$$\begin{aligned} S_{vv}^{(4)} = &-t\frac{e^4}{4!}\int \frac{d^3x\, d^3y\, d^3z\, d^3w}{(4\pi)^2|\boldsymbol{x}-\boldsymbol{y}||\boldsymbol{z}-\boldsymbol{w}|}\phi_v^{\dagger\beta}(\boldsymbol{x})\phi_v^\sigma(\boldsymbol{w}) \\ &\times\int \frac{dE_1}{2\pi}\frac{dE_3}{2\pi}G^{\beta\sigma}(\boldsymbol{x},\boldsymbol{w};E_1)G^{\lambda\nu}(\boldsymbol{z},\boldsymbol{y};E_1+E_3-\varepsilon_v)G^{\nu\lambda}(\boldsymbol{y},\boldsymbol{z};E_3). \end{aligned} \tag{C.16}$$

Finally, to extract the energy correction we can equate this to the fourth order term in the Dyson expansion of the energy correction, $-\delta^{(4)}Et/4!$, which gives us

$$\begin{aligned}\delta^{(4)}E = e^4 \int \frac{d^3x\, d^3y\, d^3z\, d^3w}{(4\pi)^2|\boldsymbol{x}-\boldsymbol{y}||\boldsymbol{z}-\boldsymbol{w}|}\phi_v^{\dagger\beta}(\boldsymbol{x})\phi_v^{\sigma}(\boldsymbol{w}) \\ \times \int \frac{dE_1}{2\pi}\frac{dE_3}{2\pi}G^{\beta\sigma}(\boldsymbol{x},\boldsymbol{w};E_1)G^{\lambda\nu}(\boldsymbol{z},\boldsymbol{y};E_1+E_3-\varepsilon_v)G^{\nu\lambda}(\boldsymbol{y},\boldsymbol{z};E_3).\end{aligned} \tag{C.17}$$

Defining the new integration variables, $\omega = E_1 - \varepsilon_v$ and $E_3 = \varepsilon'$, allows us to write the energy correction above as,

$$\begin{aligned}\delta^{(4)}E = \frac{e^4}{(4\pi)^2}\int \frac{d^3x\, d^3y\, d^3z\, d^3w}{|\boldsymbol{x}-\boldsymbol{y}||\boldsymbol{z}-\boldsymbol{w}|}\int \frac{d\omega}{2\pi}\frac{d\varepsilon'}{2\pi}\phi_v^{\dagger\beta}(\boldsymbol{x})G^{\beta\sigma}(\boldsymbol{x},\boldsymbol{w};\varepsilon_v+\omega)\phi_v^{\sigma}(\boldsymbol{w}) \\ \times G^{\lambda\nu}(\boldsymbol{z},\boldsymbol{y};\varepsilon'+\omega)G^{\nu\lambda}(\boldsymbol{y},\boldsymbol{z};\varepsilon').\end{aligned} \tag{C.18}$$

which agrees exactly with the direct part of the second-order energy correction in Eq. (4.4), if we recall that $\alpha = e^2/4\pi$ and $\alpha = 1$ in atomic units. If we suppress the spinor indices, and use the shorthand $G_{\boldsymbol{xy}}(E) = G(\boldsymbol{x},\boldsymbol{y};E)$, then this can be written in the form

$$\delta^{(2)}E_v = \int \frac{d^3x\, d^3y\, d^3z\, d^3w}{|\boldsymbol{x}-\boldsymbol{y}||\boldsymbol{z}-\boldsymbol{w}|}\int \frac{d\omega}{2\pi}\frac{d\varepsilon'}{2\pi}\phi_v^{\dagger}(\boldsymbol{x})G_{\boldsymbol{xw}}(\varepsilon_v+\omega)\phi_v(\boldsymbol{w})\mathrm{Tr}\left[G_{\boldsymbol{zy}}(\varepsilon'+\omega)G_{\boldsymbol{yz}}(\varepsilon')\right], \tag{C.19}$$

where $\mathrm{Tr}(A)$ denotes the trace of the propagator A over its spinor indices, and where the product $\phi^\dagger G\phi$ implies summation over the spinor indices.

C.1.1 Polarisation operator analytical frequency integration

The polarisation operator, as discussed in the body of this thesis, is defined as the fermion loop in Eq. (C.19),

$$\Pi(\boldsymbol{x},\boldsymbol{y};\omega) = \int \frac{d\alpha}{2\pi}\,\mathrm{Tr}\left[G(\boldsymbol{y},\boldsymbol{x};\omega+\alpha)G(\boldsymbol{x},\boldsymbol{y};\alpha)\right] \tag{C.20}$$

$$= \int \frac{d\alpha}{2\pi}\,G^{\mu\nu}(\boldsymbol{y},\boldsymbol{x};\omega+\alpha)G^{\nu\mu}(\boldsymbol{x},\boldsymbol{y};\alpha). \tag{C.21}$$

Using the full expression for the Feynman HF Green's function in Eq. (C.14), this becomes

$$\begin{aligned}\Pi(\boldsymbol{x},\boldsymbol{y};\omega) = \int \frac{d\alpha}{2\pi}\lim_{\delta\to0}\left[\sum_a^{\text{core}}\frac{\phi_a^{\mu}(\boldsymbol{y})\phi_a^{\dagger\nu}(\boldsymbol{x})}{\omega+\alpha-\varepsilon_a-i\delta}+\sum_n^{\text{exc.}}\frac{\phi_n^{\mu}(\boldsymbol{y})\phi_n^{\dagger\nu}(\boldsymbol{x})}{\omega+\alpha-\varepsilon_n+i\delta}\right] \\ \times\lim_{\varepsilon\to0}\left[\sum_b^{\text{core}}\frac{\phi_b^{\nu}(\boldsymbol{x})\phi_b^{\dagger\mu}(\boldsymbol{y})}{\alpha-\varepsilon_b-i\varepsilon}+\sum_m^{\text{exc.}}\frac{\phi_m^{\nu}(\boldsymbol{x})\phi_m^{\dagger\mu}(\boldsymbol{y})}{\alpha-\varepsilon_m+i\varepsilon}\right].\end{aligned} \tag{C.22}$$

To evaluate these four integrals, we can use Cauchy's integral formula, which states that for any function $f(z)$ that is analytic inside and on the boundary of some closed, positively-oriented contour C [111],

$$\oint_C \frac{f(z)}{z-a}\,dz = 2\pi i\, f(a). \tag{C.23}$$

We see that of the four integrals in Eq. (C.22), only two will be nonzero. This is because for the ab term, for a given a, b, we will have simple poles at $\alpha = \varepsilon_a - \omega + i\delta$ and $\alpha = \varepsilon_b + i\varepsilon$. Therefore, the poles of the integrand each lie above the real axis, and since $G(\boldsymbol{x}, \boldsymbol{y}; \alpha) \to 0$ as $\alpha \to \pm\infty$, we can choose our integration contour to be a semi-circle that encloses the lower half plane, completely missing both poles. Likewise, the last (nm) term also gives zero by choosing our integration contour to enclose the upper half plane. For the remaining two integrals, we have one pole in the upper half plane and one pole in the lower half plane, so these integrals are nonzero.

For the first of the nonzero integrals (the one involving the sum over a and m), we can choose our contour to enclose the upper half-plane, which captures the pole at $\omega = \varepsilon_a - \omega + i\delta$ and misses the pole at $\alpha = \varepsilon_m - i\varepsilon$, so using Cauchy's integral formula gets us,

$$\lim_{\delta,\varepsilon\to 0} \sum_{a,m} \int \frac{d\alpha}{2\pi} \frac{\phi_a^\mu(\boldsymbol{y})\phi_a^{\dagger\nu}(\boldsymbol{x})\phi_m^\nu(\boldsymbol{x})\phi_m^{\dagger\mu}(\boldsymbol{y})}{(\omega + \alpha - \varepsilon_a - i\delta)(\alpha - \varepsilon_m + i\varepsilon)} = i \lim_{\delta,\varepsilon\to 0} \sum_{a,m} \frac{\phi_a^\mu(\boldsymbol{y})\phi_a^{\dagger\nu}(\boldsymbol{x})\phi_m^\nu(\boldsymbol{x})\phi_m^{\dagger\mu}(\boldsymbol{y})}{\varepsilon_a - \omega + i\delta - \varepsilon_m + i\varepsilon} \tag{C.24}$$

$$= i \sum_{a,m} \frac{\phi_a^{\dagger\nu}(\boldsymbol{x})\phi_m^\nu(\boldsymbol{x})\phi_m^{\dagger\mu}(\boldsymbol{y})\phi_a^\mu(\boldsymbol{y})}{\varepsilon_a - \omega - \varepsilon_m} \tag{C.25}$$

$$= i \sum_{a,n} \frac{\phi_a^\dagger(\boldsymbol{x})\phi_n(\boldsymbol{x})\phi_n^\dagger(\boldsymbol{y})\phi_a(\boldsymbol{y})}{\varepsilon_a - \omega - \varepsilon_n}, \tag{C.26}$$

where in the last line we have relabelled $m \to n$ and removed the spinor indices to leave the summations in $\phi^\dagger\phi$ implicit. Similarly, for the other nonzero term in Eq. (C.22) (the one with the sum over b and n), we can again integrate in the upper half-plane, which captures the pole at $\alpha = \varepsilon_b + i\varepsilon$ and misses the pole at $\alpha = \varepsilon_n - \omega - i\delta$, so using Cauchy's integral formula gives us

$$\lim_{\delta,\varepsilon\to 0} \sum_{b,n} \int \frac{d\alpha}{2\pi} \frac{\phi_n^\mu(\boldsymbol{y})\phi_n^{\dagger\nu}(\boldsymbol{x})\phi_b^\nu(\boldsymbol{x})\phi_b^{\dagger\mu}(\boldsymbol{y})}{(\omega + \alpha - \varepsilon_n + i\delta)(\alpha - \varepsilon_b - i\varepsilon)} = i \sum_{b,n} \frac{\phi_n^\mu(\boldsymbol{y})\phi_n^{\dagger\nu}(\boldsymbol{x})\phi_b^\nu(\boldsymbol{x})\phi_b^{\dagger\mu}(\boldsymbol{y})}{\omega + \varepsilon_b - \varepsilon_n} \tag{C.27}$$

$$= i \sum_{a,n} \frac{\phi_a^\dagger(\boldsymbol{y})\phi_n(\boldsymbol{y})\phi_n^\dagger(\boldsymbol{x})\phi_a(\boldsymbol{x})}{\omega + \varepsilon_a - \varepsilon_n}. \tag{C.28}$$

Therefore, adding together the results of Eqs. (C.26) and (C.28) gives an expression for the polarisation operator,

$$\Pi(\boldsymbol{x}, \boldsymbol{y}; \omega) = i \sum_a^{\text{core}} \sum_n^{\text{exc.}} \left[\frac{\phi_a^\dagger(\boldsymbol{x})\phi_n(\boldsymbol{x})\phi_n^\dagger(\boldsymbol{y})\phi_a(\boldsymbol{y})}{\varepsilon_a - \omega - \varepsilon_n} + \frac{\phi_a^\dagger(\boldsymbol{y})\phi_n(\boldsymbol{y})\phi_n^\dagger(\boldsymbol{x})\phi_a(\boldsymbol{x})}{\omega + \varepsilon_a - \varepsilon_n} \right] \tag{C.29}$$

$$= i \sum_a^{\text{core}} \sum_n^{\text{exc.}} \left[\phi_a^\dagger(\boldsymbol{x}) \frac{\phi_n(\boldsymbol{x})\phi_n^\dagger(\boldsymbol{y})}{\varepsilon_a - \omega - \varepsilon_n} \phi_a(\boldsymbol{y}) + \phi_a^\dagger(\boldsymbol{y}) \frac{\phi_n(\boldsymbol{y})\phi_n^\dagger(\boldsymbol{x})}{\omega + \varepsilon_a - \varepsilon_n} \phi_a(\boldsymbol{x}) \right]. \tag{C.30}$$

To simplify this, note from the definition of the HF Green's function, Eq. (4.1), that we can identify the sums over n in the above expression as HF Green's function restricted to only

the excited states,

$$G^{\text{ex}}(\boldsymbol{x},\boldsymbol{y};\varepsilon) \equiv \sum_{n}^{\text{exc.}} \frac{\phi_n(\boldsymbol{x})\phi_n^\dagger(\boldsymbol{y})}{\varepsilon-\varepsilon_n}, \tag{C.31}$$

meaning that Eq. (C.30) can be written as

$$\Pi(\boldsymbol{x},\boldsymbol{y};\omega) = i\sum_{a}^{\text{core}} \left[\phi_a^\dagger(\boldsymbol{x})G^{\text{ex}}(\boldsymbol{x},\boldsymbol{y};\varepsilon_a-\omega)\phi_a(\boldsymbol{y}) + \phi_a^\dagger(\boldsymbol{y})G^{\text{ex}}(\boldsymbol{y},\boldsymbol{x};\varepsilon_a+\omega)\phi_a(\boldsymbol{x})\right]. \tag{C.32}$$

C.2 Exchange diagram

To arrive at the exchange diagram, we again start at the fourth-order scattering matrix element,

$$\begin{aligned} S_{vv}^{(4)} = \frac{(-ie)^4}{4!}\int d^4x\, d^4y\, d^4z\, d^4w\, \langle 0|c_v T\left\{\bar\psi(x)\gamma^\mu\psi(x)A_\mu(x)\bar\psi(y)\gamma^\nu\psi(y)A_\nu(y)\right. \\ \left.\times\bar\psi(z)\gamma^\alpha\psi(z)A_\alpha(z)\bar\psi(w)\gamma^\beta\psi(w)A_\beta(w)\right\}c_v^\dagger|0\rangle, \end{aligned} \tag{C.33}$$

with the following contractions,

$$\begin{aligned} S_{vv}^{(4)} &= \frac{(-ie)^4}{4!}\int d^4x\, d^4y\, d^4z\, d^4w \\ &\times \langle 0|\overbrace{c_v T\{\bar\psi(x)\gamma^\mu\underbrace{\psi(x)A_\mu(x)}\bar\psi(y)\gamma^\nu\overbrace{\psi(y)A_\nu(y)}\bar\psi(z)\gamma^\alpha\underbrace{\psi(z)A_\alpha(z)}\bar\psi(w)\gamma^\beta\overbrace{\psi(w)A_\beta(w)}\}c_v^\dagger}|0\rangle, \end{aligned} \tag{C.34}$$

which, using the same methods outlined for the evaluation of the direct diagram, and only retaining the Coulomb parts of the photon propagator, becomes

$$\begin{aligned} S_{vv}^{(4)} &= \frac{e^4}{4!}\int \frac{d^4x\, d^4y\, d^4z\, d^4w}{(4\pi)^2|\boldsymbol{x}-\boldsymbol{z}||\boldsymbol{y}-\boldsymbol{w}|}\,\delta(x_0-z_0)\delta(y_0-w_0)e^{-i\varepsilon_v(w_0-x_0)} \\ &\qquad\times \bar\phi_v^\alpha(\boldsymbol{x})\gamma^0_{\alpha\beta}S_F^{\beta\kappa}(x,y)\gamma^0_{\kappa\lambda}S_F^{\lambda\mu}(y,z)\gamma^0_{\mu\nu}S_F^{\nu\rho}(z,w)\gamma^0_{\rho\sigma}\phi_v^\sigma(\boldsymbol{w}) \end{aligned} \tag{C.35}$$

$$\begin{aligned} &= \frac{e^4}{4!}\int \frac{d^4x\, d^4y\, d^3z\, d^3w}{(4\pi)^2|\boldsymbol{x}-\boldsymbol{z}||\boldsymbol{y}-\boldsymbol{w}|}\,\phi_v^{\dagger\beta}(\boldsymbol{x})\phi_v^\sigma(\boldsymbol{w})\int\frac{dE_1\,dE_2\,dE_3}{(2\pi)^3} \\ &\qquad\times e^{-i(x_0-y_0)(E_1+E_3-E_2-\varepsilon_v)}G^{\beta\lambda}(\boldsymbol{x},\boldsymbol{y};E_1)G^{\lambda\nu}(\boldsymbol{y},\boldsymbol{z};E_2)G^{\nu\sigma}(\boldsymbol{z},\boldsymbol{w};E_3) \end{aligned} \tag{C.36}$$

$$\begin{aligned} &= \frac{e^4 t}{4!}\int \frac{d^3x\, d^3y\, d^3z\, d^3w}{(4\pi)^2|\boldsymbol{x}-\boldsymbol{z}||\boldsymbol{y}-\boldsymbol{w}|}\,\phi_v^{\dagger\beta}(\boldsymbol{x})\phi_v^\sigma(\boldsymbol{w})\int\frac{dE_1\,dE_2\,dE_3}{(2\pi)^2} \\ &\qquad\times \delta(E_1+E_3-E_2-\varepsilon_v)G^{\beta\lambda}(\boldsymbol{x},\boldsymbol{y};E_1)G^{\lambda\nu}(\boldsymbol{y},\boldsymbol{z};E_2)G^{\nu\sigma}(\boldsymbol{z},\boldsymbol{w};E_3) \end{aligned} \tag{C.37}$$

$$\begin{aligned} &= \frac{e^4 t}{4!}\int \frac{d^3x\, d^3y\, d^3z\, d^3w}{(4\pi)^2|\boldsymbol{x}-\boldsymbol{z}||\boldsymbol{y}-\boldsymbol{w}|}\,\phi_v^{\dagger\beta}(\boldsymbol{x})\phi_v^\sigma(\boldsymbol{w}) \\ &\qquad\times\int\frac{dE_1\,dE_3}{(2\pi)^2}\,G^{\beta\lambda}(\boldsymbol{x},\boldsymbol{y};E_1)G^{\lambda\nu}(\boldsymbol{y},\boldsymbol{z};E_1+E_3-\varepsilon_v)G^{\nu\sigma}(\boldsymbol{z},\boldsymbol{w};E_3). \end{aligned} \tag{C.38}$$

Making the substitutions $\omega_1 = E_1 - \varepsilon_v$ and $\omega_2 = E_3 - \varepsilon_v$ gives the desired expression,

$$S_{vv}^{(4)} = \frac{e^4 t}{4!} \int \frac{d^3x\, d^3y\, d^3z\, d^3w}{(4\pi)^2 |\boldsymbol{x}-\boldsymbol{z}||\boldsymbol{y}-\boldsymbol{w}|} \int \frac{d\omega_1}{2\pi}\frac{d\omega_2}{2\pi}\, \phi_v^{\dagger\beta}(\boldsymbol{x})\phi_v^{\sigma}(\boldsymbol{w}) \times G^{\beta\lambda}(\boldsymbol{x},\boldsymbol{y};\omega_1+\varepsilon_v) G^{\lambda\nu}(\boldsymbol{y},\boldsymbol{z};\omega_1+\omega_2+\varepsilon_v) G^{\nu\sigma}(\boldsymbol{z},\boldsymbol{w};\omega_1+\varepsilon_v) \tag{C.39}$$

$$= \frac{\alpha^2 t}{4!} \int \frac{d^3x\, d^3y\, d^3z\, d^3w}{|\boldsymbol{x}-\boldsymbol{z}||\boldsymbol{y}-\boldsymbol{w}|} \times \int \frac{d\omega_1}{2\pi}\frac{d\omega_2}{2\pi}\, \phi_v^{\dagger}(\boldsymbol{x}) G_{\boldsymbol{xy}}(\omega_1+\varepsilon_v) G_{\boldsymbol{yz}}(\omega_1+\omega_2+\varepsilon_v) G_{\boldsymbol{zw}}(\omega_1+\varepsilon_v)\phi_v(\boldsymbol{w}). \tag{C.40}$$

This corresponds to an energy correction of

$$\delta^{(2)} E_v^{\mathrm{x}} = -\alpha^2 \int d^3x\, d^3y\, d^3z\, d^3w \int \frac{d\omega_1}{2\pi}\frac{d\omega_2}{2\pi}\, \phi_v^{\dagger}(\boldsymbol{x}) G_{\boldsymbol{xy}}(\omega_1+\varepsilon_v) Q_{\boldsymbol{xz}} \times G_{\boldsymbol{yz}}(\omega_1+\omega_2+\varepsilon_v) Q_{\boldsymbol{yw}} G_{\boldsymbol{zw}}(\omega_1+\varepsilon_v)\phi_v(\boldsymbol{w}), \tag{C.41}$$

where $Q_{\boldsymbol{xy}} = |\boldsymbol{x}-\boldsymbol{y}|^{-1}$ and I have suppressed the spinor indices on the Green's functions, which are being implicitly summed over along this expression from left to right, as in Eq. (C.39). Eq. (C.41) is equal to the second (exchange) diagram in Eq. (4.3).

References

[1] M.-A. Bouchiat and C. Bouchiat, "Parity violation in atoms", Reports on Progress in Physics **60**, 1351–1396 (1997).

[2] S. G. Porsev, K. Beloy, and A. Derevianko, "Precision Determination of Electroweak Coupling from Atomic Parity Violation and Implications for Particle Physics", Physical Review Letters **102**, 181601 (2009).

[3] S. A. Blundell, A. C. Hartley, Z. Liu, A.-M. Martensson-Pendrill, and J. Sapirstein, "Calculations of the parity non-conserving 6s → 7s transition in caesium", Theoretica Chimica Acta **80**, 257–288 (1991).

[4] C. S. Wood, S. C. Bennett, D. Cho, et al., "Measurement of Parity Nonconservation and an Anapole Moment in Cesium", Science **275**, 1759–1763 (1997).

[5] V. Dzuba, V. Flambaum, and O. Sushkov, "Summation of the high orders of perturbation theory for the parity nonconserving E1-amplitude of the 6s–7s transition in the caesium atom", Physics Letters A **141**, 147–153 (1989).

[6] S. A. Blundell, J. Sapirstein, and W. R. Johnson, "High-accuracy calculation of parity nonconservation in cesium and implications for particle physics", Physical Review D **45**, 1602–1623 (1992).

[7] A. Derevianko, "Reconciliation of the Measurement of Parity Nonconservation in Cs with the Standard Model", Physical Review Letters **85**, 1618–1621 (2000).

[8] V. A. Dzuba, J. C. Berengut, V. V. Flambaum, and B. Roberts, "Revisiting Parity Nonconservation in Cesium", Physical Review Letters **109**, 203003 (2012).

[9] C. Zhang, T. Ooi, J. S. Higgins, et al., "Frequency ratio of the ^{229m}Th nuclear isomeric transition and the ^{87}Sr atomic clock", Nature **633**, 63–70 (2024).

[10] R. Elwell, C. Schneider, J. Jeet, et al., "Laser Excitation of the ^{229}Th Nuclear Isomeric Transition in a Solid-State Host", Physical Review Letters **133**, 013201 (2024).

[11] J. Tiedau, M. V. Okhapkin, K. Zhang, et al., "Laser Excitation of the Th-229 Nucleus", Physical Review Letters **132**, 182501 (2024).

[12] E. Peik and C. Tamm, "Nuclear laser spectroscopy of the 3.5 eV transition in Th-229", Europhysics Letters (EPL) **61**, 181–186 (2003).

[13] V. V. Flambaum, "Enhanced Effect of Temporal Variation of the Fine Structure Constant and the Strong Interaction in ^{229}Th", Physical Review Letters **97**, 092502 (2006).

[14] V. Dzuba, V. Flambaum, and O. Sushkov, "Summation of the perturbation theory high order contributions to the correlation correction for the energy levels of the caesium atom", Physics Letters A **140**, 493–497 (1989).

[15] B. M. Roberts, *Atomic many-body perturbation theory in the screened coulomb interaction*, `https://github.com/benroberts999/ampsci`.

[16] A. Derevianko, "Correlated many-body treatment of the Breit interaction with application to cesium atomic properties and parity violation", Physical Review A **65**, 012106 (2001).

[17] T. Lancaster and S. Blundell, *Quantum field theory for the gifted amateur*, 1. ed., repr. with corr (Oxford Univ. Press, Oxford, 2018).

[18] G. Breit, "The Fine Structure of HE as a Test of the Spin Interactions of Two Electrons", Physical Review **36**, 383–397 (1930).

[19] W. R. Johnson, *Atomic Structure Theory: Lectures on Atomic Physics* (Springer Science & Business Media, Mar. 8, 2007), 318 pp.

[20] J. J. Sakurai and J. Napolitano, *Modern Quantum Mechanics*, 3rd ed. (Cambridge University Press, Cambridge, 2020).

[21] I. Lindgren and J. Morrison, *Atomic Many-Body Theory* (Springer, Berlin, Heidelberg, 1986).

[22] L. Armstrong and S. Feneuille, "Relativistic Effects in The Many-Electron Atom", in *Advances in Atomic and Molecular Physics*, Vol. 10 (Elsevier, 1974), pp. 1–52.

[23] H. A. Bethe and E. E. Salpeter, *Quantum Mechanics of One- and Two-Electron Atoms* (Springer, Berlin, Heidelberg, 1957).

[24] J. D. Jackson, *Classical electrodynamics*, 3rd ed (Wiley, New York, 1999), 808 pp.

[25] L. D. Landau and E. M. Lifshitz, *The classical theory of fields*, 4th rev. English ed, Course of Theoretical Physics v. 2 (Pergamon Press, Oxford ; New York, 1975), 402 pp.

[26] G. Breit, "The Effect of Retardation on the Interaction of Two Electrons", Physical Review **34**, 553–573 (1929).

[27] J. A. Gaunt and R. H. Fowler, "The triplets of helium", Philosophical Transactions of the Royal Society of London. Series A, Containing Papers of a Mathematical or Physical Character **228**, 151–196 (1997).

[28] A. S. Eddington, "The charge of an electron", Proceedings of the Royal Society of London. Series A, Containing Papers of a Mathematical and Physical Character **122**, 358–369 (1997).

[29] P. A. M. Dirac, *The principles of quantum mechanics*, 4. ed. (rev.), repr, International Series of Monographs on Physics 27 (Clarendon Press, Oxford University Press, Oxford, 2010), 314 pp.

[30] J. B. Mann and W. R. Johnson, "Breit Interaction in Multielectron Atoms", Physical Review A **4**, 41–51 (1971).

[31] M. G. Kozlov, S. G. Porsev, and I. I. Tupitsyn, *Breit interaction in heavy atoms*, (Apr. 28, 2000) pre-published.

[32] C. Darwin, "The dynamical motions of charged particles", The London, Edinburgh, and Dublin Philosophical Magazine and Journal of Science **39**, 537–551 (1920).

[33] W. Heisenberg and W. Pauli, "On the quantum dynamics of wave fields", Zeitschrift für Physik **56**, 1–61 (1929).

[34] G. Breit, "Dirac's Equation and the Spin-Spin Interactions of Two Electrons", Physical Review **39**, 616–624 (1932).

[35] W. Heisenberg and W. Pauli, "On the quantum theory of wave fields, II", Zeitschrift für Physik **59**, 168–190 (1929).

[36] H. M. Quiney, I. P. Grant, and S. Wilson, "On the Relativistic Many-Body Perturbation Theory of Atomic and Molecular Electronic Structure", in *Many-Body Methods in Quantum Chemistry*, Vol. 52, edited by U. Kaldor, red. by G. Berthier, M. J. S. Dewar, H. Fischer, et al. (Springer Berlin Heidelberg, Berlin, Heidelberg, 1989), pp. 307–344.

[37] V. B. Berestetskii, E. M. Lifshitz, L. P. Pitaevskii, and L. D. Landau, *Relativistic quantum theory*, 1st ed., Course of theoretical physics v. 4 (Pergamon Press, Oxford, New York, 1971), 2 pp.

[38] W. Greiner and J. Reinhardt, eds., *Quantum Electrodynamics*, Fourth Edition, Springer-Link Bücher (Springer Berlin Heidelberg, Berlin, Heidelberg, 2009).

[39] G. E. Brown and D. G. Ravenhall, "On the interaction of two electrons", Proceedings of the Royal Society of London. Series A. Mathematical and Physical Sciences **208**, 552–559 (1951).

[40] W. R. Johnson, S. A. Blundell, and J. Sapirstein, "Many-body perturbation-theory calculations of energy levels along the lithium isoelectronic sequence", Physical Review A **37**, 2764–2777 (1988).

[41] Y.-K. Kim, "Relativistic Self-Consistent-Field Theory for Closed-Shell Atoms", Physical Review **154**, 17–39 (1967).

[42] H. M. Quiney, I. P. Grant, and S. Wilson, "The Dirac equation in the algebraic approximation. V. Self-consistent field studies including the Breit interaction", Journal of Physics B: Atomic and Molecular Physics **20**, 1413–1422 (1987).

[43] J. Sucher, "Foundations of the relativistic theory of many-electron atoms", Physical Review A **22**, 348–362 (1980).

[44] Y. Ishikawa and K. Koc, "Relativistic many-body perturbation theory based on the no-pair Dirac-Coulomb-Breit Hamiltonian: relativistic correlation energies for the noble-gas sequence through Rn ($Z = 86$), the group-IIB atoms through Hg, and the ions of Ne isoelectronic sequence", Physical Review A **50**, 4733–4742 (1994).

[45] E. Lindroth, A.-M. Martensson-Pendrill, A. Ynnerman, and P. Oster, "Self-consistent treatment of the Breit interaction, with application to the electric dipole moment in thallium", Journal of Physics B: Atomic, Molecular and Optical Physics **22**, 2447–2464 (1989).

[46] B. M. Roberts, C. J. Fairhall, and J. S. M. Ginges, "Electric-dipole transition amplitudes for atoms and ions with one valence electron", Physical Review A **107**, 052812 (2023).

[47] S. G. Porsev, K. Beloy, and A. Derevianko, "Precision determination of weak charge of ^{133}Cs from atomic parity violation", Physical Review D **82**, 036008 (2010).

[48] J. R. Oppenheimer, "Note on the Theory of the Interaction of Field and Matter", Phys. Rev. **35**, 461–477 (1930).

[49] I. Tamm, "Relativistic interaction of elementary particles", J. Phys. (USSR) **9**, 449 (1945).

[50] S. M. Dancoff, "Non-Adiabatic Meson Theory of Nuclear Forces", Physical Review **78**, 382–385 (1950).

[51] F. J. Dyson, "The Use of the Tamm-Dancoff Method in Field Theory", Physical Review **90**, 994–994 (1953).

[52] F. J. Dyson, "Mass-Renormalization with the Tamm-Dancoff Method", Physical Review **91**, 421–422 (1953).

[53] J. Schwinger, "On the Green's functions of quantized fields. I", Proceedings of the National Academy of Sciences **37**, 452–455 (1951).

[54] J. Schwinger, "On the Green's functions of quantized fields. II", Proceedings of the National Academy of Sciences **37**, 455–459 (1951).

[55] M. Gell-Mann and F. Low, "Bound States in Quantum Field Theory", Physical Review **84**, 350–354 (1951).

[56] E. E. Salpeter and H. A. Bethe, "A Relativistic Equation for Bound-State Problems", Physical Review **84**, 1232–1242 (1951).

[57] N. D. Son and J. Sucher, "Bound States of a Relativistic Two-Body Hamiltonian; Comparison with the Bethe-Salpeter Equation", Physical Review **153**, 1496–1501 (1967).

[58] J. Sucher, "Energy Levels of the Two-Electron Atom to Order α^3 Ry; Ionization Energy of Helium", Physical Review **109**, 1010–1011 (1958).

[59] M. Douglas and N. M. Kroll, "Quantum electrodynamical corrections to the fine structure of helium", Annals of Physics **82**, 89–155 (1974).

[60] J. Sapirstein, "Quantum electrodynamics of many-electron atoms", Physica Scripta **36**, 801–808 (1987).

[61] B. M. Roberts, *Ampsci documentation*, July 12, 2024.

[62] T. Koopmans, "Ordering of wave functions and eigenenergies to the individual electrons of an atom", Physica **1**, 104–113 (1934).

[63] W. R. Johnson, J. Sapirstein, and S. A. Blundell, "Atomic structure calculations associated with PNC experiments in atomic cesium", Physica Scripta **T46**, 184–192 (1993).

[64] V. A. Dzuba, V. V. Flambaum, P. G. Silvestrov, and O. P. Sushkov, "Relativistic many-body calculations in atoms and parity violation in caesium", Journal of Physics B: Atomic and Molecular Physics **18**, 597–613 (1985).

[65] E. Avgoustoglou, W. R. Johnson, Z. W. Liu, and J. Sapirstein, "Relativistic many-body calculations of $[2p^5 3s]$ excited-state energy levels for neonlike ions", Physical Review A **51**, 1196–1208 (1995).

[66] U. I. Safronova, W. R. Johnson, and M. S. Safronova, "Excitation energies, polarizabilities, multipole transition rates, and lifetimes of ions along the francium isoelectronic sequence", Physical Review A **76**, 042504 (2007).

[67] I. Lindgren, H. Persson, S. Salomonson, and L. Labzowsky, "Full QED calculations of two-photon exchange for heliumlike systems: Analysis in the Coulomb and Feynman gauges", Physical Review A **51**, 1167–1195 (1995).

[68] O. P. Sushkov, "Breit-interaction correction to the hyperfine constant of an external s electron in a many-electron atom", Physical Review A **63**, 042504 (2001).

[69] C. Wu, R. Zhao, D. Zhang, et al., "The influence of relativistic, Breit interaction, and QED effects on the $1s^2 2p^2$ and $2s2p^3$ energy levels of Be-like ($4 \leq Z \leq 74$) isoelectronic sequence", The European Physical Journal D **77**, 129 (2023).

[70] I. Grant, "Relativistic calculation of atomic structures", Advances in Physics **19**, 747–811 (1970).

[71] M. Reiher and J. Hinze, "Self-consistent treatment of the frequency-independent Breit interaction in Dirac-Fock and MCSCF calculations of atomic structures: I. Theoretical considerations", Journal of Physics B: Atomic, Molecular and Optical Physics **32**, 5489–5505 (1999).

[72] R. Shankar, *Principles of Quantum Mechanics* (Springer US, New York, NY, 1994).

[73] M. S. Safronova, W. R. Johnson, and A. Derevianko, "Relativistic many-body calculations of energy levels, hyperfine constants, electric-dipole matrix elements, and static polarizabilities for alkali-metal atoms", Physical Review A **60**, 4476–4487 (1999).

[74] S. A. Blundell, W. R. Johnson, and J. Sapirstein, "Relativistic all-order calculations of energies and matrix elements in cesium", Physical Review A **43**, 3407–3418 (1991).

[75] V. A. Dzuba, V. V. Flambaum, and M. S. Safronova, "Breit interaction and parity nonconservation in many-electron atoms", Physical Review A **73**, 022112 (2006).

[76] W. J. Marciano and J. L. Rosner, "Atomic parity violation as a probe of new physics", Physical Review Letters **65**, 2963–2966 (1990).

[77] A. Derevianko and S. G. Porsev, "Theoretical overview of atomic parity violation: Recent developments and challenges", The European Physical Journal A **32**, 517–523 (2007).

[78] J. Ginges and V. Flambaum, "Violations of fundamental symmetries in atoms and tests of unification theories of elementary particles", Physics Reports **397**, 63–154 (2004).

[79] T. D. Lee and C. N. Yang, "Question of Parity Conservation in Weak Interactions", Physical Review **104**, 254–258 (1956).

[80] S. C. Bennett and C. E. Wieman, "Measurement of the 6S → 7S Transition Polarizability in Atomic Cesium and an Improved Test of the Standard Model", Physical Review Letters **82**, 2484–2487 (1999).

[81] V. A. Dzuba and V. V. Flambaum, "Off-diagonal hyperfine interaction and parity nonconservation in cesium", Physical Review A **62**, 052101 (2000).

[82] R. Casalbuoni, S. De Curtis, D. Dominici, and R. Gatto, "Bounds on new physics from the new data on parity violation in atomic cesium", Physics Letters B **460**, 135–140 (1999).

[83] J. L. Rosner, "Atomic parity violation and precision electroweak physics — An updated analysis", Physical Review D **61**, 016006 (1999).

[84] V. A. Dzuba, C. Harabati, W. R. Johnson, and M. S. Safronova, "Breit correction to the parity-nonconservation amplitude in cesium", Physical Review A **63**, 044103 (2001).

[85] J. Erler and P. Langacker, "Indications for an Extra Neutral Gauge Boson in Electroweak Precision Data", Physical Review Letters **84**, 212–215 (2000).

[86] M. J. Ramsey-Musolf, "Low-energy parity-violation and new physics", Physical Review C **60**, 015501 (1999).

[87] T. Aaltonen, A. Abulencia, J. Adelman, et al., "Search for New Physics in High-Mass Electron-Positron Events in $p\bar{p}$ Collisions at $\sqrt{s} = 1.96\,\text{TeV}$", Physical Review Letters **99**, 171802 (2007).

[88] P. Langacker, "The Physics of Heavy Z' Gauge Bosons", Reviews of Modern Physics **81**, 1199–1228 (2009).

[89] J. L. Rosner, "Role of present and future atomic parity violation experiments in precision electroweak tests", Physical Review D **65**, 073026 (2002).

[90] A. Kramida, "Update of Atomic Data for the First Three Spectra of Actinium", Atoms **10**, 42 (2022).

[91] B. M. Roberts, *Private correspondence*, Jan. 30, 2025.

[92] E. Gibney, "Father time: the physicist on a mission to build the world's first nuclear clock", Nature **636**, 544–545 (2024).

[93] P. Fadeev, J. C. Berengut, and V. V. Flambaum, "Sensitivity of ^{229}Th nuclear clock transition to variation of the fine-structure constant", Physical Review A **102**, 052833 (2020).

[94] E. Peik, T. Schumm, M. S. Safronova, et al., "Nuclear clocks for testing fundamental physics", Quantum Science and Technology **6**, 034002 (2021).

[95] L. Kroger and C. Reich, "Features of the low-energy level scheme of ^{229}Th as observed in the α-decay of ^{233}U", Nuclear Physics A **259**, 29–60 (1976).

[96] G. Zitzer, J. Tiedau, Ch. E. Düllmann, M. V. Okhapkin, and E. Peik, "Laser spectroscopy on the hyperfine structure and isotope shift of sympathetically cooled $^{229}Th^{3+}$ ions", Physical Review A **111**, L050802 (2025).

[97] M. S. Safronova, U. I. Safronova, A. G. Radnaev, C. J. Campbell, and A. Kuzmich, "Magnetic dipole and electric quadrupole moments of the ^{229}Th nucleus", Physical Review A **88**, 060501 (2013).

[98] K. Beloy and A. Derevianko, "Application of the dual-kinetic-balance sets in the relativistic many-body problem of atomic structure", Computer Physics Communications **179**, 310–319 (2008).

[99] V. A. Dzuba, V. V. Flambaum, and O. P. Sushkov, "Relativistic many-body calculations of energy levels and of fine-structure intervals in the caesium atom", Journal of Physics B: Atomic and Molecular Physics **16**, 715–722 (1983).

[100] V. Dzuba, V. Flambaum, P. Silvestrov, and O. Sushkov, "Relativistic many-body calculation of parity-violating E1-amplitude for the 6S $\rightarrow$ 7S transition in atomic cesium", Physics Letters A **103**, 265–269 (1984).

[101] J. S. M. Ginges and A. V. Volotka, "Testing atomic wave functions in the nuclear vicinity: The hyperfine structure with empirically deduced nuclear and quantum electrodynamic effects", Physical Review A **98**, 032504 (2018).

[102] B. M. Roberts and J. S. M. Ginges, "Hyperfine anomaly in heavy atoms and its role in precision atomic searches for new physics", Physical Review A **104**, 022823 (2021).

[103] W. Johnson, "Relativistic Random-Phase Approximation", in *Advances in Atomic and Molecular Physics*, Vol. 25 (Elsevier, 1989), pp. 375–391.

[104] C. J. Fairhall, B. M. Roberts, and J. S. M. Ginges, "QED radiative corrections to electric dipole amplitudes in heavy atoms", Physical Review A **107**, 022813 (2023).

[105] M. S. Safronova, D. Budker, D. DeMille, et al., "Search for new physics with atoms and molecules", Reviews of Modern Physics **90**, 025008 (2018).

[106] V. Dzuba, V. Flambaum, P. Silverstrov, and O. Sushkov, "Screening of Coulomb interaction and many-body perturbation theory in atoms", Physics Letters A **131**, 461–465 (1988).

[107] A. A. Abrikosov and L. P. Gor'kov, *Methods of quantum field theory in statistical physics*, Rev. English ed (Dover Publications, New York, 1975), 352 pp.

[108] R. D. Mattuck, *A guide to Feynman diagrams in the many-body problem*, 2. ed (McGraw-Hill, New York, 1976), 429 pp.

[109] A. L. Fetter and J. D. Walecka, *Quantum Theory of Many-Particle Systems*, Dover Books on Physics (Dover Publications, Newburyport, 2012), 1118 pp.

[110] M. D. Schwartz, *Quantum Field Theory and the Standard Model*, 1st ed. (Cambridge University Press, Dec. 15, 2013).

[111] G. B. Arfken, H.-J. Weber, and F. E. Harris, *Mathematical methods for physicists: a comprehensive guide*, 7th ed (Elsevier, Amsterdam ; Boston, 2013), 1205 pp.

[112] S. A. Blundell, W. R. Johnson, and J. Sapirstein, "Higher-order many-body perturbation-theory calculations of energy levels in cesium", Physical Review A **38**, 4961–4966 (1988).

[113] W. H. Press, S. A. Teukolsky, W. T. Vetterling, and B. P. Flannery, *Numerical Recipes: The Art of Scientific Computing*, 3. ed (Cambridge University Press, Cambridge, 2007), 1235 pp.

[114] V. A. Dzuba, V. V. Flambaum, and J. S. M. Ginges, "High-precision calculation of parity nonconservation in cesium and test of the standard model", Physical Review D **66**, 076013 (2002).

[115] P. Indelicato, "Effects of the Breit interaction on the 1s binding energy of superheavy elements", Journal of Physics B: Atomic and Molecular Physics **19**, 1719–1730 (1986).

[116] J. Hata and I. P. Grant, "Comments on relativistic two-body interaction in atoms", Journal of Physics B: Atomic and Molecular Physics **17**, L107–L113 (1984).

[117] G. Brown, "XLII. Electron-electron interaction in heavy atoms", The London, Edinburgh, and Dublin Philosophical Magazine and Journal of Science **43**, 467–471 (1952).

[118] M. H. Mittleman, "Structure of Heavy Atoms: Three-Body Potentials", Physical Review A **4**, 893–900 (1971).

[119] M. H. Mittleman, "Configuration-Space Hamiltonian for Heavy Atoms and Correction to the Breit Interaction", Physical Review A **5**, 2395–2401 (1972).

[120] M. H. Mittleman, "Theory of relativistic effects on atoms: Configuration-space Hamiltonian", Physical Review A **24**, 1167–1175 (1981).

[121] K.-N. Huang, "Graphical evaluation of relativistic matrix elements", Reviews of Modern Physics **51**, 215–236 (1979).

[122] K.-N. Huang, "Relativistic radiationless transitions in atoms", Journal of Physics B: Atomic and Molecular Physics **11**, 787–795 (1978).

[123] I. P. Grant and N. C. Pyper, "Breit interaction in multi-configuration relativistic atomic calculations", Journal of Physics B: Atomic and Molecular Physics **9**, 761–774 (1976).

[124] W. R. Johnson, S. A. Blundell, and J. Sapirstein, "Many-body perturbation-theory calculations of energy levels along the sodium isoelectronic sequence", Physical Review A **38**, 2699–2706 (1988).

[125] V. V. Flambaum and J. S. M. Ginges, "Radiative potential and calculations of QED radiative corrections to energy levels and electromagnetic amplitudes in many-electron atoms", Physical Review A **72**, 052115 (2005).

[126] A. Derevianko, B. Ravaine, and W. R. Johnson, "Relaxation effect and radiative corrections in many-electron atoms", Physical Review A **69**, 054502 (2004).

[127] J. S. M. Ginges and J. C. Berengut, "QED radiative corrections and many-body effects in atoms: vacuum polarization and binding energy shifts in alkali metals", Journal of Physics B: Atomic, Molecular and Optical Physics **49**, 095001 (2016).

[128] A. Kramida, Yu. Ralchenko, J. Reader, and and NIST ASD Team, NIST Atomic Spectra Database (ver. 5.12), [Online]. Available: `https://physics.nist.gov/asd` [2025, March 16]. National Institute of Standards and Technology, Gaithersburg, MD. 2024.

[129] B. M. Roberts, V. A. Dzuba, and V. V. Flambaum, "Parity nonconservation in Fr-like actinide and Cs-like rare-earth-metal ions", Physical Review A **88**, 012510 (2013).

[130] D. L. Cooper, J. Hata, and I. P. Grant, "On the accuracy of the Breit-Pauli approximation for fine-structure intervals in light atoms: significance for molecular calculations", Journal of Physics B: Atomic and Molecular Physics **17**, L499–L503 (1984).

[131] J.-J. Wan, J. Li, and J. Gu, "Residual electronic correlation and QED effects in fine-structure splitting of ground configuration for the boron isoelectronic sequence", Results in Physics **31**, 105004 (2021).

[132] K. Cheng, Y.-K. Kim, and J. Desclaux, "Electric dipole, quadrupole, and magnetic dipole transition probabilities of ions isoelectronic to the first-row atoms, Li through F", Atomic Data and Nuclear Data Tables **24**, 111–189 (1979).

[133] B. P. Das, E. P. Venugopal, and M. Idrees, "First-principles relativistic calculations of the fine-structure intervals and magnetic dipole transition probabilities in the $1s^2 2p$ configuration of the lithium isoelectric sequence", Physical Review A **42**, 6903–6904 (1990).

[134] S. G. Porsev, K. V. Koshelev, I. I. Tupitsyn, et al., "Transition frequency shifts with fine-structure-constant variation for Fe II: Breit and core-valence correlation corrections", Physical Review A **76**, 052507 (2007).

[135] P. J. Mohr, J. Griffith, and J. Sapirstein, "Bound-state field-theory approach to proton-structure effects in muonic hydrogen", Physical Review A **87**, 052511 (2013).

[136] P. J. Mohr and J. Sapirstein, "Evaluation of two-photon exchange graphs for excited states of highly charged heliumlike ions", Physical Review A **62**, 052501 (2000).

[137] P. J. Mohr, "Quantum electrodynamics of high-Z few-electron atoms", Physical Review A **32**, 1949–1957 (1985).

[138] S. A. Blundell, P. J. Mohr, W. R. Johnson, and J. Sapirstein, "Evaluation of two-photon exchange graphs for highly charged heliumlike ions", Physical Review A **48**, 2615–2626 (1993).

[139] P. J. Mohr, "Quantum electrodynamics calculations in few-electron systems", Physica Scripta **T46**, 44–51 (1993).

[140] J. Sapirstein, "QED of high-Z three-electron ions", Nuclear Instruments and Methods in Physics Research Section B: Beam Interactions with Materials and Atoms **31**, 70–78 (1988).

[141] S. A. Blundell, W. R. Johnson, and J. Sapirstein, "Third-order many-body perturbation theory calculations of the ground-state energies of cesium and thallium", Physical Review A **42**, 3751–3762 (1990).

[142] W. H. Furry, "On Bound States and Scattering in Positron Theory", Physical Review **81**, 115–124 (1951).

[143] D. Kleppner and F. M. Pipkin, eds., *Atomic Physics 7* (Springer US, Boston, MA, 1981).

[144] I. P. Grant, "On the relativistic electron-electron interaction", Journal of Physics B: Atomic and Molecular Physics **20**, L735–L740 (1987).

[145] J. Sucher, "S-Matrix Formalism for Level-Shift Calculations", Physical Review **107**, 1448–1449 (1957).

[146] F. J. Dyson, "The S Matrix in Quantum Electrodynamics", Physical Review **75**, 1736–1755 (1949).

[147] M. E. Peskin and D. V. Schroeder, *An introduction to quantum field theory*, The Advanced Book Program (CRC Press, Taylor & Francis Group, Boca Raton London New York, 2019), 842 pp.

[148] G. C. Wick, "The Evaluation of the Collision Matrix", Physical Review **80**, 268–272 (1950).